

Propagation mechanisms of positive streamers in different gases

Gideon Wormeester

Cover: Bakabaka Design www.bakabaka.nl
Print: Wöhrmann Print Service Zutphen
ISBN: 978-94-6203-435-8



This work was supported by project 10118 of Technology Foundation STW, which is part of the Netherlands Organization for Scientific Research (NWO).

Propagation Mechanisms of Positive Streamers in Different Gases

PROEFSCHRIFT

ter verkrijging van de graad van doctor aan de
Technische Universiteit Eindhoven, op gezag van de
rector magnificus, prof.dr.ir. C.J. van Duijn, voor een
commissie aangewezen door het College voor
Promoties in het openbaar te verdedigen
op donderdag 29 augustus 2013 om 16.00 uur

door

Gideon Wormeester

geboren te Apeldoorn

Dit proefschrift is goedgekeurd door de promotor:

prof.dr. U. Ebert

Copromotoren:

dr.ir. S. Nijdam

en

dr. A. Luque Estepa

FOR GWEN

Contents

1	Introduction	1
1.1	What are streamers?	1
1.1.1	Streamers in nature	2
1.1.2	Industrial applications of streamers	3
1.1.3	Streamer experiments & observations	4
1.2	Streamer theory	6
1.2.1	Electron avalanches	6
1.2.2	Streamer structure	6
1.2.3	Electrode configurations and breakdown fields	8
1.2.4	Distinction between negative and positive streamers	9
1.3	Modeling	10
1.4	Motivation & outline of thesis	11
2	Streamer fluid modelling - An overview of CStream	13
2.1	Fluid model	13
2.1.1	Physical model	13
2.1.2	Numerical method	18
2.1.3	Timestepping	20
2.2	Overview of refinement strategies and criteria	21
2.2.1	Overview	21
2.2.2	Size of the refined areas of the density grids	21
2.2.3	The $ \mathbf{E} $ criterium	23
2.2.4	The curvature criteria	24
2.2.5	FISHPACK refinement	24
2.2.6	Conclusion	25
2.3	CStream software	26
2.3.1	Basic overview and functionality	26
2.3.2	Handling the software, input and output	27

3	Probing photo-ionization: Simulations of positive streamers in varying $\text{N}_2:\text{O}_2$ mixtures	35
3.1	Introduction	35
3.1.1	Positive streamers in varying gases	35
3.1.2	Photo-ionization	36
3.1.3	Detachment from background ionization	37
3.1.4	Goal and organization of this chapter	37
3.2	Model	38
3.2.1	Structure of discharge model	38
3.2.2	Modeling the reactions, including electron detachment and photo-ionization	39
3.2.3	Electrode geometry, voltage and initial conditions	42
3.2.4	Numerical implementation	42
3.3	Simulations in air: photo-ionization versus background ionization	43
3.3.1	Either photo-ionization or background ionization	43
3.3.2	Combining photo-ionization and background ionization	46
3.3.3	Testing different photo-ionization models	46
3.3.4	Summary of results in air	47
3.4	Simulations in “pure” N_2	49
3.5	Comparison with experiments	54
3.5.1	Velocity, diameter and branching	54
3.5.2	Feather-like structures	55
3.6	Conclusion	57
4	Feather-like structures	61
4.1	Introduction	61
4.1.1	Positive streamers	61
4.1.2	Effect of gas composition	62
4.2	Observations of Feather-Like Structures	62
4.3	Hypothesis on the Origin of Feathers	63
4.3.1	Hairs formed by avalanches	63
4.3.2	Effect of oxygen density on hair-formation	64
4.3.3	Distinction between hairs and branches	65
4.4	Numerical Simulations and Results	66
4.4.1	Simulation model	66
4.4.2	Effect of oxygen density	67
4.4.3	Estimating the number of hairs	69
4.5	Conclusions	69
5	Determining background ionization levels	71
5.1	Introduction	71
5.2	Electron attachment	71
5.3	Recombination reactions	72
5.4	Repetition of streamer paths	74

CONTENTS

5.4.1	Recombination and diffusion	74
5.4.2	Ionization profile after a single pulse	74
5.4.3	Ionization profile after repeated discharges	76
5.4.4	Comparison with experiments	77
5.5	Constant ionization sources	79
6	Effect of transport-data on streamer propagation	81
6.1	Calculation of transport-data	81
6.1.1	Monte Carlo methods	81
6.1.2	Boltzmann equation solvers	82
6.1.3	Distinction between bulk and flux coefficients	82
6.1.4	Transport-data used in this chapter	83
6.2	Effect of transport-data on positive streamers	85
6.3	Testing predictions for macroscopic streamer properties	88
6.3.1	Uniformly translating streamers	88
6.3.2	Relation between velocity, interior field, maximal field and radius	88
6.3.3	Electron density inside the streamer	89
6.3.4	Comparison between simulation and prediction	90
6.4	Conclusions	91
7	Conclusions	95
7.1	Streamers	95
7.2	Modeling of streamers	96
7.3	CStream simulation code	96
7.4	Background ionization as alternative to photo-ionization	97
7.5	Combining background- and photo-ionization	97
7.6	The effect of impurities	98
7.7	Feather-like structures	98
7.8	Estimating background ionization levels	99
7.9	Streamer path repetition	99
7.10	Effect of choice of transport data on streamer simulations	100
7.11	Comparison with analytical predictions	100
7.12	Applications and recommendations for future research	101
	Bibliography	103
	Summary	111
	Samenvatting	117
	Dankwoord	123

CHAPTER 1

Introduction

1.1 What are streamers?

Streamers are thin channels of ionized gas that play an important role in natural phenomena such as lightning and sprite discharges as well as in industrial applications such as lighting and gas cleaning.

A streamer is essentially a channel with high conductivity that is propagating through a medium with otherwise low to vanishing conductivity, such as air, in the presence of an electric field. The channel of the streamer is an electrically neutral plasma, with ionization densities going up to 10^{14} cm^{-3} in air at standard temperature and pressure (293 K, 1 bar). In the interior of the channel, the external electric field is largely screened.

At the tip of the streamer is the so-called streamer head. This region consists of a curved layer of space charge of either positive or negative polarity. This thin space charge layer screens the interior of the streamer channel from the external electric field while enhancing the external field in the area just in front of the head. The enhanced electric field, which can exceed 200 kV/cm [1], produces additional ionization that propagates the streamer forward.

The timescales in the streamer head are insufficient for the background gas to be heated considerably. Therefore, in a streamer, most of the electrical energy put into the system is transferred into ionization and into kinetic energy of the electrons in the head and while the electron energy increases, the temperature of the ions and neutral species remains almost unchanged, making a streamer a plasma that is far out of thermal equilibrium. In addition, the electron energy distribution function (EEDF) is far from its thermal equilibrium as well. Eventually, the kinetic energy of the electrons is converted into excitations of the gas molecules.

Under the right conditions, streamers may branch into separate channels, each with its own streamer head. Both channels can then continue to propagate on their own. Streamer branching is for a large part determined by the gas composition. For example, streamers

in high purity nitrogen branch more often than streamers in air. While the branching process can be accelerated by perturbations of the streamer [2], it also occurs without any such perturbations [3].

1.1.1 Streamers in nature

Sparks and lightning

The most basic example of a streamer in nature is as a precursor to a spark. When a sufficiently high voltage is applied to a non-ionized gas, a streamer can form to create a conductive channel. This channel can then heat up, leading to further ionization and thermal expansion which causes a drop of the resistance of the channel, allowing more current to flow through it. This stage is called a spark; it is clearly visible (and often audible depending on the size and intensity of the discharge). The preceding streamer phase is too short and produces significantly lower light emissions than the spark, which means that if a streamer is followed by a spark, it is often not visible to the naked eye. If the voltage is removed before a spark forms, the streamer may be seen by the naked eye in a dark room.

Streamers often occur in nature in atmospheric electricity. The most well known example of atmospheric electricity is lightning. Before the lightning stroke can be seen and heard, a conductive channel has to be created between the charged cloud and the earth. This channel is formed by a so-called lightning leader. The leader is a growing ionized channel, very similar to a streamer except for its larger size and the fact that thermal heating occurs in the leader channel, where typically no significant amount of heating takes place in the streamer channel. At the head of the leader, a cloud of streamers, called the streamer-corona, produces the ionization in the area through which the leader will be propagating.

Once a leader has connected with the other side of the system (in lightning, most commonly the earth or another cloud) or with another leader propagating in the opposite direction, a full conductive channel is formed between the charged and grounded electrodes in the system (the cloud and the ground) and current increases. In lightning, this "return stroke" lasts longer and produces far more light than the preceding streamer/leader phase, which is why the streamer/leader phase typically isn't seen. The current in the lightning channel causes rapid thermal expansion of the channel, which can be heard as the characteristic thunder.

Sprites & TLEs

In addition to lightning, streamers are a crucial component of electric discharges above thunderclouds. In the 1920s, C.T.R. Wilson predicted the occurrence of discharges above thunderclouds [4]. It wasn't until 1989 that such discharges were recorded photographically [5, 6]. These discharges were named sprites, after a character in Shakespeare's *A Midsummer Night's Dream*.

Sprites are large clusters of streamers that propagate in the upper atmosphere above thunderclouds. Sprite discharges originate from an ionization wave propagating down-

wards from the ionosphere and breaking up into thin channels, streamers [7]. Sprites typically occur a few milliseconds after a lightning strike, though the delay may be up to 100 ms [8, 9].

After the discovery of sprites, additional types of discharges were discovered in the atmosphere above thunderclouds. Collectively these discharges are referred to as transient luminous events or TLEs. The study of TLEs has become an active area of research in the field of atmospheric electricity.

1.1.2 Industrial applications of streamers

Streamers are efficient in transferring electrical energy into kinetic energy of the electrons and thereby creating a reactive plasma without affecting the temperature of the background gas. Therefore a streamer plasma can be used for various industrial applications.

Ignition of HID lamps

In the ignition of high-intensity discharge (HID) lamps, a streamer-discharge propagates between the electrodes of the lamp to form a conducting channel in the background gas, typically a noble gas at high pressure. After the initial high voltage pulse, the conductive channel is formed and current flows between the electrodes, allowing the lamp to be operated at a much lower voltage than the initial pulse.

One of the main challenges in the development of HID lamps is to lower the high voltage pulse required to ignite a cold lamp. An additional challenge comes from the fact that in a lamp that was recently used, the gas composition is different from a lamp that has been off for some time, since liquid components have vaporized. Since these vaporized components cause the ignition voltage to be significantly higher, the ignition behaves differently when a hot lamp is reignited. Finally, in some situations, the filamentary streamer channels do not take the shortest path between the two electrodes, but instead jump from the electrode to the dielectric boundary of the lamp, travel over the dielectric to the other side and then jump back to the other electrode [10]. Creating a highly reactive plasma on the dielectric material can damage it and this behavior is to be prevented.

Gas cleaning

Streamer plasmas are effective in removing various pollutants from gases, which can be applied to the cleaning of exhaust gases from factories as well as vehicle exhaust gases. In confined spaces with existing ventilation systems, such as tunnels, the polluted air can be pumped through a so-called corona reactor, which removes some of the pollutants from the gas [11, 12].

For the purpose of gas cleaning, a balance must be found between input energy, reduction of pollutant content and the volume of gas that can be treated per unit of time.

Biomedical applications & sterilization

The highly reactive streamer plasma can be used to sterilize medical equipment. Plasma treatment has proven to be very effective at reducing the number of bacteria in test samples [13]. Additionally, the application of a streamer plasma has a positive effect on the rate with which wounds heal [14]. When applied externally, the highly reactive species generated by the streamer transfer into the wound fluids, where they positively affect the healing process.

The main advantage of streamer plasmas for biomedical applications is the fact that streamers are far out of thermodynamic equilibrium, with high electron energy and density and therefore high chemical excitation and reaction rates, but without much gas heating. This means that streamers can be applied directly to unprotected skin without the risk of burning, as the gas that flows out of the plasma device onto the skin is near room temperature.

1.1.3 Streamer experiments & observations

Electrode configurations

Laboratory experiments on streamers are typically performed by setting up a pair of electrodes and applying a high voltage to one of the electrodes while grounding the other. The shape of the electrodes can be altered to alter streamer properties. Many experiments use a sharp tip on the charged electrode to locally enhance the electric field for streamer inception. An example of an electrode configuration is needle-plane, such as used by Briels *et al* and Nijdam *et al* [15], where the streamer develops from the charged needle and propagates towards the grounded plate.

The electrode configuration can also be influenced by the intended application of the research: A wire-cylinder configuration, with a charged wire in a cylinder, allows for a high streamer density in the gas, allowing for efficient production or destruction of specific species [16]. For research on lamp ignition, experiments by Sobota *et al* [10] were performed using a needle-needle configuration.

Observable quantities

Excited molecules in the gas where the streamer propagates emit photons that can be observed. These observed photons form the primary mode of measuring streamers. These observations can be done with a sensitive high-speed camera. Most of the excitation occurs at the tip of a propagating streamer. If these excited molecules emit light almost instantly, as in air and nitrogen, only the tip emits light. Since only the tip of a propagating streamer emits light, it is possible to measure the velocity of a streamer by using a short exposure time (less than the time that streamer needs to cross the gap between electrodes) and measuring the length of the visible streak left by the propagating streamer tip.

Observing streamer emissions can be difficult in certain gases. In argon, the decay time of the excited states is very long, which means that constructing a profile of the temporal

evolution of the streamer is difficult [15]. In oxygen, the total light emission is very low, making it hard to obtain a sufficient signal-to-noise ratio.

While camera observations are the most important form of streamer measurements, additional information can be obtained by measuring currents and emission spectra. In addition, active laser diagnostics may be used on discharges that can be easily repeated [17].

Scaling laws

Since the relative ionization density in streamers is low and electron-electron collisions don't play an important role, the amount of energy an electron can gain is determined by the time between collisions with neutral molecules of the background gas [18]. This determines the mean free path length of an electron, the average distance traveled before colliding with a neutral molecule. The mean free path length determines a characteristic length scale and many streamer properties scale with the mean free path length of the electrons. The mean free path length is inversely proportional to the number density of the background gas. If the temperature is kept constant, this means that the mean free path is inversely proportional to the pressure. So the characteristic length scale in streamer processes is inversely proportional to the pressure in an ideal gas.

This leads to a very useful scaling law for streamers: Increasing the pressure is equivalent to decreasing the length scales by the same factor. As a result, very large discharges such as sprites, that occur high in the atmosphere where the pressure is low, can be studied experimentally in the lab by scaling up the pressure. With air pressure at 80 km altitude, in the mesosphere, being 5 orders of magnitude lower than at sea level, a 20 km system can be reduced to a 20 cm lab setup at 100 mbar, as was done by Dubrovin *et al* [19].

The scaling law for streamers applies only when interactions are primarily 2-body reactions. At higher pressures, 3-body reactions (such as 3-body attachment) become increasingly relevant and the applicability of the scaling law is diminished.

Sprite observations

In nature, many occurrences of streamers are followed immediately by a much brighter discharge, such as the leader in lightning. Sprite discharges are an exception, as they consist purely of streamers without a leader or return stroke. Since sprites appear above thunderclouds, they are difficult to observe directly from the ground, as the observer needs to be far enough away from the sprite to be able to see the area above the thundercloud. Nevertheless, various ground-based sprite observations have been done [20, 21]. Alternatively, balloons, aircraft and satellites can be used to obtain a more favorable point of view for sprite observations [6, 22, 23].

The scaling laws for streamers allow sprites to be studied in the lab. This has been done not only for streamers and sprite in the Earth atmosphere, but also in gas-mixtures resembling the atmospheres of Venus, Jupiter and Saturn [19]. These observations can be used to make predictions for the occurrence of sprites on these planets and also to provide the relevant spectra to which detection devices on upcoming satellite missions should be tuned.

1.2 Streamer theory

1.2.1 Electron avalanches

When an electron is placed in an electric field, it gains energy as it is being accelerated. While moving in a background gas, this kinetic energy can be lost in inelastic collisions with neutral molecules. If the electron has sufficient energy, such a collision can result in the excitation of the heavy particle or even ionization, where an electron is removed from the heavy particle via the following reaction:



where M denotes any molecule. In such an impact ionization event, the number of free electrons increases. In a low electric field, electrons will lose most of their energy through collisions with heavy particles before obtaining sufficient energy to ionize a molecule (15.58 eV for N_2 and 12.07 eV for O_2). If a sufficiently high electric field is applied, the electrons will be accelerated sufficiently between collisions to obtain these ionization energies and a so-called electron avalanche can start. In an electron avalanche, the number of electrons is multiplied through repeated impact ionization events.

While electrons move easily under the influence of an electric field, most ions are 4 or more orders of magnitude heavier and will therefore undergo almost no acceleration due to the electric field. Consequently, the electrons formed in an electron avalanche move against the electric field while the ions remain mostly stationary on the time scales involved. This process leads to charge separation: the spatial distribution of negative charge (primarily electrons, but potentially also negative ions) and of positive charge (positive ions) are not equal. This charge separation, depicted schematically in figure 1.1, leads to the appearance of space charges that will generate an additional electric field, enhancing or reducing the background field. In the region of this enhanced electric field, electrons are accelerated more than in areas where the field is lower, leading to higher ionization rates in the area with the enhanced field, which reinforces the formation of space charges in this area.

1.2.2 Streamer structure

A streamer is a thin, filamentary structure that is a result of the process described above. The streamer consists of the streamer head, a curved, thin layer of space charge, trailed by the streamer channel, an electrically neutral, but highly ionized region. A streamer propagates under the influence of an external electric field, but in the region in front of the streamer head, the background field is strongly enhanced by the space charge layer in the streamer head (the field can exceed 200 kV/cm in air at standard temperature and pressure). This results in high ionization rates in the area in front of the streamer head and the high electric field will separate these newly freed electrons from the positive ions, thereby pushing the front of the streamer forward.

We distinguish between positive and negative streamers, where the sign is determined by the charge of the head. In negative streamers, the streamer head is negatively charged and the streamer propagates in the same direction as the electron drift. The electric

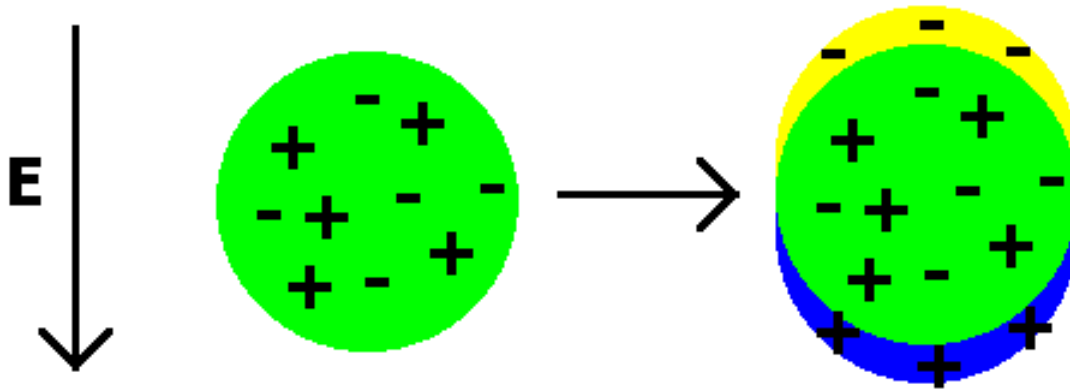


Figure 1.1: Schematic depiction of charge separation. The circle on the left represents an initially neutral seed of charged particles (in streamers, these are electrons and positive ions). A downward pointing electric field is applied resulting in the situation on the right-hand side, with the positive charges shifted towards the bottom and the negative charges towards the top, while the center area remains neutral.

field pushes the electrons forward, while leaving the positive ions behind, resulting in a forward moving negative charge layer. In a positive streamer, the streamer head is positively charged and the streamer propagates against the electron drift. Electrons are drawn from the region in front of the streamer head into the streamer channel, leaving behind a net positive charge. The differences between positive and negative streamers are further discussed in section 1.2.4.

The streamer channel is the region behind the streamer head. The channel is highly ionized, with ionization densities of up to 10^{14} cm^{-3} (in air at standard temperature and pressure) as well as electrically neutral. The channel therefore has a high electrical conductivity, which means that the electric field in the streamer channel is low. Here, the space charge in the streamer head as well as the space charge on the edge of the streamer channel help to screen the interior of the channel from the external electric field. Figure 1.2, taken from [24], shows the general shape as well as the various parts of a typical positive streamer.

The filamentary nature of the streamer makes it a system that encompasses many relevant lengthscales. A positive streamer in air at standard temperature and pressure may have a propagation length of several centimeters, while the width of the space charge layer is on a micrometer scale. Nevertheless, the small scale dynamics of the space charge layer determine the large scale properties of the entire streamer. Similarly for sprites, while the entire sprite can be tens of kilometers in size, processes on the scale of meters govern the large scale dynamics.

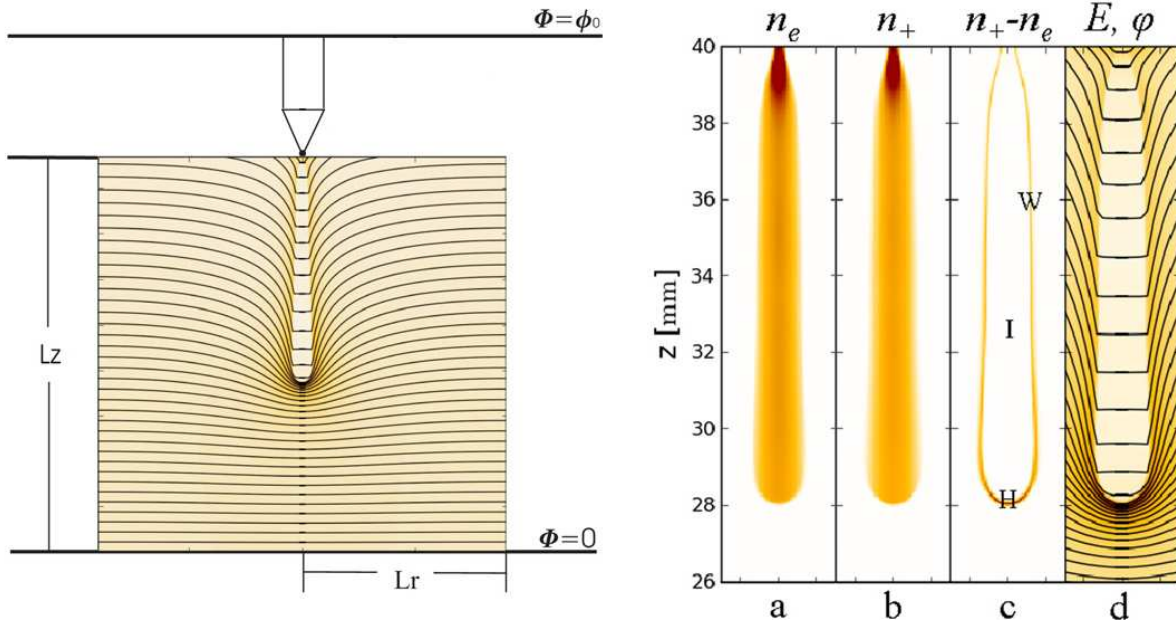


Figure 1.2: Simulation of positive streamer in air showing the various parts of the streamer structure. Full domain is shown in the left panel, panel a and b show electron and positive ion density respectively. Panel c shows the net charge density and marks the different parts of the streamer: H - streamer head, W - channel wall, I - streamer interior. Panel d shows the electric field strength (colour coded) and equipotential lines. Figure taken from [24].

1.2.3 Electrode configurations and breakdown fields

The configuration of the electrodes that generate the external electric field in which the streamer propagates has an influence on the inception of the streamer. Since electrons need a certain minimum energy to ionize neutral molecules, the electric field needs to be high enough. If the field is too low, electrons will not accelerate sufficiently between collisions to obtain the energy required for ionization. In addition, in gases that contain an electronegative admixture, such as oxygen, electrons can be lost due to attachment. The electric field strength above which there is a net growth in ionization density, i.e. where the ionization rate is larger than the attachment rate, is called the “breakdown field” or “critical field”. The value of this field strength depends on the gas. In air, at standard temperature and pressure, it is 32 kV/cm [25].

Before the streamer structure is formed, the only field present is the external field. If a streamer is to form, it can only occur where the external field exceeds the critical field. In a simple electrode geometry, two parallel plates, one charged, one grounded, this means that the potential on the charged electrode needs to be so high that the field exceeds the critical field in the entire region between the plates. Therefore:

$$\phi_0 > dE_{cr} \quad (1.2)$$

with d the distance between the electrode plates and E_{cr} the critical field. This situation is not always desirable, as such a setup would result in electron avalanches to occur everywhere where there is some level of initial ionization in the form of electrons. We speak of an “overvolted gap” when the entire area between the two electrodes has a field above the critical field. Even if $E < E_{cr}$, streamer formation can still occur if there is a large enough initial seed, which, after charge separation, sufficiently enhances the electric field locally [26].

If the charged planar electrode is replaced by a needle, or if a needle is attached to a planar electrode, the field close to the tip of the needle will be much higher than that of a planar electrode with the same potential. Consequently, the potential on the needle electrode can be much lower while still having a field above the critical field in the area close to the tip of the needle. In this situation, electron avalanches will initially occur near the tip of the needle, where a streamer may form. As the streamer is formed, it propagates towards the grounded electrode and even though the external field may fall below the critical field in areas that the streamer propagates through, the enhanced field in front of the streamer head will still exceed the critical field, allowing for electron avalanches to occur close to the streamer head.

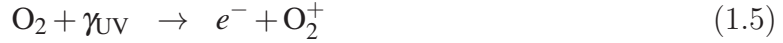
This makes a needle well suited for streamer generation, as it allows for the streamer to be started at a predetermined location (the tip of the needle) as well as requiring a lower potential to be applied. Streamers can occur in many electrode geometries other than the two mentioned above [16, 27]. However, the charged electrode should be shaped in such a way as to locally enhance the external electric field to ensure that an overvolted gap is not required.

1.2.4 Distinction between negative and positive streamers

Conceptually, negative streamers are the most straightforward; the streamer propagates in the same direction as the electron drift and the electrons that start avalanches in the area with the enhanced electric field are already flowing in from the streamer channel. In contrast, positive streamers propagate against the electron drift and the avalanches near the streamer head are initiated by the electrons that flow in from regions outside the active region with the enhanced electric field.

Because of this, positive streamers require some source of electrons in front of the streamer head in order to propagate. There are various possible mechanisms for these sources, for example a preexisting background density of electrons, but in $N_2:O_2$ mixtures, photo-ionization is the mechanism that is thought to be the primary source of these “seed electrons”. The photo-ionization mechanism in $N_2:O_2$ mixtures consists of an electron colliding with a nitrogen molecule and exciting it. The nitrogen molecule then falls back to a lower energy state and emits a photon. If this photon is in the UV range, with an energy of at least 13.62 eV, it can ionize an oxygen molecule elsewhere in the gas, creating

a free electron, which is then attracted by the positive charge of the streamer head.



Despite positive streamers propagating against the electron drift and requiring a source of electrons ahead of the streamer, positive streamers were found to emerge more easily than negative streamers as well as propagate at higher velocities. This was found both experimentally [28] and through simulations [1].

1.3 Modeling

Streamers are a strongly non-linear phenomenon and the various length scales involved in the formation and propagation of streamers make them difficult to model accurately. In general, two main approaches are used for the modeling: particle models and fluid models.

Particle models, or more precisely: Particle-In-Cell with Monte Carlo Collisions (PIC-MCC) models, model the motion of single electrons as they move through the electric field. Monte Carlo techniques are used at each timestep to randomly decide whether an electron undergoes a collision with a heavy particle and what the result of this collision is, based on cross section data for the various collision processes. After the particle positions have been updated, they are mapped onto a grid for the purpose of computation of the charge density distribution, which is then used as a source term for the Poisson equation that determines the electric field for the next timestep.

A fluid model, on the other hand, does away with discrete particles and approximates the particle distribution by a density function. From the Boltzmann equation, a set of conservation equations can be derived that govern the change of this density function. From the density functions of the various charged particles, a charge density function can be computed which can be used to obtain the electric field. Together, the equations of a fluid model form a coupled set of partial differential equations. In a simulation, this set of PDEs is discretized in space and time and solved with numerical methods. Examples of fluid models for streamer simulations are [29–31].

The main advantage of a particle model is that it is able to follow the full physics of the streamer. Since electrons are treated as discrete particles, the interactions of each electron are calculated separately. This also allows for stochastic effects to be fully explored. The downside of this is that as the streamer grows, the number of electrons grows along with it and a pure particle model will not be able to follow the streamer much beyond its initial inception due to memory constraints (particle counts higher than 10^7 become increasingly difficult on current computers). In addition, the larger the number of particles in the model, the longer each computational timestep takes.

Some approaches have been used to overcome this limitation, primarily the use of superparticles, a technique in which a single computational particle represents a large number of physical particles [32]. Especially in areas where the electric field is low (inside the streamer channel for example), this approach is justified. The precise implementation

of the superparticle method can vary on a number of points such as the amount of particles represented by a single superparticle and the conditions under which the simulation will merge particles and the method used in this merger.

Fluid models do not share the limitation of particle count as particle distributions are represented as a density. Consequently, a computational fluid model can describe streamers that are significantly longer than those realizable by particle models. However, fluid models are very limited in the physics that can typically be included. In addition, in a standard fluid model, no stochastic effects are present. In situations where the electron density is very low, the approach of a fluid model may fail as the electrons can no longer be realistically represented as a continuous density function. For example, during streamer inception, the initial amount of electrons is very low. A fluid model will not be able to accurately represent the inception process. However, it is a useful means to investigate streamer propagation, as done in this thesis.

Due to the large gap in relevant length scales involved, as discussed in section 1.2.2, a single grid is either insufficient to accurately resolve the small scale features of the streamer or it has too many cells to be computationally efficient. A technique to bridge the need for high spatial resolution and the desire to reduce the number of grid cells is adaptive mesh refinement (AMR). With AMR, a fine grid is used where spatial resolution is required, while everywhere else a coarse grid is used. Since the area that requires high spatial resolution changes with time as the streamer propagates, the grid structure has to be remade regularly.

1.4 Motivation & outline of thesis

The main subject of this thesis is captured in its title: The propagation mechanics of positive streamers. This subject was inspired by the experimental observations [15] that positive streamers still propagate in high purity nitrogen, where one would naively expect to not see any streamers once the oxygen concentration in the nitrogen-oxygen mixture has been sufficiently reduced, as the photo-ionization mechanism, that is assumed to be the source of free electrons in front of a positive streamer, is orders of magnitude less effective in high purity nitrogen than it is in air. Therefore, we have studied the effect of the magnitude and nature of the source of free electrons on the propagation of positive streamers.

In chapter 2 we describe the fluid model and simulation code used for our simulations. This code was originally written by Alejandro Luque [1] based on the work of Carolynne Montijn [33] and adapted for the purpose of the research topics discussed in this thesis. Chapter 2 also serves as a documentation for new users that want to start using this simulation code, detailing the use of the code, input parameters and output files.

Chapter 3 introduces detachment of electrons from background ionization as an alternative source of free electrons. The effect of the level of background ionization on streamer propagation is studied and compared to the effect of photo-ionization. This chapter was originally published in [34].

In nitrogen with low concentration of oxygen, streamers were found to exhibit a feath-

erlike structure which is absent in streamers in air, which are very smooth. In chapter 4 we discuss the experimental observations of these featherlike structures and propose a theoretical explanation for their appearance. This chapter was originally published in [35].

The primary source of high levels of background ionization in streamer discharges is the leftover ionization from the previous discharge(s) in setups with repetitive discharges. The effect of the repetition frequency on the level of background ionization is discussed in chapter 5. Additionally, we study the decay of the ionized streamer channel after a discharge to predict whether streamers follow the same path in repetitive discharges. The results in this chapter were published as a part of [36].

We have extended the streamer simulation code to use field-dependent transport coefficients. We discuss the effect of these coefficients in chapter 6 and compare simulation results to analytical predictions for macroscopic streamer properties.

Streamer fluid modelling - An overview of CStream

2.1 Fluid model

2.1.1 Physical model

Drift-diffusion-reaction equations

In a fluid model of a streamer, we replace the individual particles in the system by a density function $n(\mathbf{r}, t)$. The temporal evolution of this density function is governed by the physical processes of the system and this model takes the form of a set of partial differential equations (PDEs). The derivation of this so-called classical streamer model starts from the continuity equation. For particle species i , we have:

$$\frac{\partial n_i(\mathbf{r}, t)}{\partial t} + \nabla \cdot \mathbf{j}_i(\mathbf{r}, t) = S_i(\mathbf{r}, t). \quad (2.1)$$

Here $S_i(\mathbf{r}, t)$ represents the total of all sources and sinks of species i . $\mathbf{j}_i(\mathbf{r}, t)$ is the term for the particle current density of species i . Particles can drift and diffuse as described by the following expression for the particle current density \mathbf{j}_i :

$$\mathbf{j}_i(\mathbf{r}, t) = \mu_i n_i(\mathbf{r}, t) \mathbf{E}(\mathbf{r}, t) - D_i \nabla n_i(\mathbf{r}, t). \quad (2.2)$$

In equation 2.2, the first term represents the particle drift due to the electric field, with μ_i the mobility coefficient of species i . The second term represents the diffusion of particles due to the spatial gradient in particle densities with diffusion coefficient D_i . These equations can be derived from the Boltzmann equation [37, 38]. On the timescales involved, we consider only electrons to be mobile, while ions and neutrals remain stationary, which means that for heavy species, equation 2.1 is reduced to

$$\frac{\partial n_i(\mathbf{r}, t)}{\partial t} = S_i(\mathbf{r}, t). \quad (2.3)$$

The sources and sinks in equation 2.1 play a very important role in the dynamics of the streamer. In this model, the sources and sinks correspond to reactions between the different charged and neutral species present in the gas. The source term due to a single reaction is the product of the densities of the species involved in the reaction and the field-dependent rate coefficient for that reaction.

As an example, the impact ionization reaction



is modeled by

$$S_{\text{ionization}} = k_{\text{ion}}(|\mathbf{E}|)n_e[\text{N}_2]. \quad (2.5)$$

Here n_e is the local electron density, $[\text{N}_2]$ the density of N_2 and k_{ion} the reaction coefficient for impact ionization depending on the magnitude of the local electric field. The value of k can be determined in different ways, from experiments, theoretical calculations or simulations. The traditional approximation suggested by Townsend uses an empirical expression for the impact ionization term [38]:

$$\frac{dn_e}{dt} = n_e\mu_e|\mathbf{E}|\alpha_0e^{-E_0/|\mathbf{E}|}, \quad (2.6)$$

where μ_e is the electron mobility coefficient, \mathbf{E} is the local electric field and α_0 and E_0 are parameters that can be determined by fitting experimental data. In gases that contain an electronegative admixture, such as O_2 , the process of attachment can provide a sink for the electron density through the following reactions:



The first attachment process is dissociative attachment, the second an example of 3-body attachment (3-body attachment can also occur with an oxygen and nitrogen molecule). In the case of the 3-body attachment in equation 2.8, the reaction rate scales with the square of the oxygen density:

$$S_{3\text{-body-att}} = k_{3\text{-body-att}}(|\mathbf{E}|)n_e[\text{O}_2]^2. \quad (2.9)$$

Further ionization losses can occur via one or more recombination processes, but these typically have a timescale that is much longer than the timescale of streamer development and propagation and are therefore primarily interesting for the evolution of the charge density after a streamer discharge, as discussed in chapter 5. In gases with attachment, detachment may occur, resulting in an additional source of electrons. In gases that contain both nitrogen and oxygen, the photo-ionization process provides a non-local source of electrons. Since photo-ionization is non-local, it can't be modelled by simple reaction equations such as the ones for impact ionization. Instead, the local contribution of photo-ionization is calculated by spatially integrating contributions from the entire domain. The commonly used model for photo-ionization and the approximations made to make this model suitable for simulation are discussed in section 3.2.2.

The reaction model for streamer simulations can be very minimal or very extended, with many species and reactions, including metastables and various excited states. The complexity of the reaction model depends on the purpose of the simulations. For negative streamers in nitrogen, a model containing no more than 3 species (e^- , N_2 and N_2^+) and 1 reaction (impact ionization, equation 2.4) is sufficient to simulate the dynamics of the streamer head [33]. For more detailed studies of the streamer chemistry, the reaction model should be as complete as possible.

Electric potential and field

The streamer evolves under the influence of an electric field, which consists of an externally applied electric field and the electric field generated by space charges. These space charges are present at the head of the streamer as well as on the edge of the streamer channel. For the further propagation of the streamer, the enhanced electric field in front of the streamer, generated by the space charge in the streamer head is essential. We compute the net charge density $q(\mathbf{r}, t)$:

$$q(\mathbf{r}, t) = e \sum_i q_i n_i(\mathbf{r}, t), \quad (2.10)$$

where for species i , n_i denotes the density function of these species and q_i the charge of a particle in units of the electron charge e . From this we compute the potential by solving the Poisson equation

$$\nabla^2 \phi(\mathbf{r}, t) = \frac{q(\mathbf{r}, t)}{\epsilon_0} \quad (2.11)$$

and the electric field

$$\mathbf{E}(\mathbf{r}, t) = -\nabla \phi(\mathbf{r}, t). \quad (2.12)$$

Rescaling to dimensionless units

The classical fluid model for streamers can be rescaled to dimensionless units and it is with these units that the code used in this thesis works. From the Townsend approximation for ionization, equation 2.6, a characteristic field and length scale emerges: E_0 and $l_0 = \alpha_0^{-1}$ respectively. The characteristic velocity follows from the drift velocity of electrons in the characteristic field, E_0 : $v_0 = \mu_e E_0$. The characteristic time scale then follows as $t_0 = \frac{l_0}{v_0}$. The characteristic number density follows from the Poisson equation: $n_0 = \frac{\epsilon_0 E_0}{e l_0}$. And we have the characteristic diffusion $D_0 = \frac{l_0^2}{t_0}$. Values for α_0 , E_0 and μ_e were obtained from [39] and are at standard temperature and pressure:

$$\alpha_0 \simeq 4332 \text{ cm}^{-1} \quad (2.13)$$

$$E_0 \simeq 2 \times 10^5 \text{ Vcm}^{-1} \quad (2.14)$$

$$\mu_e \simeq 380 \text{ cm}^2 \text{V}^{-1} \text{s}^{-1}. \quad (2.15)$$

When we insert these values in the characteristic scales, we obtain the values with which to rescale the equations:

$$l_0 \simeq 2.3 \mu\text{m} \quad (2.16)$$

$$t_0 \simeq 3.0 \times 10^{-12} \text{ s} \quad (2.17)$$

$$n_0 \simeq 4.7 \times 10^{14} \text{ cm}^{-3} \quad (2.18)$$

$$D_0 \simeq 1.8 \times 10^4 \text{ cm}^2\text{s}^{-1}. \quad (2.19)$$

We can now make the appropriate substitutions ($t^d = t/t_0$ and similarly for the other variables; the superscript d will be used to indicate that a variable is in dimensionless form, where this isn't clear from the context. For clarity of reading, the d will be omitted where it is clear that variables are dimensionless) to obtain the classical fluid equations in dimensionless form:

$$\partial_t + \nabla \cdot \mathbf{j}_i = S_i, \quad (2.20)$$

where t is the dimensionless time, \mathbf{j}_i the dimensionless particle density current for species i and S_i the dimensionless source term for species i . S_i is obtained by rewriting reaction equations such as equation 2.5 in dimensionless form, where we remark that all rate-coefficients should also be rescaled. The particle density current \mathbf{j}_i is obtained by rescaling equation 2.2:

$$\mathbf{j}_i = -\mu_i n_i \mathbf{E} - D_i \nabla n_i, \quad (2.21)$$

where \mathbf{E} is the dimensionless electric field and n_i , D_i and μ_i are the dimensionless particle density, diffusion coefficient and mobility respectively of species i . With the electron mobility from equation 2.15, we find that in dimensionless units μ_i is equal to 1 while for heavy particles μ_i is taken as 0, since heavy particles are assumed to be stationary in this model. Equation 2.21 can therefore be simplified to

$$\mathbf{j}_e = -n_e \mathbf{E} - D_e \nabla n_e \quad (2.22)$$

for electrons and

$$\mathbf{j}_i = 0 \quad (2.23)$$

for heavy particles. The expression for the charge density q , equation 2.10, is rescaled to

$$q(\mathbf{r}, t) = \sum_i q_i n_i(\mathbf{r}, t), \quad (2.24)$$

The Poisson equation, equation 2.11 is rescaled to

$$\nabla^2 \phi = q. \quad (2.25)$$

We remark that although the code used in this thesis internally works with the dimensionless equations and variables described in this section, all results are presented in regular units unless otherwise noted. Input parameters for the simulation code are expected to be in dimensionless units. Finally we note that the rescaling to dimensionless units doesn't change the structure of the equations, it is merely a rescaling to a different set of units, where the dimensionless units yield a set of equations where some constants (such as e , ϵ_0 , μ_e) become unity.

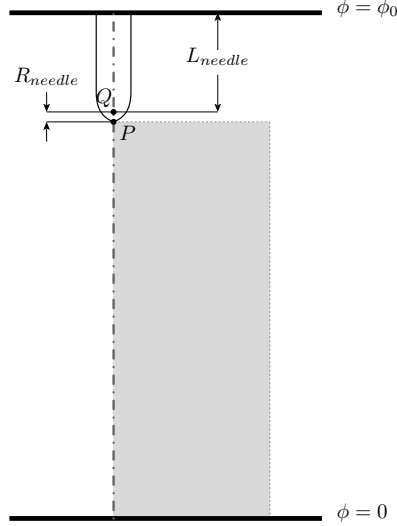


Figure 2.1: Schematic of the computational setup. The shaded rectangle represents the computational domain for the fluid equations, the thick horizontal lines the 2 planar electrodes with the needle and its parameters depicted at the anode. The area between the two planar electrodes is the computational domain for the Poisson equation. The needle is simulated by a single point charge, Q , chosen such that $\phi = \phi_0$ in the point P , which is the tip of the needle. The particle densities are calculated only in the shaded area below the electrode. The calculation assumes cylindrical symmetry around the needle axis represented by the dashed-dotted line.

Boundary and initial conditions

We consider a cylindrical computational domain with coordinates:

$$(r, z, \theta) \in (0, L_r) \times (0, L_z) \times (0, 2\pi). \quad (2.26)$$

Although the code used in this thesis is capable of performing full 3D calculations, we assume cylindrical symmetry to greatly simplify the computations to 2 dimensions. For any spatially dependent function $f(r, z, \theta)$, we assume: $\partial_\theta f(r, z, \theta) = 0$. Consequently, the coordinate system for our computations is limited to $(0, L_r) \times (0, L_z)$. We consider a setup with a powered electrode at $z = L_z$ and a grounded electrode at $z = 0$. If the powered electrode is a plate, the following boundary conditions are used for the electric potential $\phi(r, z, t)$:

$$\forall z \partial_r \phi(0, z, t) = 0 \quad (2.27)$$

$$\forall r \phi(r, 0, t) = 0 \quad (2.28)$$

$$\forall z \phi(L_r, z, t) = \frac{\phi_0 z}{L_z} \quad (2.29)$$

$$\forall r \phi(r, L_z, t) = \phi_0 \quad (2.30)$$

with ϕ_0 the potential applied to the powered electrode. If the powered electrode is a needle protruding from a plate, the needle has the same potential ϕ_0 as the plate.

For the density equations, we use homogeneous Neumann conditions on all edges:

$$\partial_r n|_{r=0} = \partial_r n|_{r=L_r} = \partial_z n|_{z=0} = \partial_z n|_{z=L_z} = 0, \quad (2.31)$$

where we remark that if the powered electrode is a needle, the computational domain for the density equations is smaller than the computational domain for the Poisson equation and the L_z values for both domains are not equal. This difference is a requirement of the numerical implementation of the needle electrode and is further detailed in section 2.3.2. See figure 2.1 for a schematic depiction of this setup.

While the boundary conditions mentioned above are the ones used in this thesis, the code that was used can also handle different choices of boundary conditions: both homogeneous Neumann and homogeneous Dirichlet boundary conditions are available for the top ($z = L_z$), bottom ($z = 0$) and right ($r = L_r$) edges of the domain for both the densities and the potential. The Neumann condition on the central axis of the cylindrical domain is required for symmetry reasons.

As initial conditions for particle densities, two types of seeds are implemented in the code. A homogeneous seed, with a constant density over the entire domain and a Gaussian seed of the form

$$n(r, z, 0) = n_{max} \exp\left(-\frac{r^2 + (z - z_0)^2}{\sigma^2}\right). \quad (2.32)$$

Here z_0 specifies the z -coordinate of the maximum of the seed (which is located on the symmetry axis with $r = 0$), where the density is n_{max} . σ is a measure of the radius of the seed, it is the distance at which the density drops to e^{-1} of the maximum value.

In typical streamer simulations, a seed of electrons and positive ions is placed at the tip of the needle to initiate the discharge. Other than these Gaussian seeds and the neutral background gas, initial particle densities are zero with the possible exception of added background ionization, a homogenous density of negative and positive ions. The initial distribution of electrons and ions is charge neutral at every point of the domain.

2.1.2 Numerical method

The physical equations in section 2.1 are to be solved numerically. The computational code we have used for this uses finite volume methods to solve a discretized version of the physical equations. Here we give a basic summary of the numerical technique used. For more details, the reader is referred to the work of Montijn *et al* [33], upon which the current code is based.

Discretization of density equations

The continuity equations 2.20 and 2.21 are discretized using finite volume methods and solved on a uniform rectangular grid with cells:

$$C_{ij} = [(i-1)\Delta r, i\Delta r] \times [(j-1)\Delta z, j\Delta z] \left(i = 1, \dots, \frac{L_r}{\Delta r}, j = 1, \dots, \frac{L_z}{\Delta z} \right), \quad (2.33)$$

where L_r and L_z are the r - and z -dimensions of the grid and Δr and Δz the size of a cell in r and z direction respectively. Particle density distributions are represented by their value in the cell center, which can be seen as an average over the cell. For some species n , we use $n_{i,j}$ to denote the density at the center of cell C_{ij} . For sake of clarity of notation we omit the superscript d indicating that variables are in dimensionless units.

The discretized continuity equations in cylindrical coordinates, with cylindrical symmetry ($\partial_\theta f = 0$) assumed, have the following form:

$$\begin{aligned} \frac{dn_{i,j}}{dt} = & \frac{1}{r_i \Delta r} \left(r_{i-\frac{1}{2}} F_{i-\frac{1}{2},j}^a - r_{i+\frac{1}{2}} F_{i+\frac{1}{2},j}^a + r_{i-\frac{1}{2}} F_{i-\frac{1}{2},j}^d - r_{i+\frac{1}{2}} F_{i+\frac{1}{2},j}^d \right) \\ & + \frac{1}{\Delta z} \left(F_{i,j-\frac{1}{2}}^a - F_{i,j+\frac{1}{2}}^a + F_{i,j-\frac{1}{2}}^d - F_{i,j+\frac{1}{2}}^d \right) + S_{i,j}. \end{aligned} \quad (2.34)$$

Here F^a and F^d represent the advective and diffusive fluxes across the cell boundaries. Since we assume ions and neutral particles to be stationary, these terms are non-zero only for electrons. For heavy particles, only the source term S_{ij} remains.

The advective flux, F^a uses an upwind scheme with flux limiting and is defined as follows:

$$\begin{aligned} F_{i+\frac{1}{2},j}^a = & E_{r, i+\frac{1}{2},j}^+ \left[n_{i,j} + \psi(P_{i,j})(n_{i+1,j} - n_{i,j}) \right] \\ & E_{r, i+\frac{1}{2},j}^- \left[n_{i+1,j} + \psi\left(\frac{1}{P_{i+1,j}}\right)(n_{i,j} - n_{i+1,j}) \right] \end{aligned} \quad (2.35)$$

$$\begin{aligned} F_{i,j+\frac{1}{2}}^a = & E_{z, i,j+\frac{1}{2}}^+ \left[n_{i,j} + \psi(Q_{i,j})(n_{i,j+1} - n_{i,j}) \right] \\ & E_{z, i,j+\frac{1}{2}}^- \left[n_{i,j+1} + \psi\left(\frac{1}{Q_{i,j+1}}\right)(n_{i,j} - n_{i,j+1}) \right], \end{aligned} \quad (2.36)$$

where $E^+ = \max(-E, 0)$ and $E^- = \min(-E, 0)$ are used to distinguish the upwind directions for the components of the electric field, E_r and E_z , and we have

$$P_{i,j} = \frac{n_{i,j} - n_{i-1,j}}{n_{i+1,j} - n_{i,j}} \quad (2.37)$$

$$Q_{i,j} = \frac{n_{i,j} - n_{i,j-1}}{n_{i,j+1} - n_{i,j}}. \quad (2.38)$$

ψ is the Koren limiter function:

$$\psi(x) = \max(0, \min(1, \frac{1}{3} + \frac{x}{6}, x)). \quad (2.39)$$

The diffusive flux F^d is calculated using a second-order central differences scheme:

$$F_{i+\frac{1}{2},j}^d = \frac{D}{\Delta r} (n_{i,j} - n_{i+1,j}) \quad (2.40)$$

$$F_{i,j+\frac{1}{2}}^d = \frac{D}{\Delta z} (n_{i,j} - n_{i,j+1}) \quad (2.41)$$

and the reaction term $S_{i,j}$ is computed as

$$S_{i,j} = \sum_{A \in \text{reactions}} \left[k_A(|\mathbf{E}|_{i,j}) \prod_{s \in \text{Spec}(A)} n_{s;i,j} \right] \quad (2.42)$$

where k_A denotes the field-dependent reaction rate coefficient of reaction A and $\text{Spec}(A)$ the set of species that appear as an input for reaction A .

Discretization of the Poisson equation

We compute the net charge $q_{i,j}$ in a cell center by adding up the contributions from the individual charged species:

$$q_{i,j} = \sum_{s \in \text{species}} n_{s;i,j} q_s. \quad (2.43)$$

With this net charge, the electric potential ϕ can be computed in the cell centers through a second-order central approximation of the dimensionless Poisson equation 2.25:

$$q_{i,j} = \frac{\phi_{i+1,j} - 2\phi_{i,j} + \phi_{i-1,j}}{\Delta r^2} + \frac{\phi_{i+1,j} - \phi_{i-1,j}}{2r_{i,j}\Delta r} + \frac{\phi_{i,j+1} - 2\phi_{i,j} + \phi_{i,j-1}}{\Delta z^2}. \quad (2.44)$$

From the potential we can compute the components of the electric field from $\mathbf{E} = -\nabla\phi$ in the cell boundaries:

$$E_{r; i+\frac{1}{2},j} = \frac{\phi_{i,j} - \phi_{i+1,j}}{\Delta r} \quad (2.45)$$

$$E_{z; i,j+\frac{1}{2}} = \frac{\phi_{i,j} - \phi_{i,j+1}}{\Delta r}. \quad (2.46)$$

The electric field strength is determined at the cell center, so we have to compute the field components in the center by averaging the values on the boundaries after which we can compute the field strength:

$$|\mathbf{E}|_{i,j} = \sqrt{\left(\frac{E_{r;i-\frac{1}{2},j} + E_{r;i+\frac{1}{2},j}}{2} \right)^2 + \left(\frac{E_{z;i,j-\frac{1}{2}} + E_{z;i,j+\frac{1}{2}}}{2} \right)^2}. \quad (2.47)$$

2.1.3 Timestepping

The code uses the explicit trapezoidal rule, a second order Runge-Kutta method, for the temporal discretization with timestep Δt . Given some timestep $t_i = i\Delta t$, density distributions $\mathbf{n}_i(r, z) = \mathbf{n}(r, z, t_i)$ and electric field $\mathbf{E}_i(r, z) = \mathbf{E}(r, z, t_i)$, the densities and field at the next timestep, t_{i+1} are calculated by first computing an intermediate result for the densities:

$$\bar{\mathbf{n}}_{i+1} = \mathbf{n}_i + \Delta t F(\mathbf{n}_i, \mathbf{E}_i). \quad (2.48)$$

Using these intermediate densities, the potential can be computed by solving the Poisson equation, after which we obtain the intermediate electric field $\bar{\mathbf{E}}_{i+1}$. With this, we compute the final values of the densities at t_{i+1} :

$$\mathbf{n}_{i+1} = \mathbf{n}_i + \frac{\Delta t}{2} F(\mathbf{n}_i, \mathbf{E}_i) + \frac{\Delta t}{2} F(\bar{\mathbf{n}}_{i+1}, \bar{\mathbf{E}}_{i+1}). \quad (2.49)$$

Finally, we again compute the potential and electric field, now using the final values of the densities.

The size of the timestep Δt is determined by using a Courant-Friederichs-Levy (CFL) restriction for stability of the advection part of the equations:

$$\max E_r \frac{\Delta t}{\Delta r} + \max E_z \frac{\Delta t}{\Delta z} < v_a. \quad (2.50)$$

There are additional restrictions from other diffusion and reaction parts of the equations, but they are dominated by the CFL criterium for the advection part [33]. The value of v_a is typically set to 0.25, which is well below the maximum required for stability [40].

2.2 Overview of refinement strategies and criteria

2.2.1 Overview

The CStream simulation code contains functions for adaptive grid refinement (also known as adaptive mesh refinement or AMR). Since streamers span different length scales, there is a need to simulate relatively large physical domains while still having high spatial resolution in areas such as the streamer head. To ensure that such large domains can be simulated without giving up resolution and accuracy, the numerical grid is refined adaptively at each timestep. The equations are solved on a coarse grid, after which the solution is analyzed using refinement criteria to determine the areas where refinement is needed. The equations are then solved on the refined subgrids after which the process is iterated. Boundary conditions for the finer grids are obtained through interpolation of the solution on the coarser grid. Grid-generation and refinement are performed separately for the density equations and for the Poisson equation.

There are three main refinement criteria. The first two concern refinement of the density-grids: Refinement based on the absolute value of \mathbf{E} and refinement based on the curvature of densities (both charge density and particle density). The grids used by the FISHPACK solver use their own refinement scheme where the decision to refine is made if the difference between the solution on a grid and the solution on a finer grid exceeds a threshold. The FISHPACK solver is used both for the Poisson equation that determines the electric potential of the system as well as for the Helmholtz equations for the photo-ionization reactions (the photo-ionization model and its translation to a set of Helmholtz equations is discussed in section 3.2.2).

2.2.2 Size of the refined areas of the density grids

All CDR (Convection-Diffusion-Reaction, CDR is the shorthand term for the density-part of the code) refinement criteria are on a per-point basis, which means that the question whether to refine or not is initially answered for every grid-cell. This is inconvenient for several reasons, primarily due to the computational cost of such a scheme. The regions containing the streamer head will almost always need to be refined, it is not necessary to evaluate this point by point in these regions.

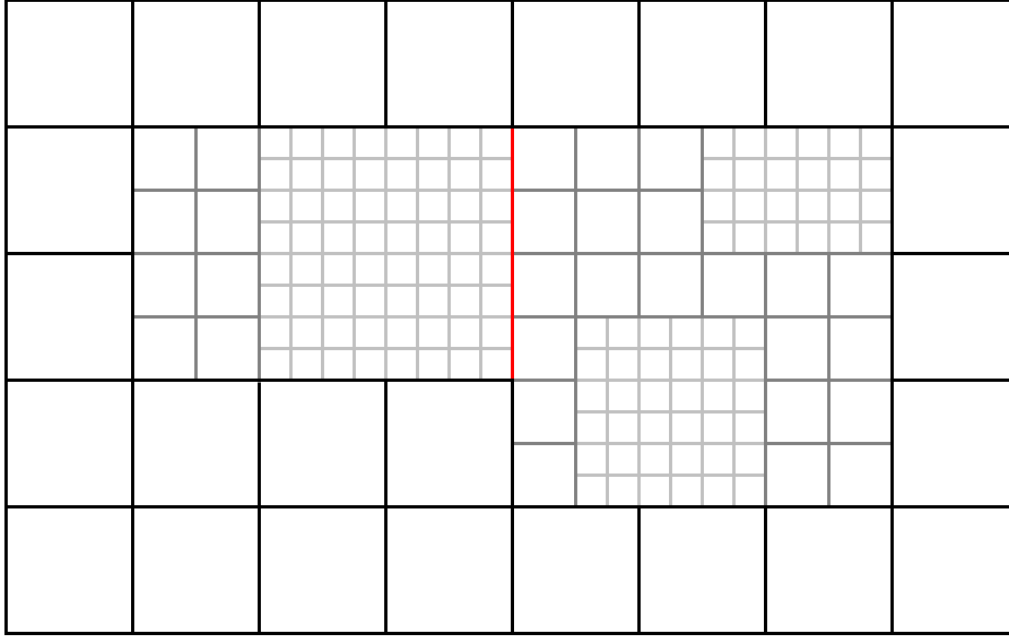


Figure 2.2: Schematic of a nested set of grids for the density equation. The black squares represent grid cells at the coarsest level (level 0), the dark gray cells are the first refined sublevel (level 1). Two rectangular grids are included at this level, their shared border is indicated by the red line. The light gray cells show grids at a further refined level (level 2).

To ease this problem, a minimal refinement area is defined by 2 parameters: `cdr_brick_dr` and `cdr_brick_dz`. The refinement module divides the grid it receives (this can be the coarsest grid covering the entire domain or a refined grid covering only part of the domain, the code and grid-structure are recursive) into "bricks" of these dimensions and searches each brick for cells that match the refinement criteria. Once such a cell is found, the entire brick containing that cell is refined.

For the **FISHPACK** module, a different approach is used. The refinement routine scans its input grid, starting at the top ($z = z_{min}$), going down per "line" (a set of cells with equal z coordinate). Once it finds a line with points that meet the refinement criterium it searches for the first line that does not contain any points that meet the criterium. It then refines the smallest rectangular area that contains all the points that meet the criterium. This process is repeated until the bottom ($z = z_{max}$) of the grid is reached.

The tree of grids for the density equations may contain refined grids that are adjacent to each other. A schematic showing the nested structure of refined density grids is shown

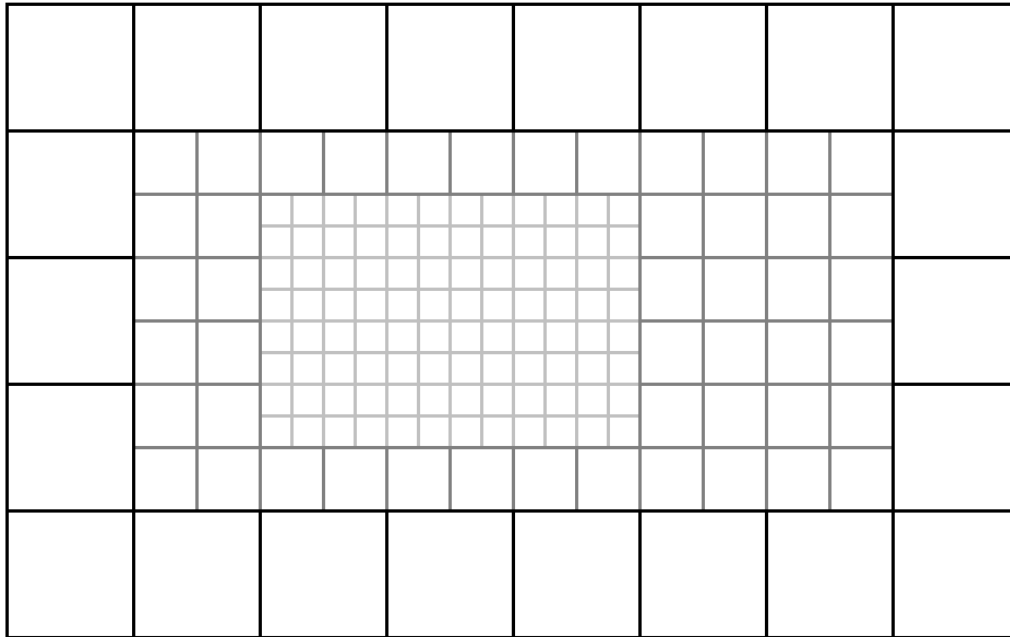


Figure 2.3: Schematic of a nested set of grids for the Poisson equation. The black grid is the coarsest level, the dark gray cells are the first refined sublevel, the light gray cells show grids at a further refined level. Each grid only has at most one subgrid.

in figure 2.2. The red line in this figure indicates the shared border between two subgrids. For the Poisson-grids, such a structure is not possible and a grid can have at most one refined child-grid as depicted in figure 2.3.

2.2.3 The $|\mathbf{E}|$ criterium

The electric field criterium is the most simple of the three refinement criteria. It is an empirical criterium that is not directly motivated by the underlying numerics. A cell with coordinates (r, z) qualifies for refinement if:

$$|\mathbf{E}(r, z)| > E_c \quad (2.51)$$

where E_c is the threshold electric field strength for refinement. E_c is a user-determined parameter that is provided in the input file for a run. Since this criterium is independent of the grid-level or the cell-size, once a cell meets the criterium at the coarsest level, it will also do so at every refined level. Because of this property, the user can limit the refinement-depth that is reached through this criterium with the `ref_level_eabs` input-parameter.

Setting `ref_level_eabs` to 1, for example, restricts the code from only refining from the coarsest level to the first refined level due to the $|\mathbf{E}|$ criterium.

The $|\mathbf{E}|$ criterium is inflexible in the sense that it requires the user to have advance knowledge of what the field strengths will be. A possible alternative would be to replace the fixed threshold value E_c by a dimensionless fraction c and refine if

$$|\mathbf{E}(r, z)| > cE_{max} \quad (2.52)$$

with E_{max} the maximum electric field strength in the computational domain. Since the electric field criterium is mostly empirical, picking the right value for the refinement threshold may be a trial-and-error process.

2.2.4 The curvature criteria

There are two criteria that use the curvature of density functions in order to determine which areas to refine. If the curvature is large compared to the size of the cells, the numerics may become unreliable and it is desirable to work with a finer grid. For a density-function $u(r, z)$ and a cell-size $\Delta r \times \Delta z$ the curvature-function $C_u(r, z)$ is a discretization of the second derivative of u in cylindrical coordinates (r, z) :

$$C_u(r, z) = \frac{1}{r + \frac{\Delta r}{2}} \left[(r + \Delta r)(u(r + \Delta r, z) - u(r, z)) - r(u(r, z) - u(r - \Delta r, z)) \right] + [u(r, z + \Delta z) - 2u(r, z) + u(r, z - \Delta z)] \quad (2.53)$$

Rather than the absolute value of the curvature, the refinement module looks at the curvature relative to the global maximum, $Max(u)$. The final criterium then reads:

Refine (r, z) if $\frac{C_u(r, z)}{Max(u)} > C_t$

with C_t the threshold curvature. This refinement criterium is checked for two density functions u . The first is the (absolute) charge density function. Here an extra condition applies: the absolute value of the charge needs to exceed a certain threshold value (which is hardcoded) before a cell can qualify for refinement based on this criterium. Secondly, the curvature criterium is applied to the particle density functions. Since only mobile particles require a high spatial resolution, any immobile species are not considered in these criteria (which currently excludes all species other than electrons). The computational grids for these immobile species are simply the same as the grids used to solve the density equations for electrons.

2.2.5 FISHPACK refinement

The FISHPACK module, for the Poisson equation and the photo-ionization equations, uses a different set of grids than the CDR module and with it a different refinement scheme. Initially, two grids are set up, one coarse and one fine grid (with the fine grid having twice the spatial resolution in each dimension, so 4 times the number of cells). The Poisson/Helmholtz equation is then solved on both grids and the solution of the coarse grid is interpolated onto the fine grid. A grid cell then qualifies for refinement if the absolute

difference between the interpolated coarse solution and the fine solution (this difference is called the error) is more than some user-defined threshold. When refinement is needed, a new set of grids is determined using the strategy mentioned earlier and the process is repeated until either the desired accuracy is reached or the maximum number of allowed refinement levels is reached. Since the **FISHPACK** module was originally only used to solve the Poisson equation for the electrostatic problem and the value of the electric field is defined on the edge of a cell, a cell that doesn't meet the error-criterion still qualifies for refinement if its neighbour does meet the error-criterion.

One limitation to this scheme is the limited number of gridcells that the **FISHPACK** routine can handle. Since **FISHPACK** applies a cyclic reduction scheme, the roundoff error increases with the number of gridcells. This places a limit on the size of grids that **FISHPACK** can solve. Once the refinement module wants to create a grid that is larger than the so-called **FISHPACK** limit, the refinement-attempt is rejected and the code relaxes the error threshold by a factor of 2 and again determines the area to refine, using the new threshold.

To solve the photo-ionization problem, 2 Helmholtz equations need to be solved (For details on the implementation of photo-ionization, the reader is referred to section 3.2.2 and references therein). Each of the so-called "photo-terms" has its own characteristic absorption length, which depends on the gas density and oxygen ratio. The term with the short absorption length is often dominated by impact ionization in the head of the streamer, while the term with the long absorption length is the main contributor of electrons in front of the streamer head that are required for a positive streamer to propagate.

The default behavior of the CStream code is to treat these two photo-ionization terms in the same manner as the Poisson problem when it comes to refinement: all user-definable parameters were equal. Since the term with the short absorption length gives rise to a solution that benefits strongly from high spatial resolution (due to the steep gradients) it will easily trigger the refinement criterium. However, it is this term that is dominated by impact ionization [41], which reduces the relevance of accurate computation of this term. The user can therefore specify the refinement criteria for each of the two photo-ionization terms separately, providing the user with the means to allow the important, long absorption length term to benefit from high spatial resolution, while reducing the computational cost incurred by the less important term. However, in tests it was found that tuning the refinement criteria for the photo-ionization terms has very little effect on computational cost or results.

2.2.6 Conclusion

The adaptive refinement scheme of CStream allows for the simulation of large domains while maintaining high spatial resolution in regions that require this. A number of refinement parameters influence both the computational performance and the accuracy of the results, which means that the user has to monitor the results carefully. Since the refinement criteria were setup by C. Montijn [33] and A. Luque [41] for simulations of air and pure nitrogen, application of the code to other gases may require changes to the values of the various thresholds used in the refinement criteria. An example is high-purity oxygen, with a small nitrogen admixture. In such a gas, ionizing photons will have a very

short characteristic absorption length and the calculation of the photo-ionization terms should be done with high accuracy close to the photon source, primarily the streamer head. However, the limitation of the FISHPACK refinement method to not permit several smaller, adjacent refined sub-grids makes it difficult to properly focus on the streamer head without including too much of the channel.

2.3 CStream software

2.3.1 Basic overview and functionality

The CStream simulation software used in this thesis was originally developed by A. Luque as a more flexible version of the adaptive refinement code developed by C. Montijn as described in [33]. The original code by Montijn was written in Fortran, while CStream is written in C. The FISHPACK package used for solving the Poisson and Helmholtz equations is written in Fortran and was developed by Adams, Swarztrauber and Sweet [42].

CStream solves the fluid equations for streamers described in section 2.1 on nested Cartesian grids using an adaptive mesh refinement technique. CStream allows for the simulation of both positive and negative streamers in the electrode configurations plate-plate and needle-plate. The needle-plate electrode geometry is included using a charge simulation method [41]. This method replaces the electrode needle by a single point charge, with the location and the size of the charge being updated at every timestep to ensure the potential at needle tip remains fixed at the predetermined value. The limitation of this method is that the potential on the rest of the surface of the simulated needle will not be accurate. Consequently, the continuity equation 2.1 is only solved on a smaller grid, not containing the simulated needle.

The effect of this is that CStream is not well suited for the study of the inception of streamers, as the area around the tip of the needle is not accurately modelled. However, since inception is often affected by the behavior of individual particles, the use of a particle code such as described in [32, 43] is recommended for studying streamer inception. The purpose of the CStream code is to study streamer propagation in the phase after the streamer has formed. Studies performed by Luque *et al.* [41] show that the dynamics of streamers in later stages hardly depends on initial conditions.

CStream allows the user full control over the numerical parameters of the simulation: Grid-size, refinement criteria and CFL numbers can be set by the user. The kinetic model, that is, the list of particle species, their reactions and initial densities as well as the diffusion and mobility coefficients can be specified via a series of input files, allowing the user to finetune the properties of the gas in which the streamer is simulated.

The use of CStream is done via terminal commands, input- and output files. CStream was developed for use on Linux systems, but does not use any Linux-specific functionality, which means compilation on Windows or MacOS should be possible as well.

The CStream code can be downloaded from the website <http://mac3wiki.project.cwi.nl/wiki/>.

2.3.2 Handling the software, input and output

Starting a simulation

The CStream program (the binary executable typically has a name such as *cstream-2d* to indicate for which task it was compiled, in the example for pure 2D simulations) takes a large number of command line parameters that govern all details of the simulation: Physical parameters such as voltage, electrode configuration, size of the gap, etc. Numerical parameters such as grid size, refinement criteria, etc. And practical details such as the location the output files should be stored and the interval at which output should be generated.

To aid the setting of these parameters, the simulation can be started through a Bash-script, called *cstream*. This startup-script reads an input file where the user can define the parameters to be used and passes these on to the main program. In addition, it provides easy options for resuming a simulation using a set of output data as initial conditions. To start a CStream-simulation using this Bash script, use the following command from the directory containing the executables:

```
./cstream example_params
```

This will read the file *example_params.cstream* (which should also be in the directory of the executables) and start a simulation with the parameters contained in this file. The CStream program will start, it will print out all parameters used (including those that were not specified in the input file - a default value is used). At this stage, the program will periodically print to screen when it has written a new set of output data. The program will run in the foreground in that terminal. The program can terminate in three different ways:

1. The preset end-time is reached.
2. The program is terminated by the user.
3. The time-step (as determined by the Courant criterium for stability, more details to come) has dropped below a preset threshold. This usually points to some form of instability.

The most convenient approach is to set a very large value for the end-time and, rather than having the program determine when to terminate, keeping track of the progress of the streamer by checking the output files and manually terminating the program when the desired output is reached (For example: the streamer has reached the electrode or it has started to branch). However, it may be necessary for the program to be able to run for a predetermined amount of time. For example when it needs to exit gracefully, which is required for profiling software to work, or if CPU walltime is limited, like on most supercomputers. After termination, the program can be restarted with very little computational overhead, using an output file from the previous execution as starting point for the new simulation. Output files have names using the format *variable.C123abc.tsv*. *variable* is a particle species or electric field (examples include *charge*, *eabs* and all names

of species defined in the kinetic input file), *123* is the sequence-number of that particular output dataset and *abc* specified the subgrid the output belongs to. More details on this in the section on output files. To resume the *example_params* simulation from output-set *123*, call:

```
./cstream example_params C123
```

The parameter file

Parameter files are required to have the *.cstream* extension and are called by providing the filename without the extension. In the parameter file, variables and their values are assigned with the following syntax

```
variable="string-value"
# <-- this starts a comment-line, which is ignored.

# White lines are also ignored.
# String-values should be between quotes, numeric values should not
pi=3.14
# (Note: The above is an approximation)
# Scientific notation can be used:
pi_times_thousand=3.14E3
```

Nonexistent or misspelled parameters are ignored. Parameters are not required, every parameter has a default value, which can be found in the include-file *parameters.h*.

The following overview lists the important parameters for the simulation. The list is not complete, but the parameters omitted are generally meant for testing purposes and changing them is not required for streamer simulations. Therefore they are best left at their default value.

File and directory handling

- **kin_input** - The filename of the input file containing the species, seeds and reactions. By convention, these files have an extension *.input*, but this is not required.
- **output_dir** - The directory where the output files will be stored. This can be a relative path to the directory with the executable or an absolute path. This directory needs to be valid and writeable.
- **output_dt** - The interval (in dimensionless units) with which an output dataset is to be saved. Decreasing this value means more frequent output, which gives finer grained time-dependent data at the cost of more disk space.
- **cdr_output_margin** - Number of margin-cells to be added to the output of the density grids. 2 layers of ghost cells are added on the edge of the computational domain for the purpose of enforcing boundary conditions. With this parameter, these can be included in the output. **cdr_output_margin** must be smaller than or equal to 2. Default 0, recommended 0.

- `pois_output` - Output the grids used in solving the Poisson equation. The grids used for solving the Poisson equation are different from those used for solving the density equations as detailed in section 2.2. Default 0. Note that the absolute value of the electric field is already saved as a density grid, so it is not required to set this parameter to 1 to obtain this data.
- `pois_output_margin` - Number of margin cells to be added to the output of the Poisson grids. `pois_output_margin` must be smaller than or equal to 2. Default 0, recommended 0.

Physical parameters

- `L_r` - Radius of the physical domain in dimensionless units.
- `L_z` - Length of the physical domain. `L_z` does not include the needle.
- `has_photoionization` - Whether to enable the photoionization module. In case `has_photoionization` is 1, photo-ionization will be applied.
- `photoionization_file` - Filename of the file containing the photoionization parameters. This file contains for each photo-ionization term a line with values $-A$ and $-\frac{1}{\lambda^2}$. For more details on these parameters and the implementation of photo-ionization in the code, see [41].
- `E0_x`, `E0_y`, `E0_z` - Components of the external electric field in dimensionless units. Since the electrodes are located at the top and bottom of the domain ($z = L_z$ and $z = 0$), only `E0_z` should be non-zero. Positive values of `E0_z` will generate an electric field in the \hat{z} direction, with the top electrode (at $z = L_z$) having a negative charge, generating negative streamers and vice versa.
- `pois_inhom` - Whether to use a needle-plane geometry. `pois_inhom = 1` means a needle-plane geometry is used, `pois_inhom = 0` denotes a plane-plane geometry. See section 2.3.2 for additional remarks regarding the needle-plane geometry.
- `pois_inhom_needle_length`, `pois_inhom_needle_radius` - The length and radius of the needle, as described in section 2.3.2, in dimensionless units. Only applies when a needle-plane geometry is used.
- `start_t` - Initial time. There's no reason to keep it at anything other than 0. This parameter is automatically set when resuming simulations and this overrides the value of `start_t` from the input file.
- `end_t` - Time at which the simulation will stop, in dimensionless units. It is recommended to use a large value here and manually stop the simulation when it has reached its desired end point as discussed in section 2.3.2.
- `max_ntheta` - Number of azimuthal grid cells. Default 1. Using a value higher than 1 will activate the full 3D simulation (without cylindrical symmetry) using a pseudo-spectral method described in more detail in [44].

Numerical parameters The adaptive mesh refinement criteria and the parameters related to them are discussed in more detail in section 2.2.

- `gridpoints_r`, `gridpoints_z` - Number of gridpoints in r and z direction for the density equations at the coarsest level.
- `cdr_max_level` - Maximum number of refinement levels of the grid for the fluid equations. `cdr_max_level` = 0 means no refinement.
- `ref_threshold_eabs` - Refine grid if $|\mathbf{E}|$ exceeds this value.
- `ref_level_eabs` - Maximum number of refinement levels of the grid for the fluid equation due to the $|\mathbf{E}|$ criterium.
- `ref_threshold_charge` - Refinement threshold for the curvature of the charge density.
- `ref_threshold_dens` - Refinement threshold for the curvature of the particle densities.
- `cdr_brick_r`, `cdr_brick_z` - Size of bricks in r and z direction of the minimal refinement area. See section 2.2.
- `cdr_bnd_bottom`, `cdr_bnd_top`, `cdr_bnd_right` - Boundary condition for the density equations at the bottom ($z = 0$), top ($z = L_z$) and right ($r = L_r$) of the domain. The value 1 means homogeneous Neumann boundary conditions, -1 means homogeneous Dirichlet boundary conditions.
- `pois_max_level` - Maximum number of refinement levels of the grid for the Poisson equation. `pois_max_level` = 0 means no refinement.
- `pois_max_error` - An area of the Poisson grid is further refined if the relative error between two consecutive refined levels exceeds this value.
- `pois_bnd_bottom`, `pois_bnd_top`, `pois_bnd_right` - Boundary conditions for the Poisson equation at the bottom ($z = 0$), top ($z = L_z$) and right ($r = L_r$) of the domain. The value 1 gives homogeneous Neumann boundary conditions, -1 gives homogeneous Dirichlet.
- `nu_a`, `nu_d`, `nu_rt` - Courant number based on advection, diffusion and relaxation time respectively to determine the time step. Must be less than 1 to satisfy CFL stability. In streamer simulations, the time step restriction based on advection (`nu_a`) will dominate over the other parameters (`nu_d` (diffusion) and `nu_rt` (relaxation)). More details on the timestepping can be found in 2.1.3.

Implementation of the needle-plane configuration

As mentioned in section 2.3.1, the needle-plane electrode geometry is implemented using a charge simulation technique, which means that the entire needle is represented by a single point charge located on the axis. The position and strength of this charge is updated each timestep to ensure that the potential at the point that would be the tip of the needle remains fixed. A schematic depiction of this setup can be seen in figure 2.1. This provides a reasonable approximation of the potential in the area below the needle (the needle is always located at the top of the domain), but the potential will be wrong in the areas to the sides of the needle. Consequently, the density equations are only solved from the tip of the needle and downwards. This means that the computational domain for the density equations is smaller than that for the Poisson equation.

In the specification of the external electric field, $E0_z$ is interpreted as the electric field between the 2 planar electrodes, far away from the needle. The applied potential is computed as follows:

$$V = E_{0,z} * (L_z + L_{needle}) \quad (2.54)$$

Output

The code generates a large amount of output files at every `output_dt` units of simulated time. These output files combined are sufficient to resume the simulation from that timestep and can also be used for data analysis. Output files are named `variable.C123abc.tsv`. `variable` is a particle species or electric field. Output is available for all particle species in the simulation. Examples include `electrons`, `n2plus` and `eabs` (the latter being $|\mathbf{E}|$). `123` is the sequence number or output timestep (which does not coincide with, but is proportional to the timestep of the numerical scheme) of that output set, it starts at 000 for the first set. This is the initial condition of the system before the simulation starts at $t = 0$. The alphabetic part of the filename after the output timestep, `abc` denotes the subgrid contained in that file and this extension is defined recursively. The coarsest grid covering the entire domain has no such alphabetical extension (example: `electrons.C123. tsv`). At every next level, the subgrids at that level are named `a`, `b`, `c`, ... and this letter is appended to the alphabetical extension. The file `electrons.C123ba.tsv` contains electron densities at the 123th timestep (so at $t = 123 * \text{output_dt}$) for the first subgrid of the second subgrid of the main grid. Beware that since the grid refinement is adaptive, each timestep has different subgrids.

Data is stored as plain text, with each line containing a single number. Data is ordered in columns (with fixed r coordinate). So to read the data, use the following pseudo-code:

```
for (i = 0, i < rmax*zmax; i++)
{
    r = floor(i / zmax);
    z = i % zmax;
    data[r,z] = read_line_from_file();
}
```

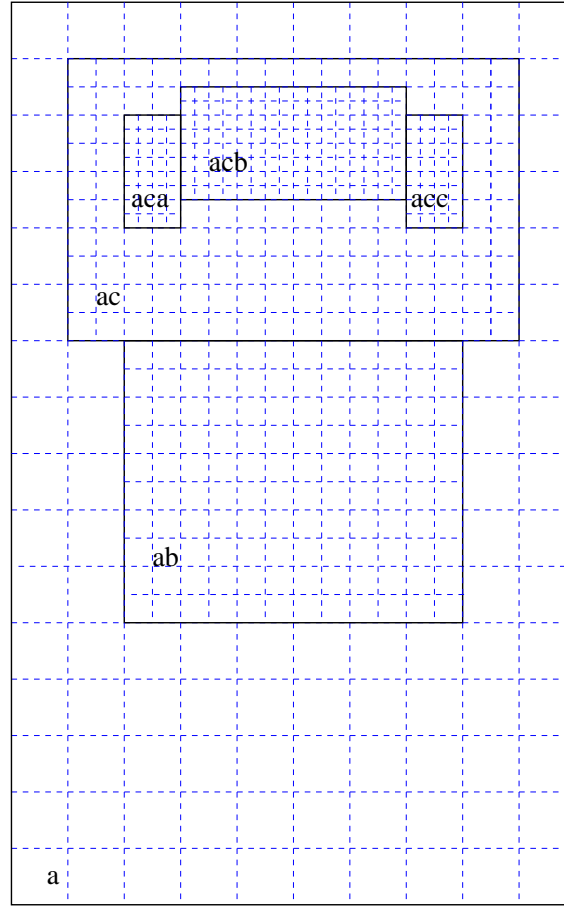


Figure 2.4: Schematic depiction of the naming convention for output files. Each next letter corresponds to a new refined level.

The dimensions of the grid are not contained in the data files. Instead, for each sub-grid and output-step, 2 additional files are created: *r.C123abc.tsv* and *z.C123abc.tsv* corresponding to subgrid *abc* of output step 123. The structure of these files is identical to that of the regular data files, but instead of particle densities or electric field strengths, these files contain the *r* and *z* coordinates of the center of the cell corresponding to that line-number. So to determine the coordinates of the n^{th} line in a regular data file, simply read the n^{th} line of the corresponding *r* and *z* files.

Source files

The CStream simulation software was written in C and its source code is split up in several files, each dealing with a separate part of the program. Most source files have an associated header file in the directory `include` (the source file `example.c` has header file `example.h`) containing the type definitions and preprocessor macros. The function prototypes are aggregated in the header file `proto.h`. A schematic of the directory structure can be seen in figure 2.5. Below is a short summary of the important source files in the directory `src`

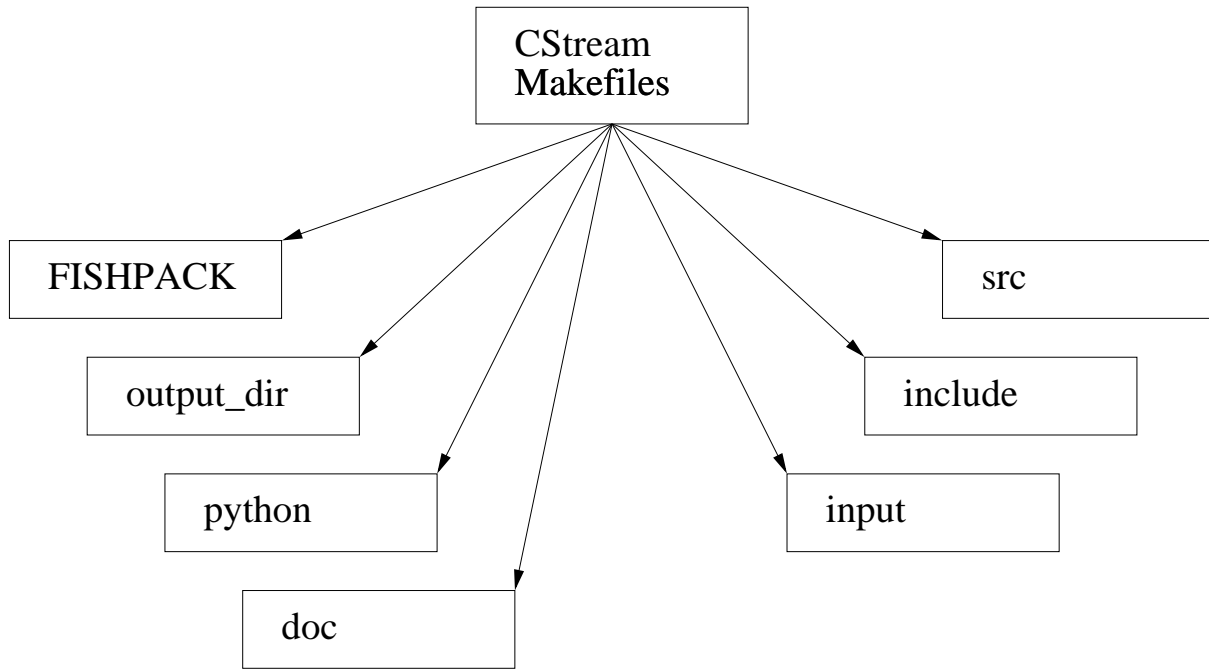


Figure 2.5: Schematic depiction of the folder structure of the CStream source code as it can be found on our website <http://mac3wiki.project.cwi.nl/wiki/>.

and the functionality that is contained within them.

- `cdr.c` - Functions for solving the convection-diffusion-reaction (CDR) equations, creation, manipulation and refinement of CDR grids and timestepping.
- `cstream.c` - Contains some general initialization and termination functions.
- `grid.c` - Low-level functions for handling of grids, both CDR and Poisson grids.
- `interp1.c` and `interp12.c` - Interpolation functions for the mapping of one grid to another (for example during refinement).
- `main.c` - Functions for reading input parameters, starting of the code and the main loop.
- `mapper.c` - Mapping of one grid-tree onto another.
- `photo.c` - Photo-ionization functions.
- `poisson.c` - Functions for solving the Poisson equation, including manipulation of Poisson grids and calling the external **FISHPACK** solver.
- `reaction.c` - Functions for computation of reactions between species as part of the density equations.

- `react_table.c` - Performs initialization of reaction coefficient tables as well as table lookups.
- `read_input.c` - Handles the loading of the input file containing the kinetic model (species, reactions, seeds).
- `rz_array.c` - Low-level functions for handling Fortran-compatible arrays.
- `proto.h` - Prototypes for all functions that are called from source files other than the one they're declared in.
- `parameters.h` - Declares the variables that can be initialized through input parameters and their default values.

Comments contained in the source and include files has been converted into a set of html documents by Doxygen [45], which takes comments from source files and generates a website where users can easily follow the connections between different functions and files. This chapter of this thesis, updated with new additions and changes, has also been included in this documentation. The html documentation can be found in the `doc/documentation/html/index.html` directory of the CStream distribution and can be viewed in a browser.

Probing photo-ionization: Simulations of positive streamers in varying $N_2:O_2$ mixtures

This chapter was reproduced from *Probing photo-ionization: Simulations of positive streamers in varying $N_2:O_2$ mixtures*, G. Wormeester, S. Pancheshnyi, A. Luque, S. Nijdam and U. Ebert, J. Phys. D: Appl Phys, **43** (2010) 505201.

3.1 Introduction

3.1.1 Positive streamers in varying gases

Streamers are thin channels of ionized gas that appear when a high voltage is applied to a large gas volume [38, 46–48]; they are of significant importance in atmospheric electricity (for example, in lightning and sprites [18, 49]) as well as in industrial applications such as lighting, removal of volatile organic components and disinfection [16] and plasma-assisted combustion [50]. We distinguish between positive and negative streamers, where positive streamers carry a net positive charge at their heads and propagate in the direction of the ambient electric field, while negative streamers carry a negative head charge and propagate against the field. This means that negative streamers propagate in the direction of the electron drift, while positive streamers move against the electron drift direction; therefore they require a source of electrons ahead of the streamer to support the impact ionization process and the further growth of the ionized area at the streamer head. Despite the fact that positive streamers propagate against the electron drift velocity, in air they appear more easily than negative streamers and they propagate faster. This faster propagation was observed in experiments [28] and explained in [1]: in negative streamers, the electrons at the side of the streamer channel drift outwards and reduce the field focussing at the streamer tip while positive streamers stay narrow and therefore enhance the electric field at the streamer tip to higher values.

While most work focusses on positive streamers in air, positive streamers have been observed in varying nitrogen:oxygen ratios [15, 51–53], in argon [54] as well as in gas mixtures presenting the atmospheres of Venus ($\text{CO}_2\text{:N}_2$) and of Jupiter-like gas giants ($\text{H}_2\text{:He}$) [19]. In a recent experiment [15], positive streamers were observed in nitrogen, oxygen and argon with impurity levels below 1 ppm; they propagate with essentially the same velocity as in air, but are thinner and less straight, they branch more, move more in a zigzag fashion or even can form feathery structures.

The traditional explanation for positive streamer propagation in air is photo-ionization; a review of the history of the concept can be found in [15]. But photo-ionization according to the traditional model critically depends on the ratio between oxygen and nitrogen and should completely stop when either nitrogen or oxygen are absent. For $\text{H}_2\text{:He}$ mixtures (as in the atmospheres of the planetary gas giants) a photo-ionization model has been outlined in [19], but a photo-ionization mechanism on Venus ($\text{CO}_2\text{:N}_2$) is unlikely to exist [19], and in pure gases it cannot exist either. An alternative is propagation through background ionization, this background can be generated by radiation or by previous discharges in a mode of repetitive pulses [55]. Though reaction rates and electron densities ahead of the streamers can vary by several orders of magnitude between different gases, the experiments show that the propagation of positive streamers is relatively unaffected. E.g., in the recent experiments by Nijdam *et al.* [15] the oxygen fraction changed by 5 to 6 orders of magnitude while the streamer velocity changed by less than 10%. This suggests that positive streamers can propagate due to several mechanisms; and that they are quite robust against changes of the underlying physical mechanisms. In the present article, we test this behavior through simulations of positive streamers in different nitrogen:oxygen ratios, and through varying the parameters of photo-ionization and of background ionization.

3.1.2 Photo-ionization

Photo-ionization in air is thought to work as follows. Electrons accelerated by high electric fields in the streamer head excite electronic states of nitrogen (the species with the higher ionization energy) by impact; the excited nitrogen can then emit a photon with sufficient energy to ionize an oxygen molecule at some distance. The presence of this ionizing radiation with significant penetration length in air was demonstrated in numerous experiments [56]. A similar mechanism was proposed by Dubrovin *et al.* in section 2.2 of [19] for the $\text{H}_2\text{:He}$ mixtures on Jupiter-like planets; she argues that there are electronically excited He states that can emit photons with sufficient energy to ionize H_2 while no such mechanism exists for Venus ($\text{CO}_2\text{:N}_2$). However, the only quantitative photo-ionization model exists for the moment, to our best knowledge, for $\text{N}_2\text{:O}_2$ mixtures like air [57]. We note that this model uses excitation efficiency, quenching parameters and absorption coefficients from different experiments [58, 59] and doing so, it is not a self-consistent model. In addition, this model does not treat the appearance of various "secondary" species in the plasma region (like N and O atoms, ozone, nitrogen-oxides in the case of $\text{N}_2\text{-O}_2$ mixtures) which can contribute to the photo-ionization process.

In pure gases, a one-step photo-ionization scheme cannot exist. A step-wise photo-ionization process (multi-photon excitation of the same species) could be an efficient

source of ionization ahead of a streamer, but such processes are much slower due to the low electron and excitation densities in streamers (see, for example, [60]); therefore this mechanism can not support the high propagation speed of streamer discharges.

3.1.3 Detachment from background ionization

Electron detachment from negative ions in the gas is another possible source of seed electrons. These negative (and positive) ions can appear due to various reasons. Natural radioactivity often governs the background ionization in initially non-excited gases (see [55] and references therein). In buildings, radioactive decay of radon is the main source of ionization. The level of background ionization lies normally within 10^3 - 10^4 positive and negative ions per cm^3 ; this is the value established by the equilibrium between ionization and recombination processes. We note that this level weakly changes with pressure, and that it can decrease due to diffusion and drift of charged species towards metal electrodes. Inside a closed metal container with controlled gas filling, the ionization density is lower.

In pulse-repetitive discharges, residual ions can be accumulated from discharge to discharge and the density of background ionization can be much higher than when it is governed by the natural sources only. A background level of about 10^7 cm^{-3} can exist for a gap of a few centimeters in air at atmospheric pressure at a 1 Hz repetition rate according to simple theoretical estimates [55] that will be recalled in section 3.2.2.

Negative ions themselves (as well as positive ions) cannot create ionization while moving in an electric field (for the range of reasonable electric fields existing at elevated pressures), while they can be a source of electrons. These free electrons appear in collisions of negative ions with other gas species. For the case of oxygen mixtures, the rate of detachment was measured as a function of applied electric field at low pressures [61, 62]. Measurements at elevated pressures in air [63] demonstrate an even higher efficiency of the detachment processes, probably due to oxygen atoms [64] and vibrationally excited species [65].

It must be noted that both mechanisms of electron production ahead of positive streamers exist normally even in "pure" electropositive gases. The level of impurities in the experiments [15] was kept below 1 ppm with much effort (carefully designed vacuum vessel, no plastic parts except for the o-ring seals, baking to reduce outgassing); and relative impurity concentrations of 10^{-4} or higher are much more frequent. In both cases, these impurities include, among others, electronegative admixtures at densities sufficient for both photo-ionization and detachment to produce a sufficient level of seed electrons, since a 1 ppm level at atmospheric pressure is still 10^{13} particles per cm^3 . Therefore it is not sufficient to simply model a pure gas without contamination.

3.1.4 Goal and organization of this chapter

We investigate the role of photo-ionization versus background ionization for the propagation of positive streamers in artificial air and in nitrogen with 1 ppm oxygen through simulations. We also briefly test the case of 1 ppb oxygen in nitrogen.

In section 3.2.2, we describe the model used for our simulations. First we detail the physical model and the relevant processes and their parameters. We discuss the relation between repeated discharges and background ionization levels. Then we provide some details of the numerical implementation. Section 3.3 contains the results of simulations in air and their interpretation as well as a quick comparison of different photo-ionization models. Section 3.4 covers results in N_2 with small (1 ppm or less) admixtures of O_2 . In section 3.5, the numerical results are compared to experiments, first by comparing streamer properties such as velocity and width, followed by a discussion on the presence of feather-like structures in streamers and their cause. Finally, we present our conclusions and an outlook on future research.

3.2 Model

3.2.1 Structure of discharge model

We simulate streamers in $N_2:O_2$ -mixtures with mixing ratios 80:20 for artificial air and 99.9999:0.0001 for pure nitrogen with a 1 ppm (a relative concentration of 10^{-6}) contamination of oxygen. We study the role of photo-ionization and of varying levels of background ionization; negative background ions can deliver free electrons through detachment in sufficiently high electric fields. The model is a density model for the electrons, the positive ions N_2^+ , O_2^+ and the negative ions O_2^- , O^- in a given $N_2:O_2$ gas mixture. The space charge densities are coupled to the electric field, and the reactions are specified in the next subsection. The ionization density stays so low that the change of neutral particle densities can be neglected. All ions are approximated as immobile on the time scale of the simulation; therefore their densities change only due to reactions. Electrons drift in the electric field and diffuse. Therefore the model is written as

$$\frac{\partial n_e}{\partial t} = \nabla \cdot (n_e \mu_e \mathbf{E}) + D_e \nabla^2 n_e + S_e, \quad (3.1)$$

$$\frac{\partial n_i}{\partial t} = S_i, \quad i = 1, \dots, N, \quad (3.2)$$

where n_e and n_i are the local number densities of the electrons or of the N ion species labeled by i . μ_e and D_e are the electron mobility and diffusion coefficients taken from [39] and [66], respectively. \mathbf{E} is the local electric field. The source terms S_e or S_i contain all production or loss reactions for the electrons or the ions of species i . The local space charge density q is the sum of the individual charge densities of all particles,

$$q = \sum_i q_i n_i - e n_e, \quad (3.3)$$

where $q_i = \pm e$ is the charge of ion species i , and e is the elementary charge. The electric field is coupled to the charge density through the Poisson equation

$$\epsilon_0 \nabla \cdot \nabla \phi = -q; \quad (3.4)$$

We calculate in electrostatic approximation

$$\mathbf{E} = -\nabla \phi. \quad (3.5)$$

Reactions	Reference
Impact ionization: $e^- + N_2 \rightarrow e^- + e^- + N_2^+$ $e^- + O_2 \rightarrow e^- + e^- + O_2^+$	BOLSIG+ [68] BOLSIG+
Photo-ionization: $e^- + N_2 \rightarrow e^- + N_2^* + \text{UV-photon},$ then $\text{UV-photon} + O_2 \rightarrow O_2^+ + e^-$	Luque <i>et al.</i> [41]
Attachment of electrons: $e^- + O_2 + O_2 \rightarrow O_2^- + O_2$ $e^- + O_2 \rightarrow O + O^-$ $e^- + O_2 + N_2 \rightarrow O_2^- + N_2$	BOLSIG+ BOLSIG+ Kossyi <i>et al.</i> [67]
Detachment of electrons: $O_2^- + O_2 \rightarrow e^- + O_2 + O_2$ $O_2^- + N_2 \rightarrow e^- + O_2 + N_2$	Capitelli <i>et al.</i> [69] Capitelli <i>et al.</i>
Recombination: $e^- + X^+ \rightarrow \text{neutrals}$ $O^- + X^+ \rightarrow \text{neutrals}$ $O_2^- + X^+ \rightarrow \text{neutrals}$ $O^- + X^+ + X \rightarrow \text{neutrals}$ $O_2^- + X^+ + X \rightarrow \text{neutrals}$	Kossyi <i>et al.</i> Kossyi <i>et al.</i> Kossyi <i>et al.</i> Kossyi <i>et al.</i> Kossyi <i>et al.</i>

Table 3.1: Overview of the reactions included in our model and the references for their rate coefficients. X denotes any neutral species and consequently, X^+ denotes any positive ion.

3.2.2 Modeling the reactions, including electron detachment and photo-ionization

Reactions

The reactions included in the model are impact ionization of nitrogen and oxygen, photo-ionization, attachment of electrons to oxygen, detachment of electrons from O_2^- , electron-ion- and ion-ion-recombination; they are listed in table 3.1. The reaction rates depend on the densities of the interacting species and a field-dependent rate coefficient. The rate coefficients for impact ionization, electron attachment and recombination are based on the kinetic model of Kossyi *et al.* [67] with some of the rate coefficients generated by the BOLSIG+ Boltzmann-solver [68]. The electron detachment rates are taken from Kossyi *et al.* [67] and are discussed in more detail by Capitelli *et al.* [69]. The photo-ionization model is from Luque *et al.* [41]. Both detachment and photo-ionization can be a source of free electrons ahead of the streamer; therefore we discuss them now in more detail.

Detachment

Electron detachment from O_2^- can occur when the negative ion collides with a neutral gas particle. The rate at which electrons detach from negative ions depends on the collision

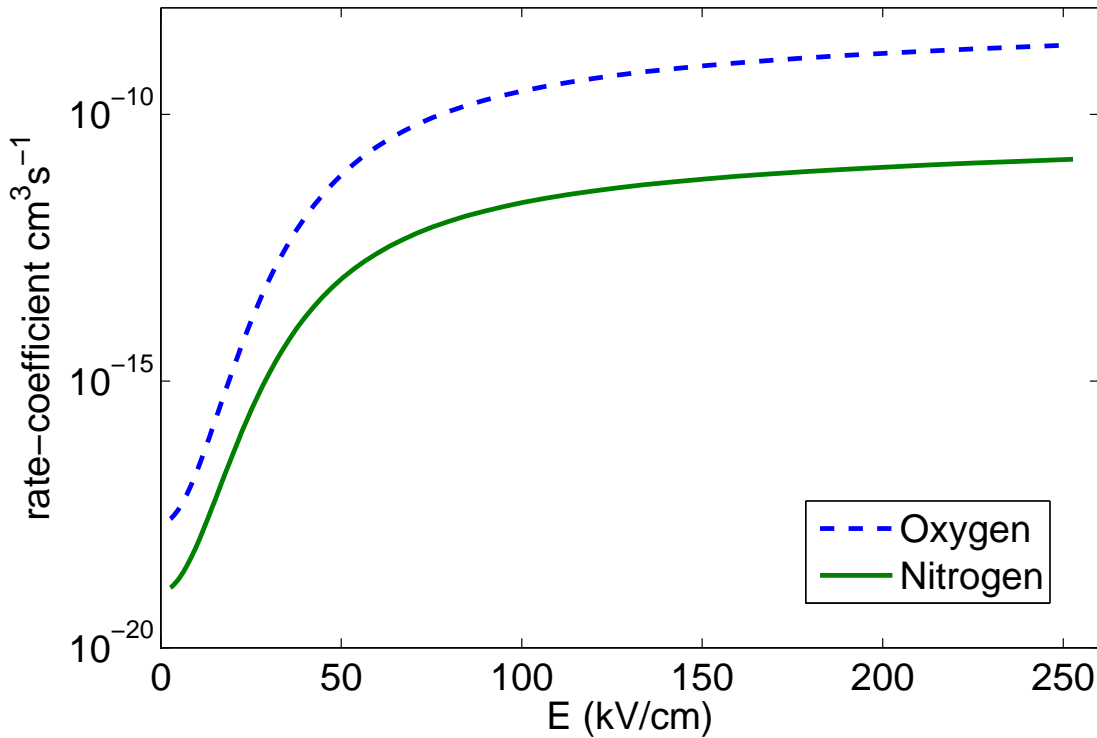


Figure 3.1: Rate coefficients for detachment mediated by two different neutral species as a function of the local electric field. The dashed curve shows the rate coefficient for detachment via collision with O_2 (8), the solid curve shows the rate coefficient for detachment via collision with N_2 (9). All data is for standard temperature and pressure.

frequency, on the local electric field and on the density of the neutral gas. Since we consider $N_2:O_2$ mixtures, we have two separate detachment reactions as listed in table 3.1. The rate coefficients for these reactions are plotted in figure 3.1.

Various processes can contribute to the presence of O_2^- in the gas. First of all, external sources such as radioactive materials in buildings (primarily radon) and cosmic rays can generate an equilibrium level of background ionization. This level is estimated to be 10^3 - 10^4 cm^{-3} [55]. A second source of background ionization is the residual ionization from a previous discharge. In many experiments and practical applications, discharges are generated in a repetitive way. By the time the next discharge is started, some residual ionization still remains in the form of O_2^- and positive ions.

We here give a simple estimate for the level of background ionization in the region far from the needle electrode in a repetitive discharge with repetition frequency in the range of 1 Hz. The streamers then explore a different part of space in each consecutive voltage pulse [15]. If the electron density is 10^{14} cm^{-3} in the streamer and a fraction of 10^{-3} of space is filled with streamer plasma, then the average electron density in space is 10^{11} cm^{-3} . Now these electrons will attach rapidly to O_2 to form O_2^- , even with 1 ppm of O_2 , the attachment time is only 20 ms [55]. The density of both negative and positive ions

will then be 10^{11} cm^{-3} after diffusion has smeared out the original streamer structure. The bulk recombination rate β is approximately 10^{-6} - $10^{-7} \text{ cm}^3\text{s}^{-1}$ [67,69]. We then arrive at the following differential equation for the ion densities ($n_+ = n_- = n$):

$$\partial_t n = -\beta n^2, \quad (3.6)$$

which is solved by

$$n(t) = \frac{1}{\frac{1}{n(0)} + \beta t} \simeq \frac{1}{\beta t} \quad (\text{for } t > 1 \text{ ms}). \quad (3.7)$$

Therefore one expects the level of O_2^- to be around 10^6 - 10^7 cm^{-3} when the repetition frequency of the discharges is 1 Hz.

The precise detachment rate [64,65] as well as the evolution of negative ions in the plasma in the time between two streamer discharges [70] is presently under debate and future simulations might benefit from the inclusion of a more detailed chemistry model. In our model, the critical electric field at which the rate coefficient for detachment equals the rate coefficient for attachment is 70 kV/cm in air. Since the attachment rate is orders of magnitude lower in nitrogen with 1 ppm oxygen and the detachment rate is not as strongly dependent on the electric field as, for example, the impact ionization rate, the critical field for detachment in nitrogen with 1 ppm oxygen is only 20 kV/cm.

Photo-ionization

Photo-ionization in air is based on the fact that there are excited states of nitrogen molecules that can relax through emission of a UV-photon with energy high enough to ionize an oxygen molecule. The history of the concept and the present (poor) data situation was recently reviewed in [15]. Typically, photons in two or three spectral ranges are included; the most used model is presently the one of Zheleznyak *et al.* [57]. Zheleznyak *et al.* merged the available experimental data to create this model for the process:

$$S_{ph}(\mathbf{r}) = \frac{\xi}{4\pi} \frac{p_q}{p + p_q} \int \frac{h(p|\mathbf{r} - \mathbf{r}'|) S_i(\mathbf{r}') d^3(p\mathbf{r}')}{|p\mathbf{r} - p\mathbf{r}'|^2}, \quad (3.8)$$

where ξ is a proportionality constant, p is the gas pressure, $p_q = 80 \text{ mbar}$ the quenching pressure, S_i is the local impact ionization rate of nitrogen and h the absorption function of the ionizing photons. Since integral expressions such as these are computationally costly to solve, Luque *et al.* approximated equation (3.8) by a set of Helmholtz differential equations [41] (and in parallel Bourdon *et al.* [71] did the same):

$$S_{ph} = \frac{p_q}{p + p_q} \sum_{j=1}^N A_j S_{ph,j}, \quad (\nabla^2 - \lambda_j^2) S_{ph,j} = S_i \quad (3.9)$$

where A_j and λ_j are chosen to fit the experimental model as well as possible. λ_j is related to the characteristic absorption length and A_j represents an intensity. Unless otherwise specified in the paper, we have used the original fit by Luque *et al.* with two Helmholtz terms and the following parameters: $A_1 = 4.6 \times 10^{-2} \text{ cm}^{-1} \text{ bar}^{-1}$, $A_2 = 2.7 \times 10^{-3} \text{ cm}^{-1} \text{ bar}^{-1}$,

$\lambda_1 = 45 \text{ cm}^{-1} \text{ bar}^{-1}$ and $\lambda_2 = 7.6 \text{ cm}^{-1} \text{ bar}^{-1}$. (The quantities were originally given in Torr^{-1} rather than in bar^{-1} .) All our simulations were conducted at standard temperature and pressure.

The longest of the absorption lengths is the main contribution to the non-local effects of the photo-ionization. In the fit by Luque *et al.* [41], the longest of the two absorption lengths is 1.3 mm in air at standard temperature and pressure. The absorption length scales inversely with the density of oxygen molecules in the mixture: in nitrogen with 1 ppm O_2 , the oxygen density is 2×10^5 times lower than in air and consequently, the absorption length is 2×10^5 times longer: 260 m. We note that the Zheleznyak model and the approximations that are based on it assume that the UV-photons are emitted instantaneously when the molecule is excited. This assumption is implemented in all streamer simulations we know of and its results are in good agreement with experiments. It been remarked in [72, 73] and by C. Li (unpublished) that the non-instantaneous emission can cause some retardation in the photo-ionization process. However, estimates for retardation times are not well based yet. A full model of the population dynamics of the excited states would be required to accurately predict this retardation.

3.2.3 Electrode geometry, voltage and initial conditions

We simulate a needle-plane electrode configuration as shown in figure 2.1. The needle electrode protrudes from a planar electrode and is positively charged while the planar electrode below is grounded, resulting in an electric field (in the absence of space charges) pointing from the needle towards the plane. The voltage is constant throughout the simulation. The gap between the tip of the electrode needle and the planar electrode is 4 mm or 8 mm. The length of the needle L_{needle} is 2 mm and its radius R_{needle} is 0.2 mm. The potential between the two electrodes is fixed to 12 kV for the 4 mm gap and to 20 kV for the 8 mm gap. The radius of the computational domain is 2 mm (4 mm gap) or 3 mm (8 mm gap).

As an initial condition, we place an electrically neutral seed of electrons and positive ions at the tip of the needle. The seed consists of half of a Gaussian with the peak located at the needle tip. The maximal density of this initial seed is $3.4 \times 10^7 \text{ cm}^{-3}$. The width of the Gaussian (the distance at which the density fallen to a factor of $1/e$ of the maximum) is $73.6 \text{ }\mu\text{m}$. As was shown by Luque *et al.* in [1], the density of the initial seed hardly influences a positive streamer when it starts from a pointed electrode. In the cases where field detachment is studied, a uniform and electrically neutral density of O_2^- ions and positive ions is added.

3.2.4 Numerical implementation

We assume cylindrical symmetry of the simulated system. As a consequence, only the radial and longitudinal coordinates r and z are considered. We use the numerical code developed by Montijn *et al.* [33] and extended with photo-ionization by Luque *et al.* [41]; it uses an adaptive grid-refinement scheme to increase the spatial resolution where necessary:

most notably in the head of the streamer. Different grids with different refined areas are used for the particle densities and for the electric field.

The needle electrode is modeled by a floating point charge using a “charge simulation technique” as described in [1], and earlier in [74]. The computational domain of the density equations starts at the tip of the needle electrode and extends towards the planar electrode, depicted by the shaded area in figure 2.1. The computational domain for the Poisson equation is the region between the two planar electrodes, including the simulated needle. This area is depicted in figure 2.1 by the area between the two bold horizontal lines and to the right of the vertical dashed-dotted line. The implementation of this needle-plane setup is discussed further in section 2.3.2.

The computational domain for the density equations is initially covered by a rectangular grid of 360×200 cells for the 4 mm gap and 720×300 cells for the 8 mm gap, resulting in a cell-size of approximately $11.1 \mu\text{m} \times 10 \mu\text{m}$ at the coarsest level. At every level of refinement, the refined grid contains cells of half the length and height of the cells at the coarser level. We have used up to 3 levels of refinement, leading to a cell-size at the finest level of approximately $1.39 \mu\text{m} \times 1.25 \mu\text{m}$. The criteria for refinement are such that the head of the streamer is always in the area of maximal refinement, though this area is not necessarily restricted to the streamer head. In figure 2.1, the computational domain of the density equations is depicted by the gray area.

For the density equations we use homogeneous Neumann boundary conditions at the top, bottom and outer edges of the domain. A homogeneous Neumann boundary condition represents the symmetry on the central axis. For the Poisson equation as well as for the Helmholtz equations calculating the photo-ionization, we use homogeneous Dirichlet boundary conditions at the top, bottom and outer edges of the domain and again a symmetric Neumann boundary condition on the central axis. The homogeneous electric field created by the planar electrodes is added in a second step. Note that the top boundary for the Poisson equation is not the same as the top boundary for the density equations.

3.3 Simulations in air: photo-ionization versus background ionization

3.3.1 Either photo-ionization or background ionization

We here consider streamers in artificial air which is a mixture of 80% N_2 molecules and 20% O_2 molecules. We use standard temperature and pressure (STP), i.e., the pressure is 1 bar and the temperature 300 K. The distance between the two planar electrodes is 6 mm with a 2 mm needle protruding from the anode. Consequently, the propagation length of the streamer and the length of the computational domain for the density equations is 4 mm. The applied voltage is 12 kV, therefore the average field between the planar electrodes is 20 kV/cm. The initial electron and ion density near the electrode needle is described in section 3.2.3. We consider four scenarios:

1. Photo-ionization, no initial background ionization.

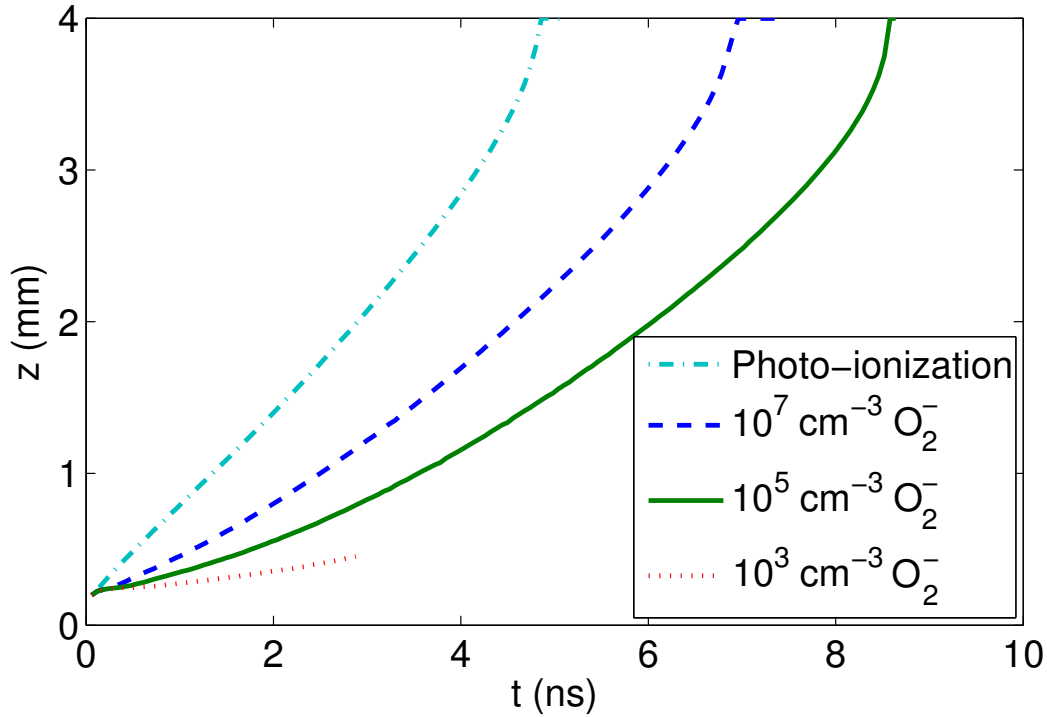


Figure 3.2: Position of the streamer head as function of time. The top curve corresponds to an air streamer with photo-ionization (scenario 1), the curves below that to streamers without photo-ionization, and with a decreasing amount of background ionization (scenarios 2, 3 and 4). The $z = 0$ point corresponds to the tip of the needle.

2. No photo-ionization, initial uniform background ionization $[\text{O}_2^-] = 10^7 \text{ cm}^{-3}$.
3. No photo-ionization, initial uniform background ionization $[\text{O}_2^-] = 10^5 \text{ cm}^{-3}$.
4. No photo-ionization, initial uniform background ionization $[\text{O}_2^-] = 10^3 \text{ cm}^{-3}$.

The first scenario is the usual streamer model in air with the standard photo-ionization model for $\text{N}_2:\text{O}_2$ mixtures. In the other scenarios, photo-ionization is excluded, but different levels of background ionization are included. The second scenario corresponds with a streamer in a series of repeated discharges of approximately 1 Hz while the fourth scenario represents the background ionization present due to ambient sources such as radioactive materials in buildings, see discussion in section 3.2.2.

Figure 3.2 shows the position of the streamer head as a function of time for the 4 scenarios. The position of the streamer head is defined as the position of the charge maximum on the axis of symmetry. At the start of the simulation, both the positively charged and the negatively charged initial seeds are equal and no space charge is present. Immediately thereafter, however, charges separate under the influence of the electric field and a space charge layer is formed at some distance from the origin. This explains the initial jump in position that can be seen in figure 3.2 as well as the increased initial velocity in later figures.

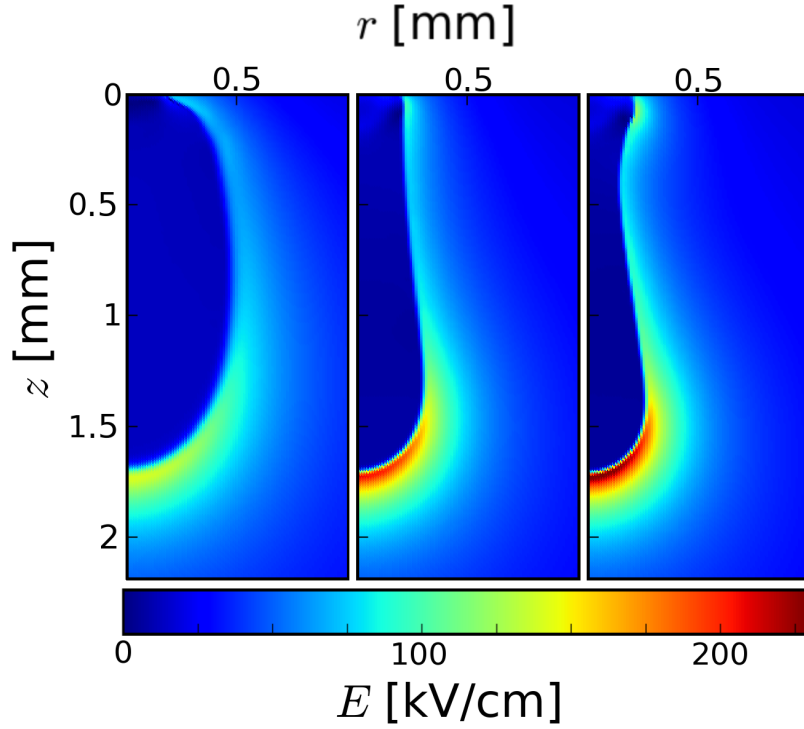


Figure 3.3: Absolute value of the electric field for streamers with photo-ionization (left, scenario 1), 10^7 cm^{-3} background ionization (middle, scenario 2) and 10^5 cm^{-3} background ionization (right, scenario 3). The images are taken after simulation times of approximately 3, 4 and 6 ns, respectively. The computational domain is larger than the plotted area.

We see that streamers with photo-ionization are the fastest under the conditions of the present simulations. But a sufficiently high level of background ionization, e.g., in a repetitive discharge produces enough free electrons in front of the streamer head for the streamer to propagate. The streamer propagates about 40% faster with photo-ionization than with a background ionization of 10^7 cm^{-3} ; according to the discussion in section 3.2.2, this is roughly the background ionization for a discharge with repetition frequency of 1 Hz. When the background ionization density decreases by a factor of 100 from 10^7 to 10^5 cm^{-3} (corresponding to a frequency of 0.01 Hz), the time it takes for the streamer to cross the gap increases by only 20%. However, a background ionization density of 10^3 cm^{-3} was not sufficient to start a streamer that would propagate more than a few hundreds of micrometers under the modeled circumstances (the width of the initial Gaussian seed is $70 \text{ }\mu\text{m}$); this background density characterizes ambient air at ground level without previous discharges. Note that as the streamer approaches the cathode, the electric field in front of the streamerhead increases, since the total potential remains unchanged and the streamer interior is almost completely screened. As a consequence, streamers accelerate when they approach the cathode.

Streamer diameter and shape and maximum value of the enhanced electric field are shown in figure 3.3. When photo-ionization is present, the streamer is wider by a factor of

2 and the maximal electric field is 30% lower than in the case of background ionization. In addition, the electric field profile is less steep with photo-ionization than with background ionization. Streamers with photo-ionization are wider and smoother than those with background ionization, because detachment from background ionization is mostly a local effect (the critical electric field for detachment in air is 70 kV/cm in our model), while photo-ionization is highly non-local with a characteristic absorption length of the ionizing photons of 1.3 mm in air at atmospheric pressure (cf. section 3.2.2). Therefore, free electrons are generated in a much larger region by photo-ionization than by detachment; this will be illustrated later in figure 3.8.

It is worth noting that although the background ionization differs by 2 orders of magnitude between scenarios 2 and 3, the diameter of the streamer and the maximal electric field are practically the same when the streamer head has reached the same point, though the evolution times differ. However, a certain minimum level of background ionization is required to generate propagating streamers. For this reason, scenario 4 was omitted from figure 3.3, because the streamer did not propagate sufficiently far, in accordance with figure 3.2.

3.3.2 Combining photo-ionization and background ionization

To determine the relative influence of photo-ionization and background ionization, we run another simulation that combined scenarios 1 and 2: a 10^7 cm^{-3} density of O_2^- was added to a model with photo-ionization. The results of this simulation were virtually indistinguishable from the results of scenario 1 with photo-ionization only. We therefore conclude that since both mechanisms are present in air, photo-ionization dominates over the effect of detachment from background ionization for the generally accepted photo-ionization model.

As discussed in section 3.2.2, in discharges with repetition frequencies as high as 1 kHz the background ionization can reach a level of 10^{10} cm^{-3} . We therefore have investigated two additional cases with photo-ionization as well as background ionization. Figure 3.4 shows, that only at a level of 10^{11} cm^{-3} negative oxygen ions starts to increase the streamer velocity. At lower levels of O_2^- , streamers propagate due to photo-ionization and are insensitive to the additional background ionization. We remark that at these high repetition frequencies, there may not have been enough time for the residual ionization to diffuse into a homogeneous density distribution. This may cause memory-effects, where streamer propagation is easier over a path taken by the previous discharge.

3.3.3 Testing different photo-ionization models

It is well known [15,55,75], that the actual parameters of photo-ionization are not very well known. We therefore test here how much the simulation results depend on the parameters of the photo-ionization model. We compare streamers in air without background ionization in three cases. The first includes photo-ionization according to Luque's approximation [41]. Bourdon *et al.* [71] suggest that the 2-term Helmholtz model for photo-ionization is insufficient and propose to replace it by a similar model with 3 terms. This 3-term model

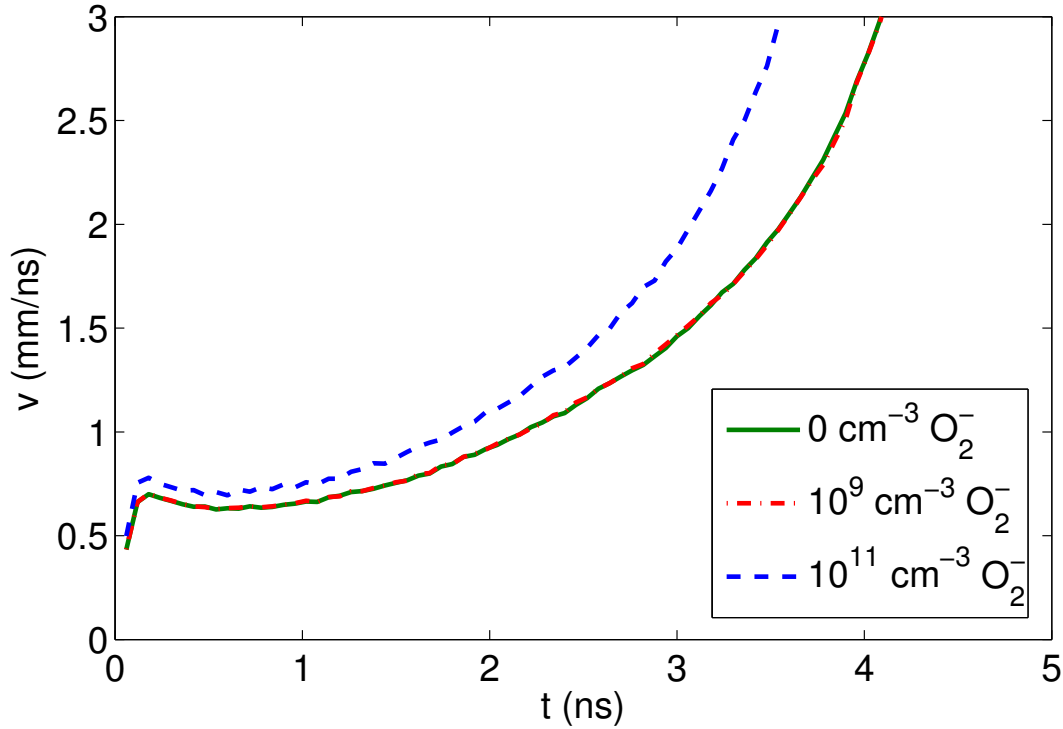


Figure 3.4: Propagation speed of streamers in air with different levels of background ionization. Photo-ionization is present in all 3 cases.

we call the Bourdon model here. The final test-case uses our default 2-term model, but with the number of emitted photons artificially reduced by a factor of 10; this serves as a model for our lack of knowledge of the actual parameters. The longest characteristic absorption length in Bourdon’s 3-term model is 0.5 mm in STP air, while it is 1.3 mm in Luque’s 2-term model.

The gap between the electrodes is here increased to 8 mm so that any differences would have time to develop; and the applied voltage is now 20 kV. The positions of the streamer heads as a function of time are plotted in figure 3.5; it shows that the difference between the unaltered scenario (which is identical to the aforementioned scenario 1, only with a larger electrode gap) and the weakened one is rather small: The weakened scenario has 10 times less source electrons in front of the streamer head, but it only takes 20% longer to cross the gap between the electrodes. The results with Bourdon’s 3-term approximation lie between the other two curves, i.e., they deviate from the results with Luque’s photo-ionization model by 10%.

3.3.4 Summary of results in air

With our simulations in air, we have found that while background ionization levels of 10^5 cm^{-3} or more can provide sufficiently many electrons for positive streamers to prop-

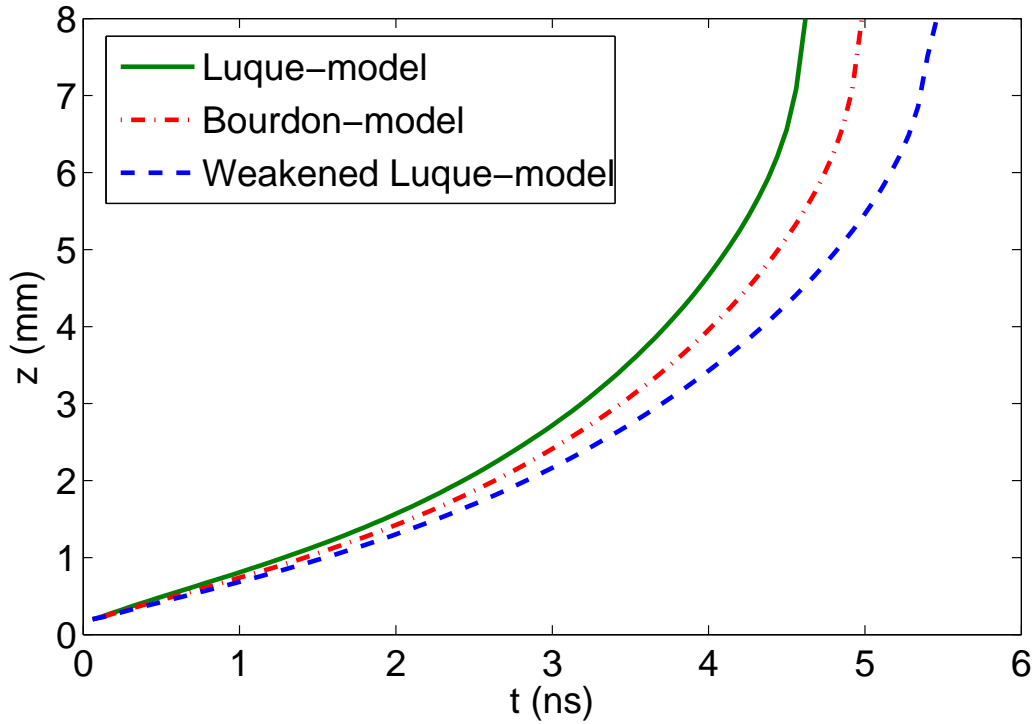


Figure 3.5: Comparison of three photo-ionization models. The curve labeled “Luque-model” refers to scenario 1 and uses the photo-ionization model by Luque *et al* [41]. The curve labeled “Bourdon-model” shows the result of a 3-term Helmholtz model for photo-ionization by Bourdon *et al* [71] as opposed to our default 2-term model. The bottom curve uses the Luque-model, where the source term for the photo-ionization equation was artificially reduced by a factor of 10. Note that the weakened scenario does not represent an actual physical scenario; its purpose is to demonstrate the influence of the accuracy of the photo-ionization parameters.

agate in the absence of photo-ionization, in real-life experiments and applications, the photo-ionization mechanism will dominate the effects of any background ionization level of 10^9 cm^{-3} or less. Therefore, we only expect to see the effects of background ionization on streamer propagation in experiments with repeated discharges with a repetition frequency of 1 kHz or more.

Additionally, we found that positive streamers in air are remarkably insensitive to the precise conditions of the source of the seed electrons (both the mechanism and the number of electrons produced). Changing the background ionization level by two orders of magnitude only resulted in a 20% difference in the time it takes to cross the electrode gap. Also, changing the photo-ionization model to an artificial one with ten times less photo-ionization events has similarly small effects on streamer propagation.

3.4 Simulations in “pure” N₂

We now investigate streamers in nitrogen of high purity. In Nijdam’s experiments [15], the impurity level was kept below 1 ppm. We here simulate an admixture of 1 ppm oxygen in nitrogen. The different ratio of nitrogen and oxygen changes both the number of emitted photons and their absorption lengths. The artificially weakened photo-ionization from section 3.3 amounts to lowering the N₂ density for the purpose of photo-ionization, while keeping the overall gas pressure constant, as it results in a lower number of emitted photons. The other parameters in our photo-ionization model are the absorption lengths of the ionizing photons of different wave lengths. These lengths are inversely proportional to the O₂ density. The longest of these, denoted by l_a , has the strongest effect on the non-local characteristics of the process. In artificial air at atmospheric pressure, we have $l_a = 1.3$ mm. In N₂ with a 1 ppm admixture of O₂, this absorption length is increased to 260 m. In cases where l_a is much larger than the size of the modeled domain, the decay profile of O₂ ionization events as function of distance from the photon source (the streamer head) is dominated by a r^{-2} falloff, with r the distance to the photon source.

We remark that the approximation of the photo-ionization integral (equation 3.8) with Helmholtz equations assumes photo-ionization to fall off proportionally to $\frac{1}{r}$ rather than $\frac{1}{r^2}$, which causes an overestimation of the photo-ionization intensity in certain areas. Close to the streamer head, impact ionization dominates any photo-ionization and the discrepancy for the algebraic falloff can be neglected. At distances much larger than the longest absorption length l_a , exponential decay dominates any algebraic falloff. In near-pure nitrogen, with large absorption lengths, our current model overestimates the photo-ionization intensity in areas away from the active region near the streamer head.

Figure 3.6 shows that in N₂ with a 1 ppm admixture of O₂, both photo-ionization as well as a background ionization of 10^7 cm⁻³ can produce streamers. The propagation speeds are more similar than they are for the same scenarios in artificial air, which is an indicator of the lowered effect of photo-ionization: compared to air, the amount of ionizing photons produced is 25% higher in N₂, but the characteristic absorption length is 2×10^5 longer.

Just like the propagation speed, the maximal of the electric field and its development over time is very similar for both mechanisms, as can be seen in figure 3.7. Background ionization gives rise to slightly higher (between 15% and 20%) fields, but the evolution of the field strength in time remains the same: The field starts at a base value determined by electrode and its applied voltage, then it rises to a maximum and drops as the streamer becomes less focused until it finally branches. The branching sets in after the streamer has propagated 3.7 mm (photo-ionization case) or 4.2 mm (background ionization case). At the onset of the branching event, the rounded space charge layer becomes increasingly flat, leading to a more strongly enhanced electric field at the corners and consequently propagation in a direction that deviates from the axis, this was seen similarly in [3, 41, 47]. Simulations are halted once branching occurs, as this breaks the cylindrical symmetry of the system.

As the source of the background ionization level of 10^7 cm⁻³ is the residual ionization from repeated discharges, we expect that in virgin air the streamer would only propagate

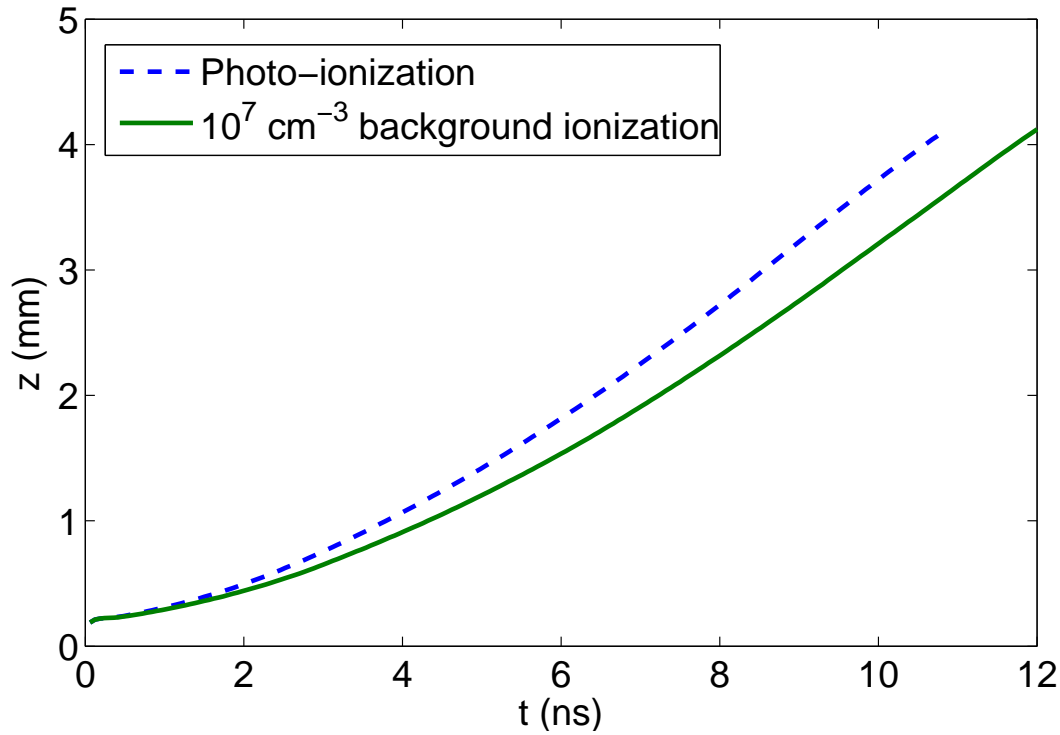


Figure 3.6: Position of streamer head as a function of time for two cases in N_2 with 1ppm O_2 . Solid curve: 10^7 cm^{-3} background ionization, no photo-ionization. Dashed curve: photo-ionization, no background ionization. The gap between the electrodes is 8 mm and the potential is 20 kV. For both cases, the available data was limited by the fact that branching occurs at around 4 mm and the simulations were halted before the streamers reached the cathode.

due to the photo-ionization mechanism. In simulations where photo-ionization and background ionization were combined, the presence of background ionization on the streamer velocity was noticeable at levels of 10^7 cm^{-3} and higher. From this we can conclude that in nitrogen with 1 ppm oxygen, the effect of the repetition frequency can be seen with repetition frequencies of 1 Hz or higher, as our estimate for ion densities (cf. section 3.2.2) applies equally in air and in N_2 with 1 ppm O_2 .

The non-local effect of photo-ionization is visible in the electron density profile in figure 3.8. While in the background ionization scenario, free electrons are only created near the streamer head, in the area with a high electric field (where the field exceeds 20 kV/cm in nitrogen with 1 ppm oxygen), the long characteristic absorption length l_a of photo-ionization causes electrons to be freed at a significant distance from the streamer head. The relatively constant, non-zero electron density in the background ionization case is due to an equilibrium between detachment (rate-coefficient is low in the low-field region ahead of the streamer, but the O_2^- density is rather high) and attachment (high rate-coefficient, but low level of e^- density) of electrons.

The effect of the absorption length of the ionizing photons can be seen when comparing

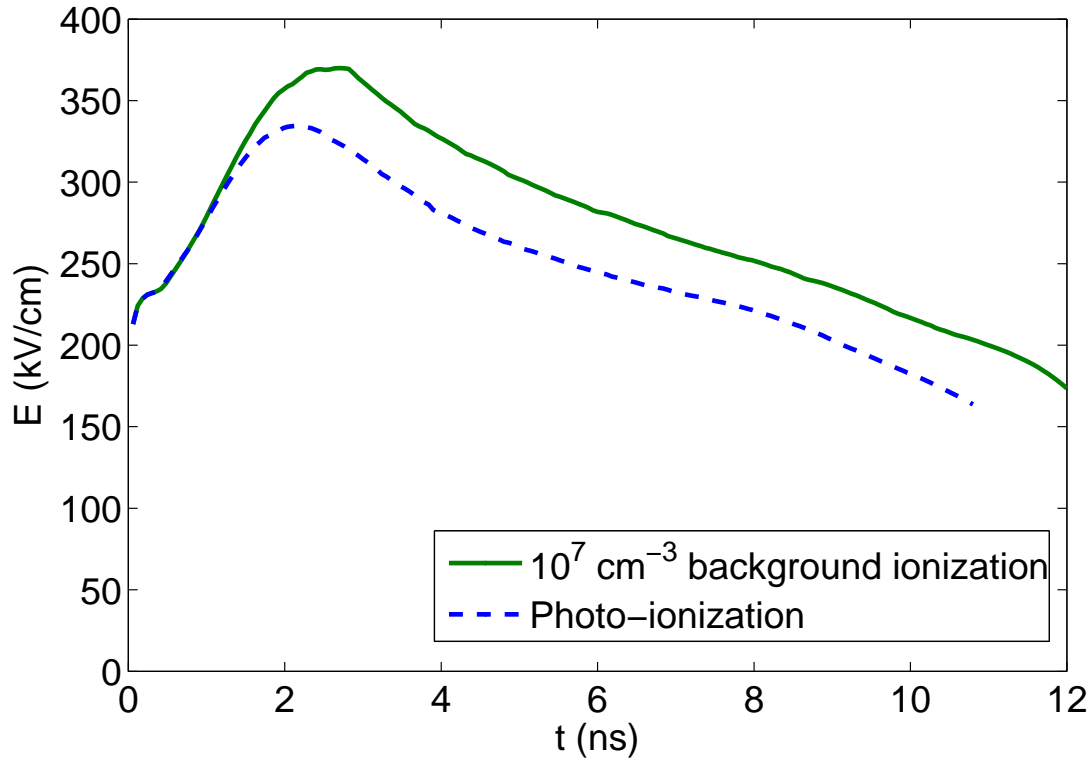


Figure 3.7: Maximal electric field on the symmetry axis of the streamer as a function of time for two cases in N₂ with 1ppm O₂. Solid curve: 10^7 cm^{-3} background ionization, no photo-ionization. Dashed curve: photo-ionization, no background ionization. The gap between the electrodes is 8 mm.

the curves from air and N₂ in figure 3.8. Ahead of the ionization front, the electron density in air is 2 to 3 orders of magnitude larger than in N₂. The long absorption length of the ionizing photons in N₂ with 1 ppm O₂ (260 m) means that most of the photons do not ionize an O₂ molecule before leaving the computational domain, while in air (1.3 mm absorption length), the opposite is true.

In general, the number of photons that reaches a point at a distance r from the streamer head is proportional to $S_{ph} \times e^{-r/l_a} \times r^{-n}$ where l_a is the absorption length and $n \geq 0$ describes the algebraic falloff of the photon intensity. n depends on the shape of the photon source. For a point-source $n = 2$, for a planar front $n = 0$. When the distance r is large, the source of the photons can be approximated by a point source and we get $n = 2$. For small r , the complex structure of the streamer head will give rise to a smaller value of n . In nitrogen with a 1 ppm admixture of oxygen, the absorption length is so large compared to the size of the domain that the exponential falloff can be neglected. In air, the absorption length is still fairly large compared to the size of the domain, but its contribution can no longer be neglected. This can be seen in figure 3.8, where the slope of the electron density curve in air is steeper than in nitrogen in the area in front of the streamer head.

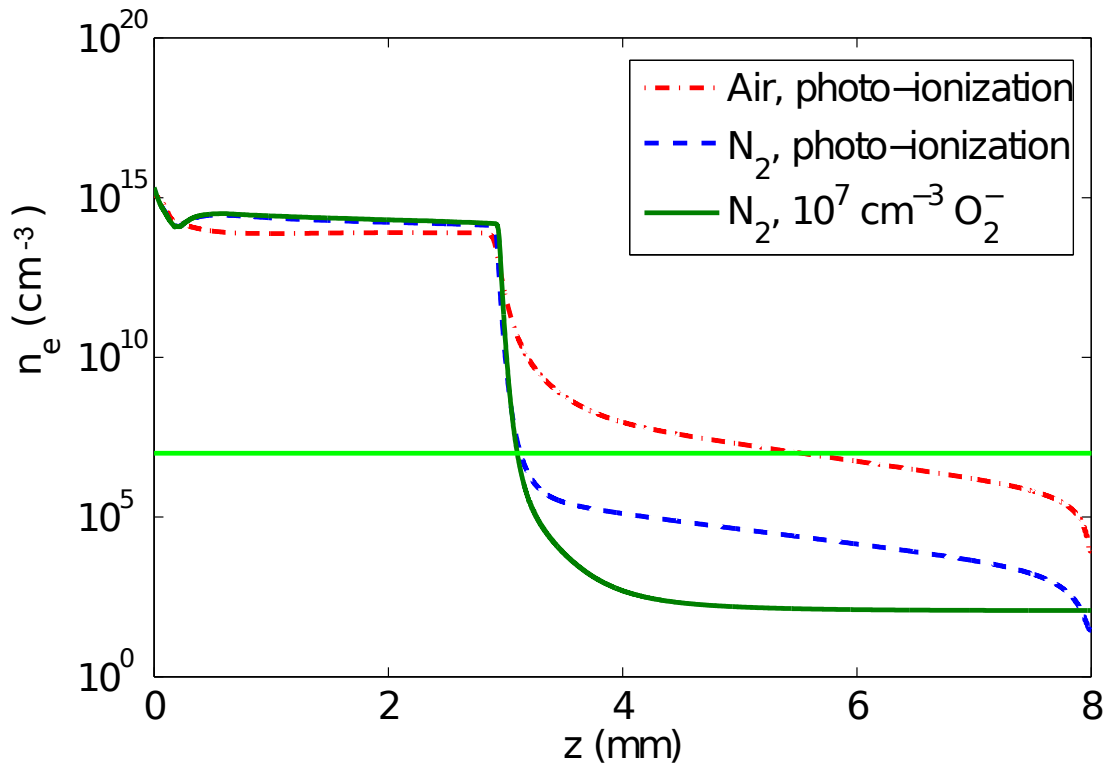


Figure 3.8: Electron density on the streamer axis where the streamer propagates from left to right. The solid curve shows N_2 with 1 ppm O_2 with a background ionization of 10^7 cm^{-3} , the dashed curve shows N_2 with 1 ppm O_2 with photo-ionization and the dashed-dotted curve shows air with photo-ionization. All three curves represent a streamer of equal length and are therefore from different time steps. Also included is the initial level of O_2^- background ionization (horizontal line).

With a naive comparison of the absorption lengths, one expects to see a 2×10^5 times lower electron density in nitrogen with 1 ppm oxygen than in air due to the difference in photo-ionization intensity: The number of photo-ionization events in a small test-volume is proportional to the number of photons entering this test volume multiplied by the number of oxygen molecules in the test volume. Assuming identical photon-sources and no loss of photons between the source and the test-volume, the number of photons entering the test-volume is independent of gas composition and the number of photo-ionization events is proportional to the oxygen density.

However, from figure 3.8, this difference seems to be about 10^3 . There are several reasons that explain the difference between the naive expectation and the obtained results. First, photon absorption in air diminishes the photon number due to the non-negligible exponential falloff e^{-r/l_a} as described in the previous paragraph. Second, the field at the streamer head is higher in nitrogen, which, along with the 25% higher N_2 density causes a higher number of photons to be emitted. Finally, in air a large part of the photo-electrons is lost due to attachment to oxygen, whereas in nitrogen this attachment is orders of

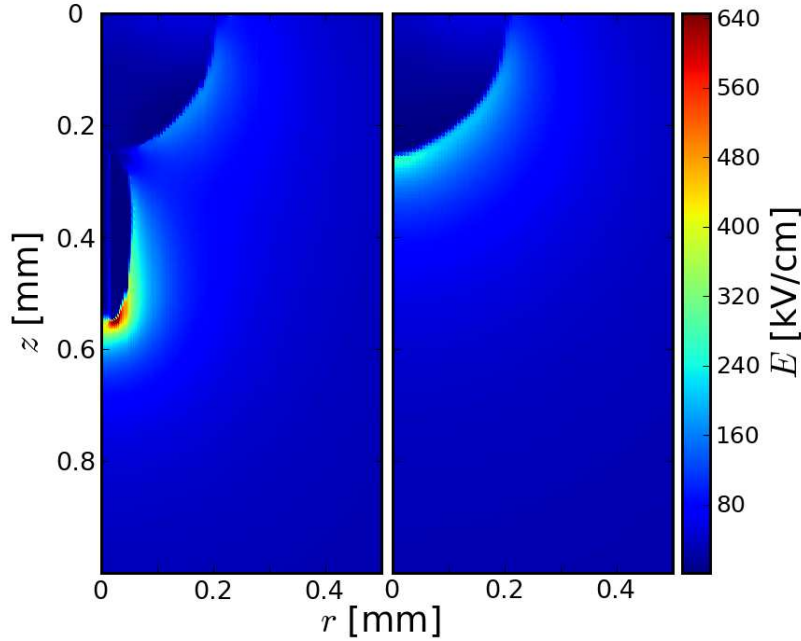


Figure 3.9: Electric field strength of simulated streamers in N₂ with 1ppb O₂ contamination. Both cases have photo-ionization, but no background ionization. The physical parameters of the two cases are identical with the exception of the size of the discharge gap. Compared to the left picture, the right picture has a shorter gap (still many times larger than the scale at which space charge processes occur), and therefore a smaller computational domain, but twice the spatial resolution on the coarsest level (5.56 μm versus 11.1 μm) and four times the spatial resolution on the finest level (0.347 μm versus 1.39 μm). We conclude that the propagating streamer in the left panel is due to a numerical artifact. (In both cases, the computational domain is larger than the plotted area.)

magnitude lower due to the lower oxygen density.

The sudden drop of the electron density near the cathode is due to the choice of a Dirichlet boundary condition for the photon density and the fact that reactions and ionization on and in the electrode are not modeled. The production of electrons due to photo-ionization falls off evenly, but the background electric field moves the electrons towards the anode. Everywhere else in the domain, the balance between electrons moving away from a point and those moving towards it results in a relatively flat density profile, but near the cathode, at any point, electrons that move away from a point are not replaced by electrons coming from the cathode. In reality, one might expect an increase in electron density near the electrode due to photo-emissions of electrons from the metal in the electrode, but this goes beyond the scope of this work.

To investigate how much photo-ionization was actually required to yield a propagating streamer, we decreased the level of oxygen contamination in the simulation. As the oxygen density decreases, the nitrogen density remains practically constant. At 10 ppb O₂ a streamer still emerged. At a lower purity of O₂, 1 ppb, we run into the limitations of the

fluid approximation used in our model, with less than one oxygen molecule per cell at the finest level. Initially, a very thin streamer slowly emerged with a very high electric field (600 kV/cm). However, after decreasing the computational domain and increasing the spatial resolution of the simulation, the streamer did not emerge anymore. In addition, the original simulation showed some artifacts near the symmetry axis. In the original simulation, cell-sizes ranged from $1.39\ \mu\text{m}$ (finest level) to $11.1\ \mu\text{m}$ (coarsest level). The follow-up simulation used cell-sizes between $0.347\ \mu\text{m}$ and $5.56\ \mu\text{m}$. Both results can be seen in figure 3.9. Since the low density of O_2 makes the applicability of the fluid approximation questionable, we can't make any claims about the possibility of photo-ionization as a mechanism for positive streamer propagation at these levels of purity. Additionally, experimentally testing nitrogen with such a high purity would require large effort and investments.

3.5 Comparison with experiments

3.5.1 Velocity, diameter and branching

The present investigations were inspired by experiments conducted by Nijdam *et al.* [15,76] on streamers in gas compositions similar to the ones we used in the numerical simulations. The experiments produce pictures of the optical emissions of streamers that typically branch repeatedly. Nevertheless, they can be compared qualitatively with the numerical results. Figure 7 in [15] shows a comparison between streamers in air and streamers in pure nitrogen. The pure nitrogen has a contamination of O_2 of less than 1 ppm. The streamers in air are about twice as thick as those in nitrogen. Both propagate with the same velocity.

Streamer initiation and propagation has also been observed in pure oxygen (less than 10 ppm contamination). However, this only occurred at higher voltages. For a given gas pressure, roughly twice the voltage was needed compared to the other nitrogen-oxygen mixtures. Unfortunately, streamers in pure oxygen emit very little light and are therefore very difficult to image and analyze [15]. Nonetheless, it seems that their general morphology, diameter and propagation velocity is not far off from the other gas mixtures. In addition, positive streamers with similar velocities and diameters were also observed in argon, while in argon properties such as branching behavior and light emission are different and the streamers emerge more easily at lower voltages than in $\text{N}_2:\text{O}_2$ mixtures.

Figure 3.10 shows similar results from the numerical simulations: The streamer in air is thicker than its nitrogen counterparts. Unlike the situation in air, the streamer generated by photo-ionization and the one generated by background ionization look remarkably similar, though it is important to note that both pictures are not from the same time step, they have been selected so that each streamer is in the same stage of its propagation and the streamer generated by photo-ionization is slightly faster, as was discussed earlier. The data used is the same as in figure 3.8. Note that both streamers in nitrogen started to branch not long after the timestep shown in the figure. Due to the cylindrical symmetry of the system, the simulations were stopped after the streamer branched.

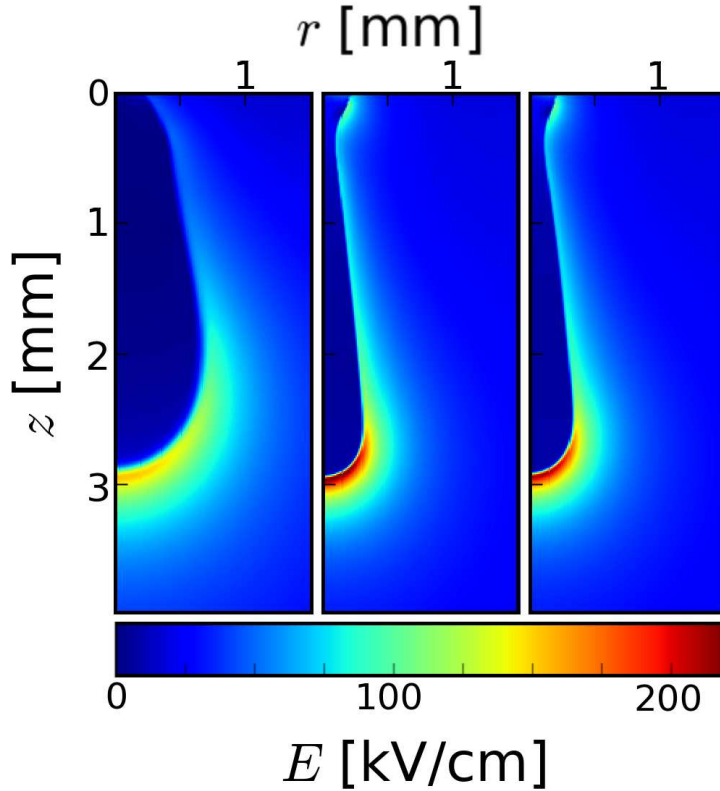


Figure 3.10: Electric field strength of three streamers of equal length in an 8 mm gap. The left figure is in air with photo-ionization and no background ionization, the middle figure is in N_2 with 1 ppm O_2 , photo-ionization and no background ionization. The right figure is N_2 with 1 ppm O_2 with 10^7 cm^{-3} background ionization and no photo-ionization. The computational domain is larger than the plotted area.

The propagation velocity of streamers in N_2 is not constant, but increases slowly up to the branching point. In figure 3.11 we see that the maximum velocity reached is approximately 0.5 mm/ns. In experiments conducted by Nijdam *et al.* [15] in a 16 cm gap at 200 mbar a linear relation was found between voltage and the velocity halfway down the discharge gap. At 20 kV, they measured a velocity of 0.4 mm/ns. We must note that we can not mimic the conditions of the experiments precisely, as we can not follow the streamer after it has branched. The same experiments show that streamers in nitrogen branch more easily than in air. In our simulations, branching was observed in nitrogen, but not in air under otherwise identical conditions.

3.5.2 Feather-like structures

In their experiments in “pure” nitrogen and argon, Nijdam *et al.* [15] observed feather-like structures on the sides of streamer channels. This was not observed in mixtures with 1% or more oxygen, in which streamer channels appear smooth. They hypothesized that these feathers are electron avalanches generated by single electrons that move into the

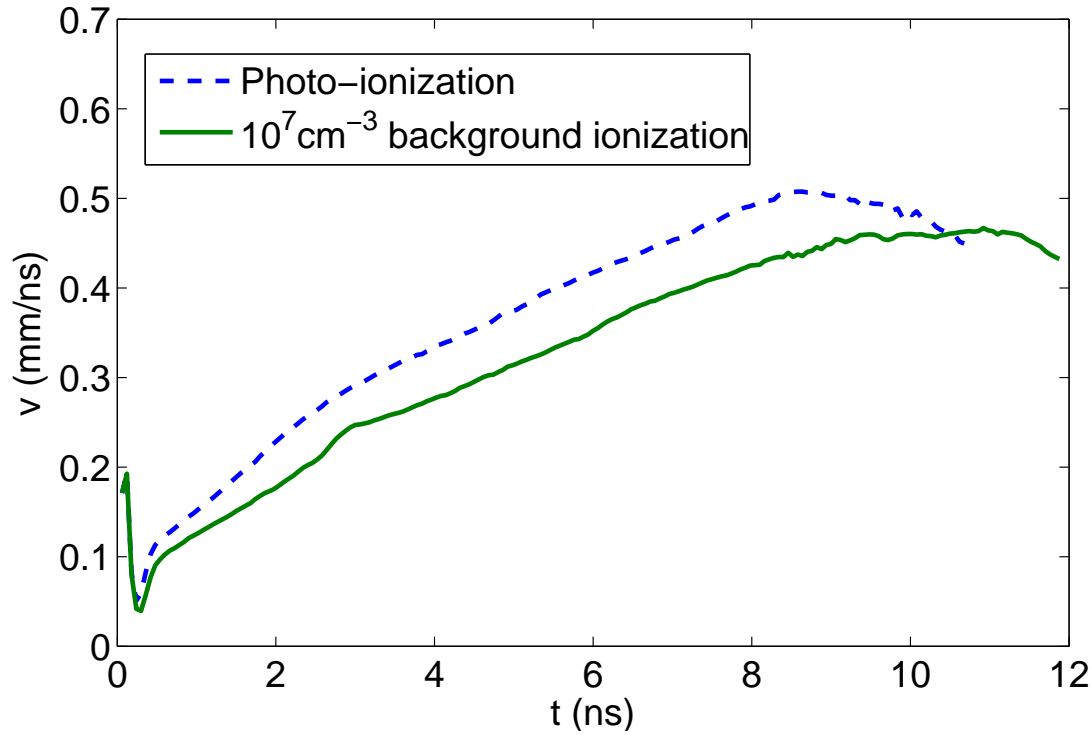


Figure 3.11: Propagation velocities of streamers in nitrogen using different propagation mechanisms.

region where the electric field is above the breakdown threshold. A distinction must be made between nitrogen and air: in nitrogen, the photo-ionization length scale is much larger than the distance from the streamer head at which the electric field exceeds the breakdown threshold. Therefore many of the electrons that are created by photo-ionization do not form avalanches. Only when an electron reaches the area in front of the streamer head, an avalanche will form. This results in a low number of avalanches that can be seen as distinct feathers.

In air on other hand, the photo-ionization length is much smaller and electrons created by photo-ionization are immediately accelerated to form an avalanche in the area of high electric field. This results in a lot of avalanches that are no longer distinct, but will instead overlap and become part of the streamer head that can become much wider for precisely this reason. This heuristic argument matches the observation that streamer channels in air are straight and wide.

In experiments in pure nitrogen at 200 mbar, the visible hairs of the feathers have a length of 0.5–1.5 mm. The angle between these hairs and the propagation direction of the streamer is 20 to 50 degrees. This value is determined from a 2D projection of the real hairs, therefore the real angles may be larger than 20 degrees. It is not clear whether the hairs bend away from the streamer channel or towards it. The maximum distance between the tip of a hair and the center of a streamer channel is about 1 mm, but most hairs do not stick out more than 0.5 mm from the axis of the channel.

About 1–1.5 hairs per mm of streamer channel can be observed. Because hairs in the path of the channel will be overrun by the channel and hairs in the same optical path as the streamer channel will be obscured by the streamer, the total number of avalanches per mm is larger than 1.5 hairs per mm.

Simulating the creation of these feathers goes beyond the capabilities of our fluid model and requires a model that tracks the individual electrons or a spatially hybrid model, such as [77], that combines the fluid approximation in the interior of the streamer with the full particle model outside of the streamer. However, we can still make some qualitative statements based on our simulation data.

There are 2 parameters that influence the presence of distinct feathers: the distance from the streamer at which avalanches are created and the number of avalanches per unit volume. If avalanches only occur close to the streamer, they will be indistinguishable from the main streamer channel. Similarly, if the electron density is high enough that they can be described as a density rather than as a probability, one can expect the number of avalanches to be so high that individual avalanches overlap and distinct feathers are no longer visible, but rather one wide channel is seen.

Due to the similarity laws [18, 53], the feather length of 1.0 mm seen in the 200 mbar experiments in nitrogen corresponds to a length of 0.2 mm in our simulations at 1000 mbar. In our simulations in air with photo-ionization, we found the electron density to be at around 10^5 mm^{-3} at distances of 1 mm (or more) from the streamer channel. Therefore we expect any effects from individual avalanches to be smoothed out and to be invisible as the density-description holds. This is in agreement with experiments, where no distinct feathers were seen in air.

In nitrogen with photoionization the situation is different, the electron density falls off more rapidly with distance and we observe that at 0.2 mm from the streamer head, the electron density drops to 10^2 mm^{-3} , which is sufficiently low to consider the electron density distribution as a probability distribution rather than as a continuous medium. We note that at 0.2 mm to the side of the streamer head, the electric field is around 80 kV/cm, well over the breakdown threshold, so avalanches should be able to start at this distance and even further from the streamer. So in nitrogen we find that we both have a sufficiently low electron density as well as a sufficiently high electric field to enable the formation of distinct avalanches at at least 0.2 mm from the streamer head.

In conclusion, we again emphasize that a proper investigation of these feather-like structures is not possible with our fluid model and requires a particle model. However, our arguments based on the density of electrons qualitatively agree with the observed differences between the smooth streamers in air and the feathered streamers in nitrogen.

3.6 Conclusion

We have simulated and analyzed the propagation of positive streamers due to photo-ionization or background ionization, in air as well as in nitrogen with 1 ppm oxygen which corresponds to the lowest impurity level reached in experiments [15]. In such pure gases, the usual photo-ionization mechanism present in air is largely suppressed. The

initial background ionization can come from natural radioactive sources or from residual ionization from a previous discharge.

We have found that in air the photo-ionization mechanism dominates the streamer propagation except when a very high density of background ionization, such as 10^{10} cm^{-3} , is present. (This background density can be associated with a repetition frequency of 1 kHz according to the estimates in section 3.2.2.) We have found that the parameters of the photo-ionization model have a very small effect, relative to the change in number of ionizing photons, on the streamer characteristics: an order of magnitude change of the number of ionizing photons results in a change of 20 % in streamer characteristics such as the velocity. Therefore we conclude that although the detailed parameters of the photo-ionization model are not well known, we still expect that the numerical results will hold up experimentally.

In nitrogen with 1 ppm oxygen, we found that photo-ionization is still dominating streamer propagation up to background ionization levels of 10^7 cm^{-3} (corresponding to a repetition frequency of 1 Hz). This is remarkable since the low oxygen concentration leads to a low number of photo-ionization events per volume. As lower impurity levels than 1 ppm are extremely difficult to reach experimentally, we conclude that streamer propagation even in "pure" nitrogen is dominated by the usual photo-ionization mechanism in non-repetitive discharges.

While for all simulations with photo-ionization or background ionization in different gas compositions, the streamer velocity changes by less than a factor of two, there are characteristic differences in shape and field enhancement. The nonlocal photo-ionization in air creates a wide electron cloud around the streamer head that can be interpreted as a density; this explains why the streamer head in air can become broad and propagate in a stable manner. On the other hand, pure background ionization in air or in nitrogen as well as the weak photo-ionization in nitrogen with 1 ppm oxygen create a steep decrease of the electron density around the streamer head. These densities become so low immediately outside the streamer head that they have to be interpreted as probabilities rather than as densities, hence creating a more stochastic propagation mode in which the streamer cannot become as wide as in air. These observations match the experiments [15] that show a more feathery structure consisting of many avalanches around thin streamer channels in "pure" nitrogen while streamers in air are straighter and wider. Velocities are comparable between air and "pure" nitrogen both in experiments and in our simulations.

The simulations show another characteristic difference between streamers in air and in "pure" nitrogen that up to now cannot be verified in experiments: The field enhancement at the streamer tip is stronger in nitrogen than in air. This is reminiscent of the difference between positive and negative streamers in air. Negative streamers in air become wider along the channel due to electron drift [1] and at their head due to the non-local photo-ionization; therefore they are not very able to keep the field focussed. For positive streamers in air, the field focussing is suppressed at their head through photo-ionization, while positive streamers in "pure" nitrogen stay narrow and focus the field at the heads to the highest values. Therefore they create higher ionization levels in the streamer channel, and they can propagate with similar velocities as in air though the electron density falls off faster ahead of the ionization front.

We have studied photo-ionization versus background ionization for positive streamers in air and in "pure" nitrogen. We showed that for sufficiently low repetition frequencies and background ionization, photo-ionization is dominant in both gases, but that streamers can propagate by pure background ionization as well, and in a similar manner. We discussed characteristic differences of propagation modes between strong or weak photo-ionization. Finally, we believe that our results are representative for other gas composition as well.

CHAPTER 4

Feather-like structures

This chapter was reproduced from *Feather-like structures in positive streamers interpreted as electron avalanches*, G. Wormeester, S. Nijdam and U. Ebert, Jap. J. Appl. Phys., **50** (2011) A01.

4.1 Introduction

4.1.1 Positive streamers

Streamers are thin channels of ionized gas that are of significant importance in processes of atmospheric electricity (for example lightning and sprites [18, 49]) as well as in industrial applications such as lighting and disinfection [16]. We distinguish between positive and negative streamers. Negative streamers propagate in the direction of the electron drift, while positive streamers move against the drift direction and therefore require a source of electrons ahead of the streamer head. Yet positive streamers emerge more easily than negative streamers, which makes them more suitable for experiments.

The source of electrons in front of a positive streamer head is typically assumed to be photo-ionization, in particular in air, but this mechanism can be replaced by detachment from background ionization. In reality, both mechanisms are present. In recent work [15, 34], the dependence of the relative influence of each mechanism on parameters such as gas composition and repetition frequency of the discharges was investigated. Detachment from background ionization is only of influence in discharges with high repetition frequencies, in the kHz range for air and above 1 Hz in near-pure nitrogen. In all other cases, photo-ionization completely dominates the effect of any background ionization present in the gas.

4.1.2 Effect of gas composition

The amount of electrons generated by photo-ionization depends on the gas composition: In $\text{N}_2\text{:O}_2$ -mixtures, the photo-ionization intensity depends both on the N_2 density (for the number of emitted photons) and on the O_2 density (that determines the absorption length). Therefore one expects streamers to be different in different $\text{N}_2\text{:O}_2$ -mixtures. However, both in experiments [15] and in numerical simulations [34], many of the streamer properties such as velocity and diameter are remarkably insensitive to order of magnitude changes in the number of photo-electrons outside the streamer.

Additionally, positive streamers have been observed in mixtures other than $\text{N}_2\text{:O}_2$, such as argon as well as mixtures representing the atmospheres of Jupiter and Venus [19], again with velocities that are very similar to the $\text{N}_2\text{:O}_2$ streamers. In these gases, the source of the electrons in front of the streamer head is not yet known. The lack of nitrogen and oxygen makes the classical $\text{N}_2\text{:O}_2$ -photo-ionization mechanism in air impossible. Some form of photo-ionization from the gases in these atmospheres is plausible, but no detailed models are available yet.

While positive streamers in different gas-mixtures have many similar properties, there are clear differences. In “pure” nitrogen as well as in argon, Nijdam *et al* [15] observed small hairs connecting to the main streamer channels, giving the entire channel a somewhat feather-like appearance. The nitrogen had at most 1 ppm of oxygen contamination, while the argon had at most 10 ppm of impurities. Independently, Takahashi *et al* [78] observed the same phenomenon in streamers in argon. In air, no such feathers were observed. Figure 4.1 shows the difference in streamer smoothness and feather formation between air (bottom panel) and two near-pure nitrogen mixtures (top panels).

4.2 Observations of Feather-Like Structures

In experiments on streamers in N_2 with at most 1 ppm O_2 as well as in argon a feather-like structure was observed around the main streamer channels [15]. More recently, experiments have been done in even purer nitrogen, where the O_2 contamination is at most 100 ppb. Lowering the oxygen density decreases the smoothness of the streamer channel and makes the feather-like structure more apparant, as can be seen in figure 4.2, which consists of closeups of figure 4.1. The protrusions from the main streamer channel, like the one indicated by the circle in figure 4.3 will be called “hairs”.

An estimate of the number of “hairs” in the feathers is made by drawing two boxes parallel to the streamer channel, as indicated in figure 4.3, and manually counting the number of visible hairs in these boxes. Dividing the hair-count by the length of the boxes yields the number of hairs per unit of streamer length. It must be noted that due to the two dimensional nature of the images, any hairs that are in front of or behind the streamer in the projection of the camera, will not be visible and will therefore not be counted. Consequently, the hair-count obtained by this method is a lower limit for the actual number of hairs.

Using this method, an estimate of about of 1 hair per mm of streamer length was found in the image plane of streamers in nitrogen with at most 1 ppm oxygen at 200 mbar. We

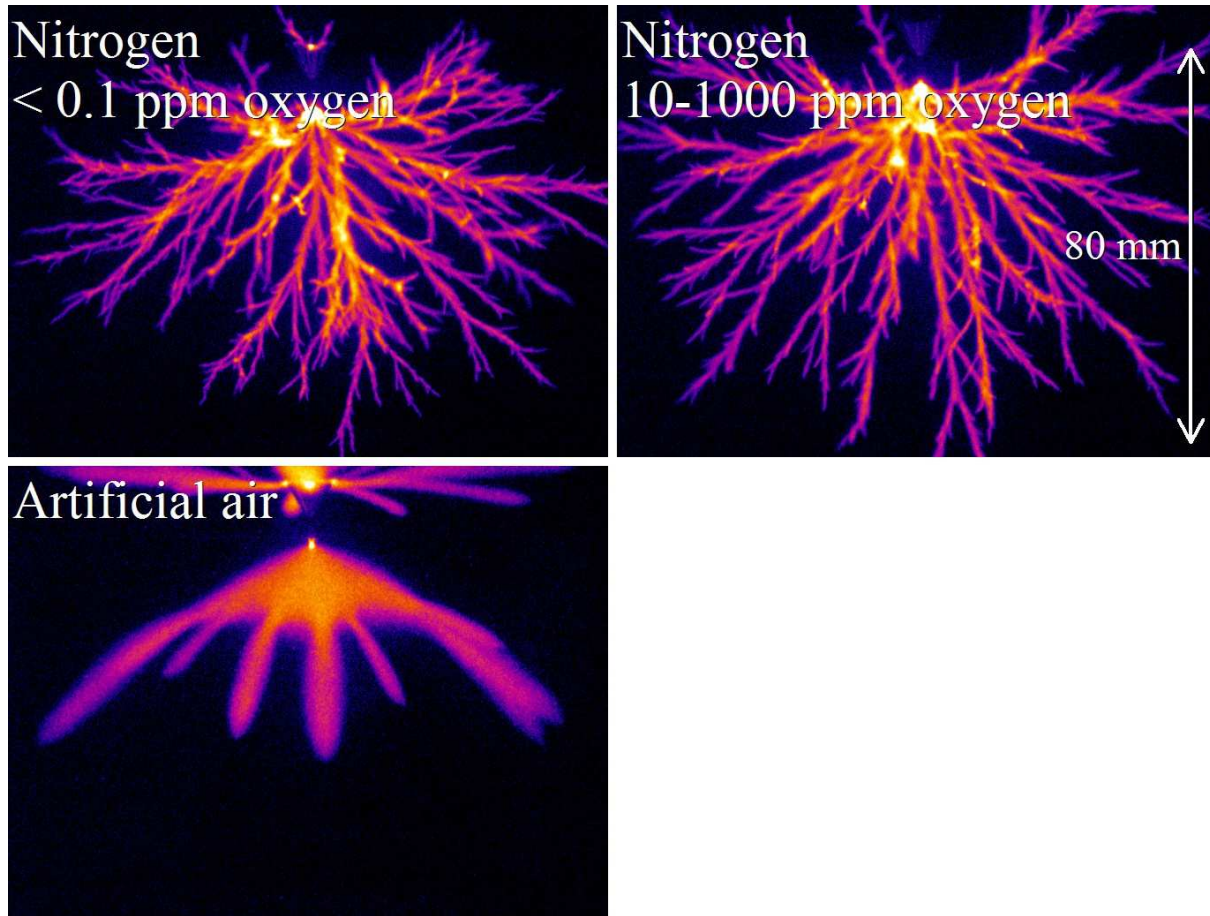


Figure 4.1: Streamers in three different $N_2:O_2$ -mixtures at 200 mbar. The top-left panel shows a mixture with an oxygen fraction of at most 10^{-7} , the top-right panel shows a less pure nitrogen source where the oxygen fraction is estimated to be between 10^{-3} and 10^{-5} and the bottom panel shows streamers in artificial air. In all cases, a positive voltage pulse of 25 kV and of 130 ns duration is applied to the upper needle electrode (with the Blumlein pulser described in [15]), the distance to the plate electrode below is 16 cm and the upper 8 cm are shown. In the artificial air image, the brightness is four times more enhanced than in the nitrogen images.

remark that this is only an order-of-magnitude estimate due to the strong stochastic nature of the phenomenon and the difficulty of counting.

4.3 Hypothesis on the Origin of Feathers

4.3.1 Hairs formed by avalanches

We hypothesize that the feathers are separate electron avalanches moving towards the streamer. Free electrons in front of the positive streamer head drift towards the streamer

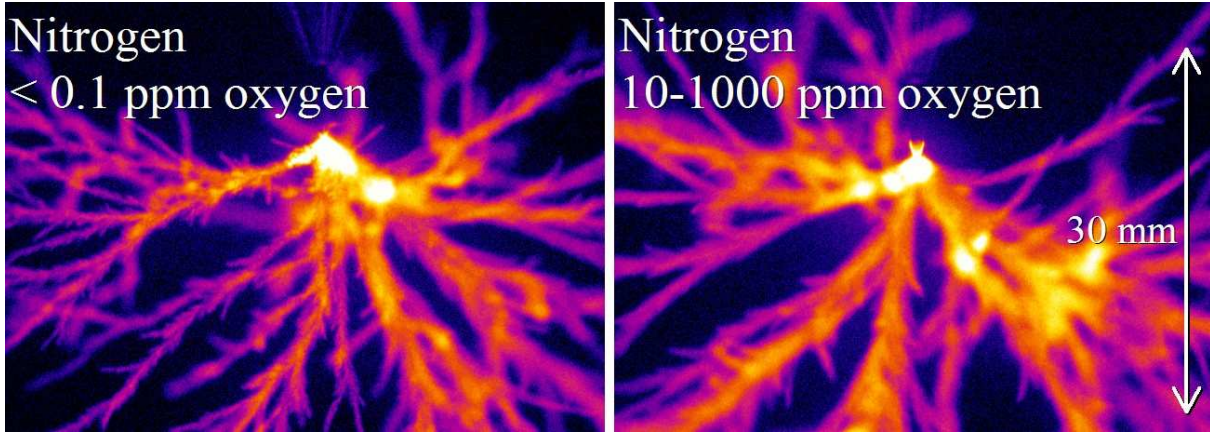


Figure 4.2: Comparison between feather-like structures in streamers in nitrogen with small oxygen admixtures. These images are closeups of the area near the needle for discharges under the same conditions as in figure 4.1. The left panel shows a mixture with an oxygen fraction of at most 10^{-7} , the right panel shows a less pure nitrogen source where the oxygen fraction is estimated to be between 10^{-3} and 10^{-5} .

due to the enhanced electric field generated by the space charge layer in the streamer head. Once the electrons enter the region where the electric field is above the breakdown value (where the impact ionization rate exceeds the attachment rate), more free electrons are created than there are lost. This results in an avalanche that drifts towards the streamer head. This can be seen schematically in figure 4.4. If the avalanche is created directly in front of the streamer head, it will be overtaken by the propagating streamer and will therefore not be visible in experiments. Avalanches seen in experiments start away from the path of streamer propagation.

If at the critical electric field, where the impact ionization and attachment rates are equal, the electron density is low, one expects that some of these avalanches do not overlap and can be seen as distinct structures. On the other hand, if the electron density is already high enough so that the average distance between free electrons is much smaller than the dimensions of the streamer, one expects so many avalanches that they will overlap and can no longer be seen as separate entities, but only as a continuum, being part of the propagating streamer.

4.3.2 Effect of oxygen density on hair-formation

The source of electrons in front and to the sides of the streamer head is assumed to be photo-ionization. An excited nitrogen molecule falls back to a state with lower energy, emitting a photon with the right energy to ionize an oxygen molecule. The characteristic ionization length of these photons scales inversely with the oxygen density and as a consequence significantly less photons will create ionization in the area around the streamer. Therefore the density of free electrons in the region away from the streamer head is expected to be orders of magnitude higher in air than in nitrogen with only a very small

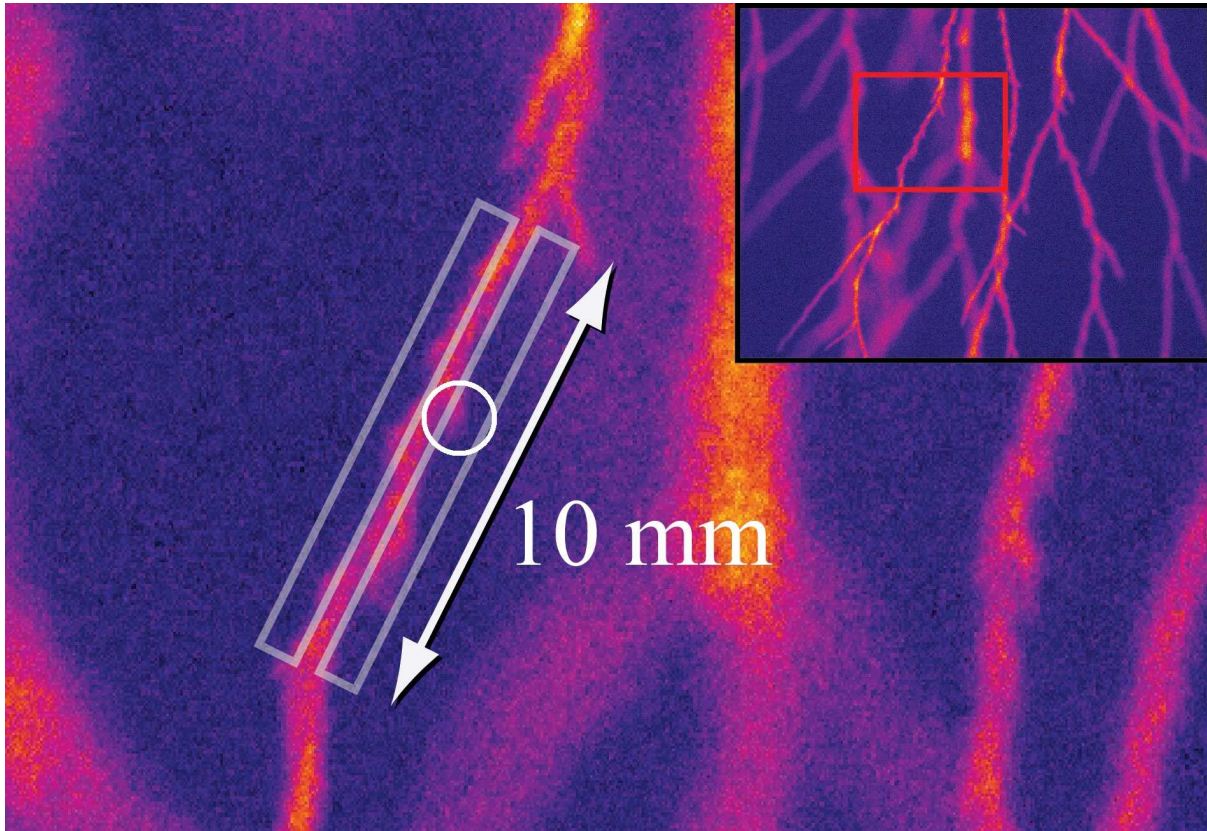


Figure 4.3: Zoom to segments of positive streamers in nitrogen with at most 1 ppm of impurities at 200 mbar. The white circle contains an example of a hair. The rectangular boxes mark the area in which hairs are counted for the purpose of determining the number of hairs per mm of streamer length. The picture is from [15].

oxygen admixture. Therefore we expect avalanches to overlap more easily in air, while in nitrogen with a 1 ppm oxygen admixture, the avalanches are more likely to be distinct; we will quantify this expectation in 4.4.3.

As the oxygen density decreases, so does the electron density outside the streamer channel. As a consequence, the avalanches that head towards the streamer channel become more and more rare, making stochastic effects visible, rather than forming a smooth channel. In experiments we see the channel being less smooth in the purest nitrogen with <0.1 ppm of oxygen (figure 4.2, left panel) than in nitrogen with an oxygen fraction between 10^{-3} and 10^{-5} (figure 4.2, right panel).

4.3.3 Distinction between hairs and branches

At first glance, the formation of hairs connected to the streamer channel seems to be similar to the branching of streamer channels. However, in the model for hair-formation we propose, there are significant differences between hairs and branches. During a branching

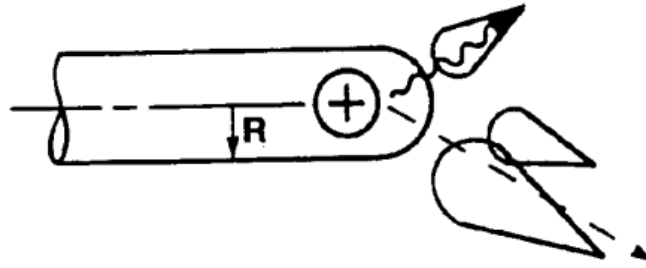


Figure 4.4: Schematic representation of a positive streamer propagating preceded by ionization avalanches as found in [79] and many other papers and textbooks. The drawing can be traced back to Raether in 1939 [80] and is discussed in more detail in [47]. We know now that the space charge is not uniformly distributed in the streamer head, but concentrated in a thin layer, in contrast to the sketch. The number and role of the avalanches is discussed in this article.

event, the streamer head is divided into fragments that due to electrostatic repulsion continue to propagate in different directions. Each fragment forms its own streamer channel with space charge layer, similar to the original streamer.

Hairs on the other hand do not form their own space charge layer. They consist of avalanches of electrons that are attracted by the positive charge in the streamer head. This property puts an upper bound on the length of the hairs, as they only start when the electric field exceeds the breakdown field. Streamer branches, on the other hand, generate their own enhanced electric field and can therefore propagate independently from the “parent” streamer. The branching of streamers is discussed in detail by Ebert *et al* [47, 81]. They concluded that an instability of the space charge layer is a necessary ingredient of streamer branching.

Despite the differences between hairs and branches, the appearance and frequency of both phenomena is correlated. Mixtures that create a high electron density outside the streamer channel will see less branching and less hairs, due to the smoother structure of the streamer head. Liu and Pasko [73] as well as Luque *et al.* [41] found that photo-ionization suppresses branching. Experiments show that streamers branch more easily in near-pure nitrogen mixtures than they do in air. Similarly, streamers in argon branch more easily than streamers in air.

4.4 Numerical Simulations and Results

4.4.1 Simulation model

Numerical simulations were performed with a code using an adaptive grid refinement scheme [33]. The model consists of a fluid description for the densities with drift, diffusion

and reaction terms. Included reactions are impact ionization, attachment, detachment and recombination. Photo-ionization is included using the widely used Zheleznyak model [57], implemented as described by Luque *et al* [41]. The electrode configuration is needle-plane. Simulations are done at standard temperature and pressure, using a voltage of 24 kV with an 8 mm gap between the tip of the needle and the planar electrode. Initially, no charged species are present in the computational domain except for a Gaussian seed located at the needle tip, serving as the source of streamer inception. Further details of the model and its parameters are described in chapter 2.

Since we use a fluid approximation, our code can not be used to model individual avalanches. For this, a particle code or a hybrid code such as the one by Li *et al* [77] is needed. However, we can still use results of the fluid code to draw conclusions on whether the presence of hairs and the corresponding feather-like structure can be expected or not.

4.4.2 Effect of oxygen density

The left panel of figure 4.5 shows the electron density and the boundary of the region where the electric field reaches the critical field and avalanches can occur; the simulation is in air at standard temperature and pressure. With the rate coefficients from BOLSIG+ [68] for impact ionization and attachment, as they were used in the simulation, this critical field is 32 kV/cm.

It is immediately obvious that at the outer boundary of the area where the electric field is above the breakdown field (see figure 4.5, left panel), the electron density is already 10^5 mm^{-3} . This will generate so many avalanches that they will overlap and are no longer distinct. Running the same simulation on a mixture of N_2 with 1 ppm O_2 gives completely different results. As can be seen in the right panel of figure 4.5, the electron density away from the streamer head is around 10^2 mm^{-3} . Additionally, the density of the attaching oxygen has been reduced by 5 orders of magnitude, so the critical field is lower than in air, around 20 kV cm^{-1} (rather than 32 kV/cm in air), which in turn means that avalanches can form further away from the streamer head. At these levels of electron-densities, 10^2 mm^{-3} , the number of avalanches in this nitrogen mixture will be low enough in number to be visually distinct, resulting in observable hairs in experiments.

In simulations performed at lower oxygen densities, the electron density away from the streamer head is even lower. With just 10 ppb of O_2 , the electron density outside the streamer is almost 2 orders of magnitude lower than in the simulation with 1 ppm of O_2 . At these levels of O_2 , the photo-ionization intensity is completely determined by the algebraic falloff of photon density when moving away from the photon source, the streamer head. With absorption lengths exceeding hundreds of meters, we can safely assume that the exponential falloff of photon density due to absorption events does not play a role.

Since we expect that the electron density outside the streamer channel is predominantly determined by the photo-ionization intensity, we expect that in these low levels of oxygen, the electron density outside the streamer is proportional to the oxygen density. The fact that this proportionality does not hold up completely is due to electron losses from attachment to oxygen. In mixtures with more oxygen, more of the electrons generated by photo-ionization are attached and consequently, the electron density is lower than

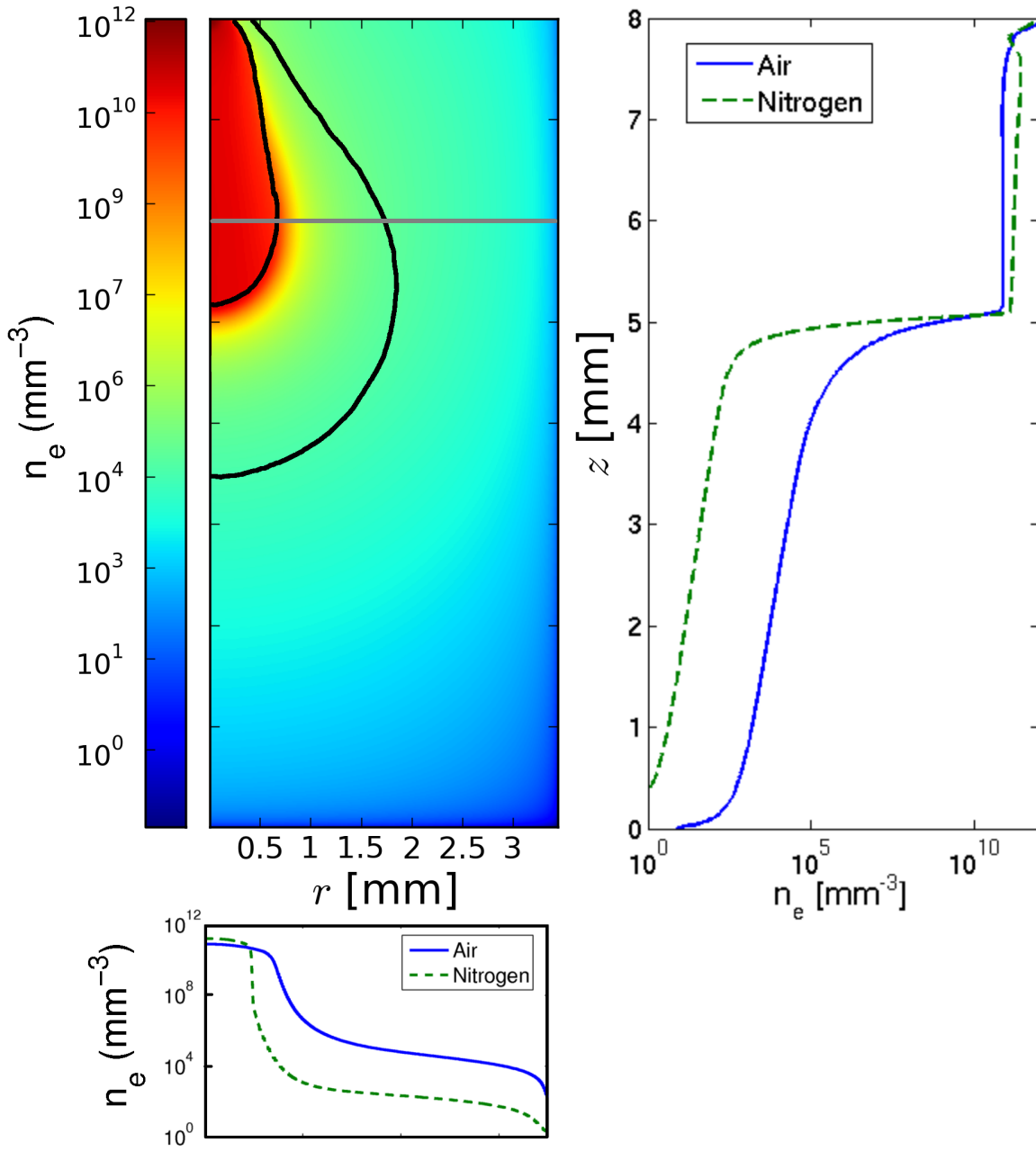


Figure 4.5: Left: Electron density in mm^{-3} of a positive streamer in air. The black lines indicate where the electric field reaches the breakdown value, so in the area between the black lines the field is above the breakdown value. Right: Electron density on the axis of positive streamers in air (solid line) and N_2 with a 1 ppm O_2 admixture (dashed line). Bottom: Electron density in mm^{-3} on a cross section of positive streamers in air (solid line) and N_2 with a 1 ppm O_2 admixture (dashed line). The gray line in the top-left panel indicates the location where the cross section was taken.

the simple proportionality argument would predict.

We must remark that at oxygen densities as low as 10 ppb (and corresponding to low electron densities outside the streamer), the density approximation used in our fluid model is no longer valid outside the streamer as the electron density in each cell becomes too low and stochastic effects start to play a role. Also, in our simulations and estimates we have ignored the effects of background ionization present in the domain. However, for these low electron densities, detachment from background ionization may be a non-negligible contribution to the electron density outside the streamer channel.

4.4.3 Estimating the number of hairs

We can estimate the number of hairs per mm of streamer length for our simulation in nitrogen with 1 ppm of oxygen by counting the number of free electrons outside the streamer. From our simulations, we can obtain the electron density in each cell of the simulation domain. In the simulation with 1 ppm of O_2 , we have an electron density of the order of 10^2 mm^{-3} to the sides of the streamer. However, the oxygen level in the experiments was probably about 0.2 ppm (with a total impurity below 1 ppm), whereas the simulations used 1 ppm. At low oxygen levels, the electron density outside the streamer is roughly proportional to the oxygen density [34]. So we would have approximately 20 electrons per mm^{-3} to the sides of the streamer in the conditions of the experiment. This translates to a distance between electrons of approximately 0.3 mm. We therefore expect to see approximately 3 hairs per mm of streamer length.

In experiments in nitrogen at 200 mbar, about 1 hair per mm of streamer length was observed in the image plane. According to scaling laws for streamers [18], the number of hairs does not depend on the pressure. This is because electron densities scale as the square of the gas density, while similar lengths scale as the inverse of the gas density.

Our theoretical estimate is only a rough estimate for the following reasons: Since our numerical code assumes cylindrical symmetry, a streamer can only be followed up to the point where it branches. This limits the length of streamers in nitrogen that we can simulate and therefore we can't directly match the parameters, such as electrode-gap, used in experiments. Furthermore, the individual hairs can't be simulated with a fluid code, which greatly limits the extent to which we can compare our estimate with experimental results.

4.5 Conclusions

Even though many streamer properties are remarkably insensitive to changes in gas composition, the formation of feather-like structures, small hairs connected to the main streamer channel, appears to be sensitive to the background gas. In air, such hairs were not observed, while in $N_2:O_2$ -mixtures with very small (less than 10^{-3}) O_2 fraction, the feather-like structures are visible. As the oxygen density is decreased, the feather-like structure becomes more pronounced as the streamer channels become less smooth.

We have proposed that the feather-like structures in positive streamers are due to

individual avalanches created by photo-ionization. As a photo-electron moves into the region where the electric field exceeds the breakdown field, repeated impact ionization creates an electron avalanche that drifts towards the positive charge in the streamer head. Since in air, the absorption length for photo-ionization is much smaller than in near-pure nitrogen, the electron density outside the streamer head is much higher and consequently avalanches overlap and are not visible as distinct hairs. In near-pure nitrogen, the electron densities outside the streamer head are much lower and individual avalanches may be seen. The numerical simulations with a fluid model, while not suited for simulation of individual hairs, have provided evidence that supports our explanation of the effect of the $\text{N}_2:\text{O}_2$ -ratio on the formation of hairs and feathers in positive streamers.

Furthermore, we have provided an estimate for the number of hairs in nitrogen with 1 ppm of oxygen and compared it with the experimental value. Our estimate has the same order of magnitude as the experimental result, but limitations of the simulation model limit the accuracy of this estimate. A particle model is required to study the phenomenon of feather-formation in more detail.

CHAPTER 5

Determining background ionization levels

This chapter was reproduced from parts of *Probing background ionization: Positive streamers with a varying pulse repetition rate and with a radioactive admixture*, S. Nijdam, G. Wormeester, E. M. van Veldhuizen and U. Ebert, J. Phys. D: Appl Phys, **44** (2011) 455201.

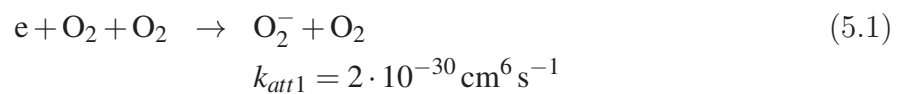
5.1 Introduction

In this chapter we will discuss the mechanisms that affect the level of background ionization that remains after a streamer discharge. With these mechanisms, we can make an estimate for the level of background ionization as a function of the repetition rate in repeated discharges or as a function of the addition of a radioactive admixture.

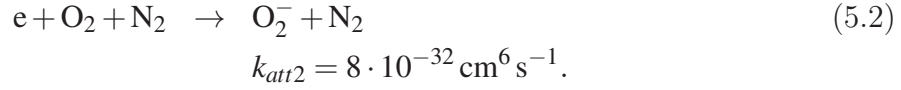
The streamer produces high (local) ionization levels (n_e up to 10^{15} cm^{-3}). After the discharge, electron density in the remainder of the streamer channel will decrease due to attachment and overall ionization density will decrease due to recombination. In addition, diffusion will cause the very localized ionization channel to spread out.

5.2 Electron attachment

In gas mixtures with high oxygen concentrations, electrons quickly attach to oxygen molecules [55, 67]:



or, in gasses with low oxygen concentrations:



Therefore the free electron density n_e will decrease as function of time as

$$\begin{aligned} \partial_t n_e = & - k_{att1} \cdot n_e \cdot [O_2]^2 \\ & - k_{att2} \cdot n_e \cdot [O_2] \cdot [N_2] \end{aligned} \quad (5.3)$$

if diffusion and drift are neglected. The attachment time t_{att} (the e-folding time of the exponential decay) is determined by equation (5.3) as

$$t_{att1} = (k_{att1} \cdot [O_2]^2)^{-1} \quad (5.4)$$

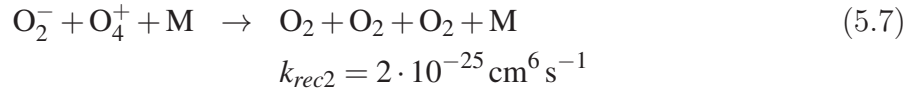
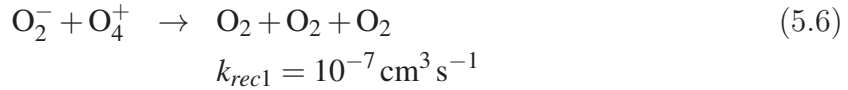
for air, or for oxygen concentrations below a few percent:

$$t_{att2} = (k_{att2} \cdot [O_2] \cdot [N_2])^{-1}. \quad (5.5)$$

The attachment time can vary significantly depending on oxygen content and pressure: in air at standard temperature and pressure, t_{att1} is about 20 ns while under the conditions used in section 3.4 ($N_2 + 1$ ppm O_2 at standard temperature and pressure) we find that t_{att2} is about 20 ms. In some of the experiments we compare with, a mixture of pure nitrogen with about 0.1 ppm of oxygen contamination at 200 mbar was used, resulting in a t_{att2} of about 5 s. The rates used here are based on a cold gas with no electric field present.

5.3 Recombination reactions

After electron attachment, the plasma will decay through recombination. In air we have two- and three-body ion-ion dissociative recombination that determine the rate of plasma decay (Pancheshnyi [55]):



where M denotes either a neutral oxygen or a neutral nitrogen molecule. The O_4^+ in these reactions is created quickly after the discharge from reactions of N_2^+ to N_4^+ , O_2^+ and finally O_4^+ , see e.g. [82]. The effective recombination rate for oxygen:nitrogen mixtures is therefore

$$k_{rec-air} \approx k_{rec1} + k_{rec2} \cdot [M]. \quad (5.8)$$

For pure nitrogen (i.e., without electron attachment), we use $k_{rec-N_2} = 5 \cdot 10^{-7} \text{ cm}^3\text{s}^{-1}$, which, at room temperature, is equal to $k_{rec-air}$ at a pressure of about 80 mbar ($[M] = 2 \cdot 10^{18} \text{ cm}^{-3}$).

If we neglect diffusion and drift of charged particles, and assume a spatially homogeneous neutral plasma, we can express the decrease of the ionization density n (with $n = n_+ = n_-$) as a function of time as:

$$\partial_t n = -k_{rec} \cdot n^2; \quad (5.9)$$

where t is time, and k_{rec} is the effective recombination rate for given gas composition and density, as described above. We can solve equation 5.9 by

$$n(t) = \frac{n(0)}{1 + n(0) k_{rec} t}, \quad (5.10)$$

where $n(0)$ is the ionization density at $t = 0$. In case of a streamer, $t = 0$ corresponds to the time where the external electric field is (instantaneously) switched off. For a streamer under standard conditions, the electrons density in the streamer channel, $n(0)$, is about 10^{13} to 10^{14} cm^{-3} . If

$$n(0)k_{rec}t \gg 1, \quad (5.11)$$

equation 5.10 can be approximated by

$$n(t) = \frac{1}{k_{rec} t}, \quad (5.12)$$

The requirement of equation 5.11 holds for all practical values of k_{rec} when $n(0)$ has the value corresponding with the density in a fresh streamer channel and t is of the order of magnitude of milliseconds or greater. That means that for streamers, the ionization density in the channel is independent of the precise level of initial ionization density.

This means that in air at atmospheric pressure, the ionization density in a streamer channel has decreased to roughly $2 \cdot 10^5 \text{ cm}^{-3}$ after 1 second, if we assume homogeneity. Since the ionization density $n(t)$ is inversely proportional to the time t in this approximation, we obtain a straightforward approximation for the ionization density as a function of repetition rate.

At other pressures, the ionization density after 1 second will be different, since k_{rec} changes according to equation 5.8. Therefore, in air, at 200 and 25 mbar, the ionization density 1 second after a discharge will be $9 \cdot 10^5$ and $4 \cdot 10^6 \text{ cm}^{-3}$ respectively. The inverse proportionality relation between time and ionization density, equation 5.12, still holds.

In pure nitrogen (with less than 1 ppm oxygen concentration), the attachment time will be much longer than the recombination time. Therefore, electrons will mostly recombine before they attach to oxygen. This means that any remaining negative charges in pure nitrogen will primarily be free electrons, while in air they are mostly negative ions.

Note that the reactions above are valid for nitrogen-oxygen mixtures at pressures close to atmospheric pressure. In mixtures with a pressure that is far from atmospheric, other processes may play a more significant role. For example, at pressures below 1 mbar, relevant for sprite discharges, dissociative attachment and recombination play an important

role as ionization loss mechanisms [83]. In addition, the equations derived above are valid only when bulk recombination is the dominant loss process. In situations where ionization losses occur due to surfaces or the refreshing of the gas by a gas flow between pulses, the above equations are no longer valid.

5.4 Repetition of streamer paths

5.4.1 Recombination and diffusion

The equations from the previous section assume a 0-dimensional situation with no spatial dependence of the ionization density. Streamers, however, are very localized, narrow channels. It is therefore to be expected that diffusion of the local channel will have an influence on ionization levels both inside and outside the channel. We include diffusion in equation 5.9 to obtain

$$\partial_t n = D_{ion} \cdot \nabla^2 n - k_{rec} \cdot n^2, \quad (5.13)$$

with $D_{ion} \approx 5 \cdot 10^{-2} \text{ cm}^2\text{s}^{-1}$ the diffusion coefficient at standard temperature and pressure in air in the absense of an electric field [38,55,84]. The diffusion coefficient scales inversely with pressure.

5.4.2 Ionization profile after a single pulse

To calculate the decay of the streamer channel through diffusion and recombination, we solve equation 5.13 with initial conditions that approximate experimental measurements of streamers by Nijdam *et al.* [36]. We assume high purity nitrogen at 200 mbar as background gas, where the diffusion coefficient is $D_{ion} \approx 0.25 \text{ cm}^2\text{s}^{-1}$. The width of the streamer channel was measured at $300 \mu\text{m}$ and we approximate the streamer channel by a Gaussian profile with a maximum ionization density of 10^{14} cm^{-3} and a full width at half maximum of $300 \mu\text{m}$. Since we investigate the time after the external electric field has been turned off and since almost all charged particles reside in the neutral channel rather than the charged skin, we neglect space charges and electric fields.

As mentioned in section 5.3, in high purity nitrogen, most electrons will stay free until they recombine with positive ions. Due to the faster diffusion of electrons compared to ions and the resulting charge separation and electric field, the electrons and ions don't diffuse independently, but rather via ambipolar diffusion. In nitrogen, the ambipolar diffusion coefficient is well approximated by the ion diffusion coefficient.

We numerically solve equation 5.13. From experimental observations [36], we know that different streamer channels are on average 30 mm apart in the conditions studied. Therefore we assume the streamers to be distributed in a hexagonal grid with 30 mm between each pair of neighbouring streamers. Such a hexagonal grid can be well approximated by a single streamer with cyllindrical symmetry and a symmetry boundary condition $\frac{\partial n}{\partial r} = 0$ (cf. illustration in [81]).

As initial condition we use a Gaussian profile centered at $r = 0$ for the streamer channel

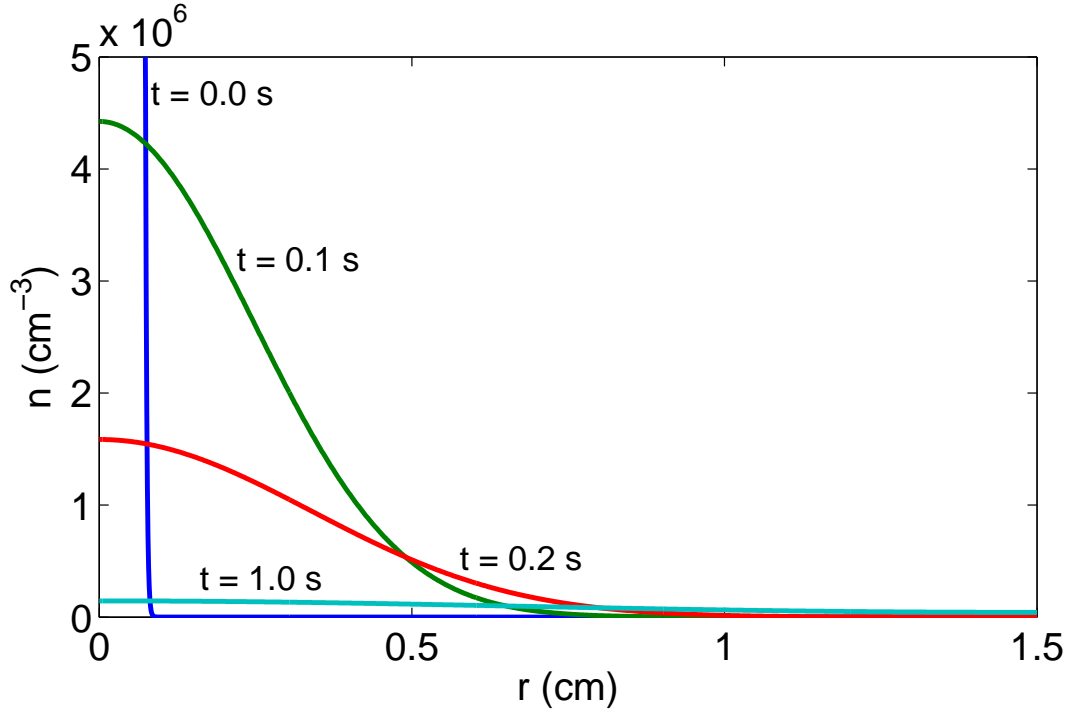


Figure 5.1: Ionization density as function of distance r from streamer axis at different times ($t = 0.0$ s, $t = 0.1$ s, $t = 0.2$ s and $t = 1.0$ s) after the streamer discharge in nitrogen at 200 mbar. Initial conditions are as described in equation 5.14, with $n_{ini,bg} = 10^3 \text{ cm}^{-3}$, $n_{ini,channel} = 10^{14} \text{ cm}^{-3}$ and FWHM = 0.3 mm. Note that the line for $t = 0$ extends outside the plotted area to its maximum of 10^{14} cm^{-3} at $r = 0$ cm.

with maximum $n_{ini,channel}$ with a homogeneous background density $n_{ini,bg}$:

$$n(0, r) = n_{ini,bg} + n_{ini,channel} \cdot e^{-\frac{r^2}{\sigma^2}}. \quad (5.14)$$

The width of the channel, taken as the full width at half maximum (FWHM) is related to σ by $\text{FWHM} = \frac{\sigma}{2\sqrt{\ln(2)}}$.

We take $n_{ini,bg} = 10^3 \text{ cm}^{-3}$, which corresponds to the ambient background ionization density in a virgin gas as discussed in section 3.1.3. $n_{ini,channel} = 10^{14} \text{ cm}^{-3}$ and FWHM = 0.3 mm. In figure 5.1 we see the ionization density after different amounts of time. After 0.1 s, the density at the center of the channel ($4 \times 10^6 \text{ cm}^{-3}$) is only 3-4 orders of magnitude higher than the density at the edge of the domain (10^3 cm^{-3} at $r = 15$ mm), down from the 11 orders of magnitude difference at $t = 0$. This means that the channel is still present, although the width of the channel has increased considerably. The full width at half maximum has increased from 0.3 mm at $t = 0$ to 5.5 mm at $t = 0.1$ s. After one second, the width of the channel has increased even more, to 15 mm, which is half the width of the system. In addition, the ratio of ionization density between the center and the edge has decreased to 3.4. So at this time, one second after the discharge, the channel of the previous discharge becomes rather faint and spread out.

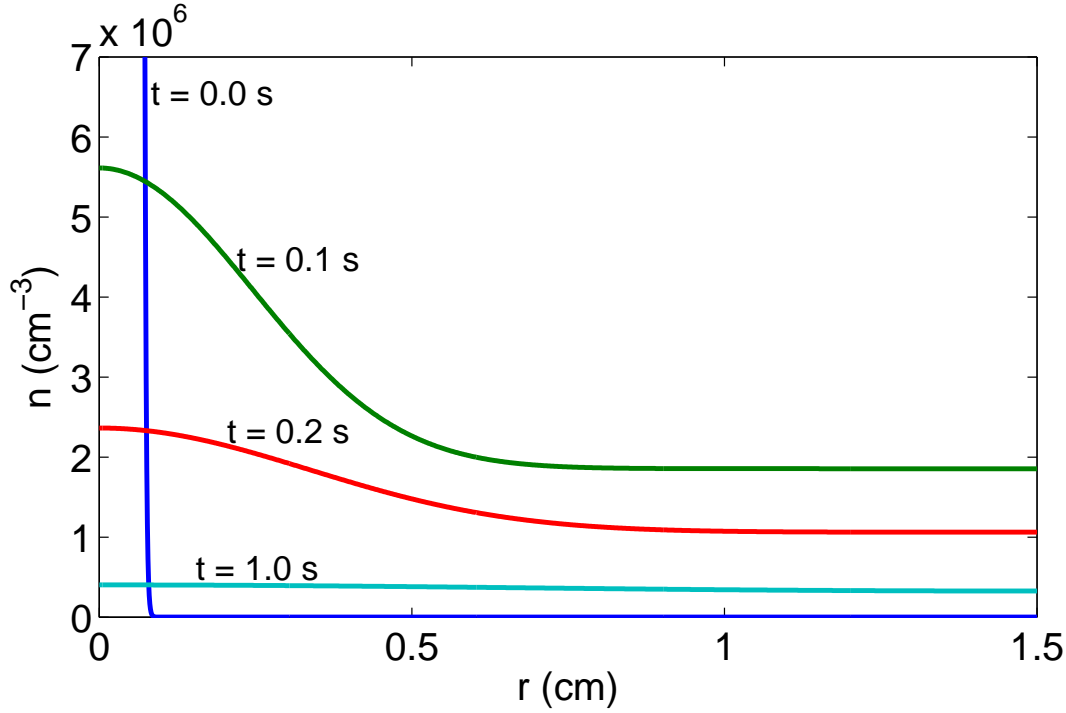


Figure 5.2: Ionization density as function of distance r from streamer axis in the equilibrium situation where spatially averaged background ionization level remains constant from pulse to pulse. Plotted curves show the ionization density directly before the next pulse in the sequence at different frequencies, 10 Hz ($t = 0.1$ s), 5 Hz ($t = 0.2$ s) and 1 Hz ($t = 1.0$ s) in nitrogen at 200 mbar. For reference, the curve $t = 0$ shows the ionization density directly after the first discharge in a sequence. Initial conditions are as described in equation 5.14, with $n_{ini,bg}$ the calculated equilibrium level n_{eq} , $n_{ini,channel} = 10^{14} \text{ cm}^{-3}$ and FWHM = 0.3 mm. Note that the line for $t = 0$ extends outside the plotted area to its maximum of 10^{14} cm^{-3} at $r = 0$ cm.

5.4.3 Ionization profile after repeated discharges

We determine the spatially averaged ionization density by numerically integrating the calculated ionization density over cylindrical coordinates

$$n_{avg}(t) = \frac{\int_0^R 2\pi r n(r,t) dr}{\pi R^2} \quad (5.15)$$

with $R = 1.5$ cm. To calculate the background ionization level after many pulses, we use the average ionization density calculated with equation 5.15 and use this value for $n_{ini,bg}$ in the initial conditions of the diffusion-recombination model, equation 5.14. We iterate this calculation until n_{avg} converges to an equilibrium value n_{eq} . For $t = 0.1$ s we found that $n_{eq} = 2.04 \cdot 10^6 \text{ cm}^{-3}$. This equilibrium value was found to be independent of the choice of the initial homogeneous background ionization level for the first pulse, as was expected.

If we use n_{eq} as $n_{ini,bg}$, we obtain the ionization density distribution in the equilibrium

case, which can be seen in figure 5.2. We find that after $t = 0.1$ s, the ratio between the ionization density at the center and at the edge has decreased to only 3.0. The width of the channel is approximately 5 mm. This means that in repetitive discharges in 200 mbar nitrogen, the channel produced by the streamer has largely dissipated by the time the next discharge starts.

At 1 Hz, the equilibrium background ionization density can be computed using the method described above. We find that with 1 s between discharges, $n_{eq} \approx 3.5 \cdot 10^5 \text{ cm}^{-3}$. With this level of background ionization, the ratio of ionization density between the center of the channel and the edge of the domain is only 1.23.

Based on these calculations, it is uncertain whether a homogenous background ionization density is a reasonable approximation when simulating repeated discharges in air with repetition frequencies of 10 to 30 kHz [85], since the diffusion coefficients and recombination rates in air are similar to those in nitrogen.

Nikipelov *et al* [86] recently showed that at the time-scales we have studied (0.1–1 s), ionization densities in the streamer channel can be lower than those outside the channel. The abundance of excited species in the channel can enhance the effective recombination rates leading to a greater loss of ionization in the channel than we calculated. Therefore the ionization density inside the channel can be lower than the density outside the channel at sufficiently long timescales.

We find that the equilibrium ionization densities calculated in this section are about an order of magnitude lower than those calculated with the assumption of a homogeneous initial distribution (equation 5.12). The cause for this is that the ionization density in the streamer channel is higher than in a homogenous distribution with the same initial amount of charged particles. Consequently, the recombination rate will be higher in this area of high density.

We found that at 1 Hz, using a homogeneous initial density results in a background density of approximately $2 \cdot 10^6 \text{ cm}^{-3}$, while the diffusion-recombination model yields a background density of $3.5 \cdot 10^5 \text{ cm}^{-3}$. Similarly, at 10 Hz, the homogenous initial density results in a background density of approximately $2 \cdot 10^7 \text{ cm}^{-3}$ and the diffusion-recombination model yields $2.0 \cdot 10^6 \text{ cm}^{-3}$. We note that the value n_{eq} calculated with the diffusion-recombination model depends on assumptions for the width of the streamer channel and the separation between different channels. As streamer density increases, either through increase of streamer width or decrease of channel separation distance), n_{eq} approaches $\frac{1}{k_{rec}t}$. In air, background ionization density can be increased due to photo-ionization increasing the ionization density outside the streamer channel.

5.4.4 Comparison with experiments

In figure 5.3, taken from Nijdam *et al* [36], three consecutive discharges in nitrogen at 200 mbar with a repetition frequency of 10 Hz are shown separately and overlayed on top of each other with different colours. If streamers follow the path of a previous discharge, it will be rendered as a composite colour. Instead, we see no channels from different discharges coinciding. From this we can conclude that even at 10 Hz, streamers do not tend to follow the path of previous discharges and that therefore the ionization trail remaining after a

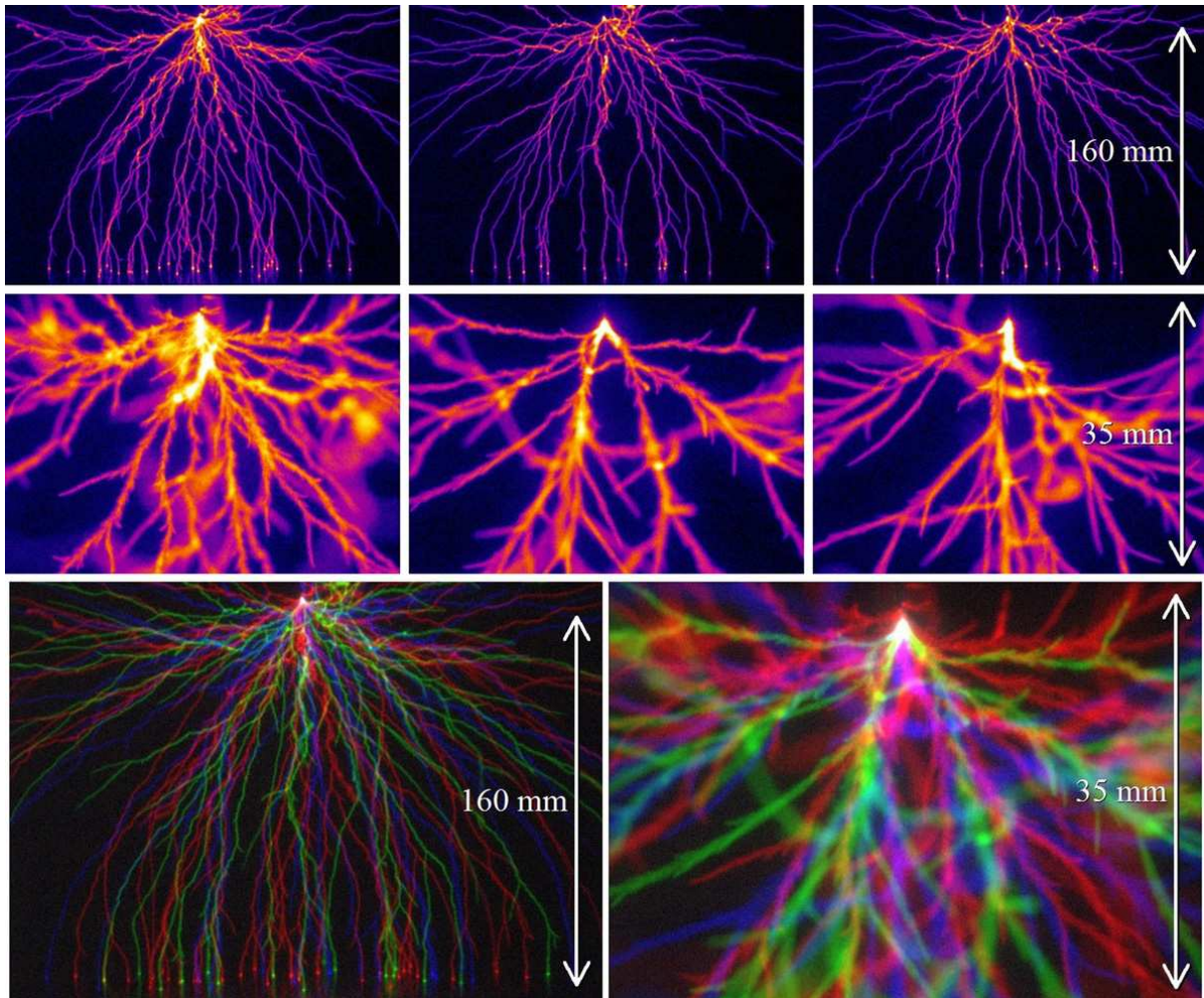


Figure 5.3: Two series of three consecutive images of streamers in nitrogen in overview (top row) and zoomed (middle row), both under similar conditions and with 10 Hz repetition rate. In the bottom row, the three consecutive images from the first or second row are coloured in red, green and blue, respectively, and overlaid. Therefore repetitive streamer paths are rendered yellow (red + green), cyan (green + blue) or white (red + green + blue), while single streamer paths are rendered red, green and blue. Magenta areas show where the paths from the first and third discharges, but not the second, overlapped. All images are acquired in 200 mbar nitrogen (impurities less than 1 ppm). In both series, the first three discharge pulses after a break of about 10 s are shown. Picture is from Nijdam etal [36].

discharge is faint enough to no longer affect the path of the next discharge.

This is in agreement with the results from our diffusion-recombination model, where we found the ionization density in the center of the streamer channel to only be 3 times as high as the ionization density in the gap between the different channels, where this difference is 9 orders of magnitude immediately after the discharge. In addition, with the results of Nikipelov *et al* [86], the ionization density in the channel will be even lower and the channel may even repulse the next discharge.

5.5 Constant ionization sources

In addition to ionization from a previous discharge, background ionization can also be introduced by means of an external source. This external source can be cosmic rays, natural radioactivity or a radioactive admixture. If we assume homogeneity, we can include a constant ionization source S in equation 5.9 to obtain

$$\partial_t n = S - k_{rec} \cdot n^2. \quad (5.16)$$

In equilibrium, we have $\partial_t n = 0$ and we can solve

$$S - k_{rec} \cdot n^2 = 0 \quad (5.17)$$

to obtain the equilibrium ionization density

$$n = \sqrt{\frac{S}{k_{rec}}}. \quad (5.18)$$

Effect of transport-data on streamer propagation

In previous chapters we have studied the effect of different levels of source electrons in front of the streamer head on the propagation of positive streamers and found streamers to be remarkably insensitive to order-of-magnitude changes to the density of free electrons ahead of the streamer front. Additionally, while replacing photo-ionization with detachment from background ionization yielded noticeably different streamers (thinner, higher maximal electric field), both mechanisms of production of source electrons were able to produce sufficiently many electrons for the propagation of positive streamers.

In these previous chapters, the parameters D and μ in the streamer model, representing the diffusion and mobility coefficients respectively, were taken as constant. This is a simplified approximation of reality as these coefficients typically depend on the local electric field. In this chapter, we study the effect of this choice on streamer simulations by comparing simulations with the previously used constant coefficients to simulations of streamers with field-dependent values of the diffusion and mobility coefficients. We briefly discuss the computation of these coefficients and then analyze their effect on our streamer simulations. Finally, we discuss an analytic relation between electric field inside and outside the streamer, velocity, radius and electron mobility, obtained by Ratushnaya *et al.* [24], which was found for streamers simulated with constant coefficients, and we verify that this relation still holds when the constant coefficients are replaced by field-dependent coefficients.

6.1 Calculation of transport-data

6.1.1 Monte Carlo methods

As a swarm of charged particles moves under the effect of an electric field, the particles collide with the neutral background gas. The various types of collisions each occur with different probabilities, determined by the cross section of the interaction. Averaging the

motion of the charged particles provides a means to obtain the mobility and diffusion coefficients. To do so computationally, one starts with an initial swarm of particles and applies Monte Carlo techniques to follow the particles as they are accelerated by the external electric field and lose energy by undergoing the various kinds of collisions. These so-called Monte Carlo swarm simulations have been used by various authors [77,87].

The disadvantage of these Monte Carlo simulations is that they are computationally expensive. To obtain high accuracy, a sufficiently large number of simulated particles as well as a sufficiently long simulation time is required, placing requirements on both the amount of available computer memory and on the time of the computation.

6.1.2 Boltzmann equation solvers

An alternative approach to obtain transport-data comes from the Boltzmann equation. A swarm of charged particles under the influence of an electric field can be described by the phase-space distribution function $f(\mathbf{r}, \mathbf{c}, t)$ with \mathbf{r} the spatial coordinates, \mathbf{c} the coordinates in velocity space and t the time. The phase-space distribution function can be obtained from the Boltzmann equation:

$$\frac{\partial f}{\partial t} + \mathbf{c} \cdot \frac{\partial f}{\partial \mathbf{r}} + \frac{q}{m} \mathbf{E} \cdot \frac{\partial f}{\partial \mathbf{c}} = -J(f, f_0). \quad (6.1)$$

Here q and m stand for the charge and mass of the particle, respectively, \mathbf{E} is the externally applied electric field and $J(f, f_0)$ represents the electron-neutral collision operator, which accounts for elastic, inelastic and non-conservative collisions, which are collisions that don't conserve the number of particles, such as ionization and attachment collisions.

Equation 6.1 can be solved by using the so-called two-term approximation where the distribution function f is expanded to first order in the deviation from isotropy [88]. This approach is employed by the BOLSIG+ program [68], which is a userfriendly tool that can be used to generate transport data and reaction rate coefficients.

Alternatively, a multi-term technique can be used to obtain more accurate results when the distribution function is further from isotropy. Such a technique was developed by Dujko *et al* [89] who have used it to generate transport data for a wide variety of gas mixtures.

6.1.3 Distinction between bulk and flux coefficients

When dealing with transport coefficients obtained from swarm experiments, one must distinguish between bulk and flux coefficients. To compute the average electron drift velocity (and from that the mobility) from swarm data, one can simply take the average displacement of the center of mass of the swarm and divide it by the duration of the experiment. Similarly, the diffusion coefficient can be obtained by calculating the average distance of particles from the center of mass of the swarm as a function of time.

However, in the presence of non-conservative collisions, there is ambiguity as to which particles to take into account when calculating these averages. If we use all particles present in the swarm, including the effects of the non-conservative collisions (such as ionization

and attachment), we obtain the so-called bulk transport data. However, if we only follow the particles that were originally present in the swarm and ignore any particles created by non-conservative collisions, we obtain the so-called flux transport data.

In the presence of high electric fields, non-conservative collisions become increasingly important and the difference between bulk and flux transport coefficients will increase. From experimental measurements, one can only obtain bulk coefficients as there is no way to distinguish between the original electrons in the swarm and those created by ionization during the experiment. In swarm simulations, both bulk and flux data can be easily computed. Details of the computation of bulk and flux transport coefficients from swarm simulations can be found in [87]. In the simulations performed in this chapter, we have used flux transport coefficients.

6.1.4 Transport-data used in this chapter

In this chapter, we use the transport data computed with this multi-term approach. For a full description of the multi-term solution of the Boltzmann equation for electrons (and light ions) in a spatially homogeneous electric field, the reader is referred to Dujko *et al* [89]. We note that the solution is obtained by expanding the directional dependence of the distribution function $f(\mathbf{r}, \mathbf{c}, t)$ in velocity space in terms of spherical harmonics. The speed dependence of $f(\mathbf{r}, \mathbf{c}, t)$ is treated by an expansion in terms of Sonine polynomials. Finally, the spatial dependence is treated by a density gradient expansion. With these decompositions, the Boltzmann equation is transformed into a hierarchy of doubly infinite coupled inhomogeneous matrix equations for the time-dependent moments. Finite truncation of the expansions allows for the hierarchy to be solved via matrix inversion. From the moments obtained this way, the desired transport coefficients can be calculated.

We assume an air-like mixture ($\text{N}_2:\text{O}_2 = 80:20$) with neutral temperature 300 K. Cross sections for electron scattering in N_2 and O_2 that were used in the computation are from [90–92].

We note that calculations of these transport data were performed using reduced electric fields measured in Td (Townsend, $1 \text{ Td} = 10^{-21} \text{ Vm}^2$).

Figures 6.1 and 6.2 show the mobility and diffusion coefficients respectively as a function of reduced electric field. The previously used, constant value for the mobility coefficient is $380 \text{ cm}^2\text{V}^{-1}\text{s}^{-1}$, which means that for $E < 63 \text{ kV/cm}$, the field-dependent mobility will be higher than in our previous simulations. Similarly, the previously used value for the diffusion coefficient is $1800 \text{ cm}^2\text{s}^{-1}$, so in the streamer head and other areas with high electric field ($E > 150 \text{ kV/cm}$), the previous simulations tended to underestimate the diffusion.

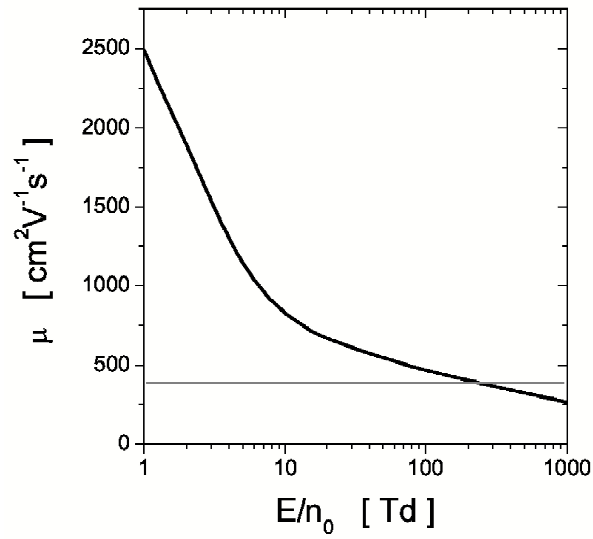


Figure 6.1: Electron mobility as a function of E/n_0 in a $N_2:O_2 = 80:20$ air-like mixture. Dark gray line indicates the previously used value.

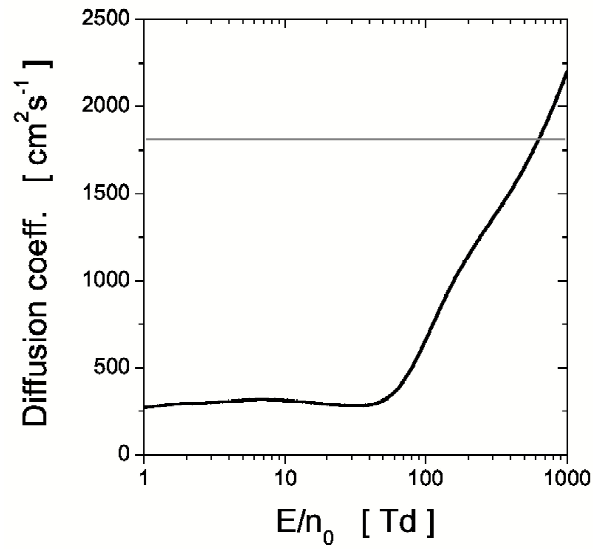


Figure 6.2: Diffusion coefficient for electrons as a function of E/n_0 in a $N_2:O_2 = 80:20$ air-like mixture. Dark gray line indicates the previously used value.

6.2 Effect of transport-data on positive streamers

We have extended our simulation code with the transport data described in the previous section (and plotted in figure 6.1 and figure 6.2). To investigate the effect of this change on streamer propagation, we have simulated a streamer in an 8 mm gap with a 24 kV potential in air. The conditions are the same as those described in chapter 3, that is, a needle-plane configuration with a positively charged needle, a background gas of N_2 and O_2 with a 80:20 mixing ratio, no initial homogeneous background ionization and a Gaussian seed of electrons and positive ions at the tip of the needle. The reactions, their rate coefficients and the photo-ionization model are also the same as in chapter 3.

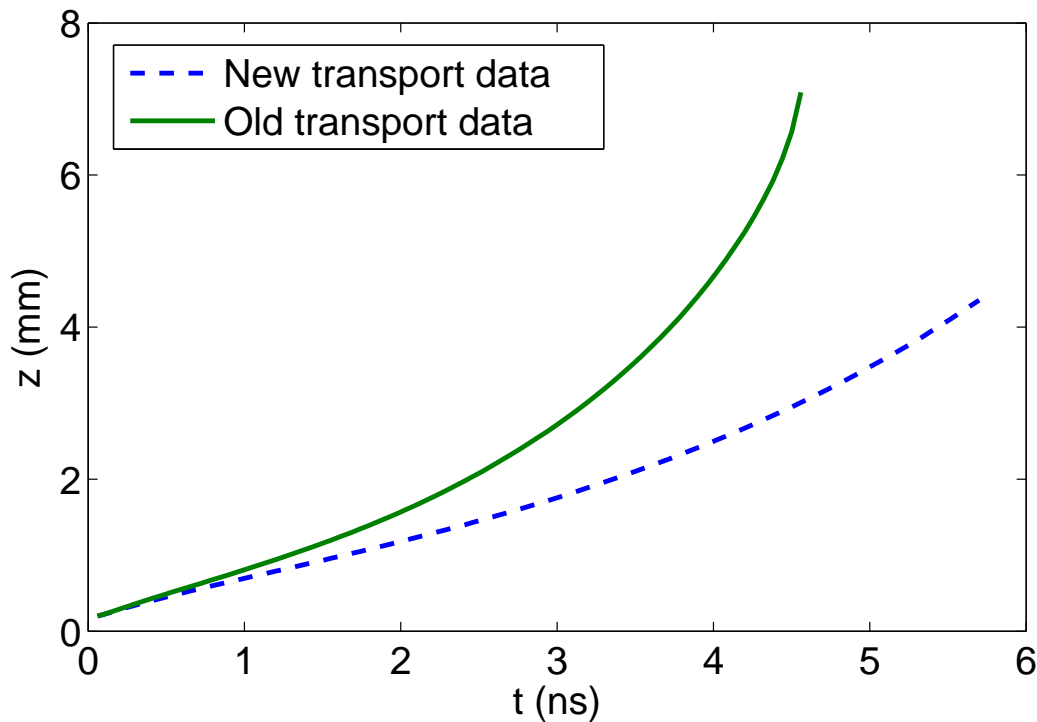


Figure 6.3: Simulation of positive streamers in air at standard temperature and pressure. The position of the streamer head is plotted as a function of time for streamers with old transport coefficients (solid curve) and new transport data (dashed curve). Streamers in a needle-plane electrode configuration with 24 kV potential over an 8 mm gap.

Figure 6.3 shows the position of the streamer head as a function of time for positive streamers both with the original, constant transport coefficients as well as with the new field-dependent transport coefficients. It is immediately obvious that with the field-dependent transport data, streamers are slower than with the constant transport coefficients. The difference in velocity is initially approximately 30%, but increases as the streamer with constant transport coefficients more rapidly approaches the cathode.

Figure 6.4 shows the electric field profile of both streamers from which we can determine the width of the streamers. The streamer with the new transport data appears

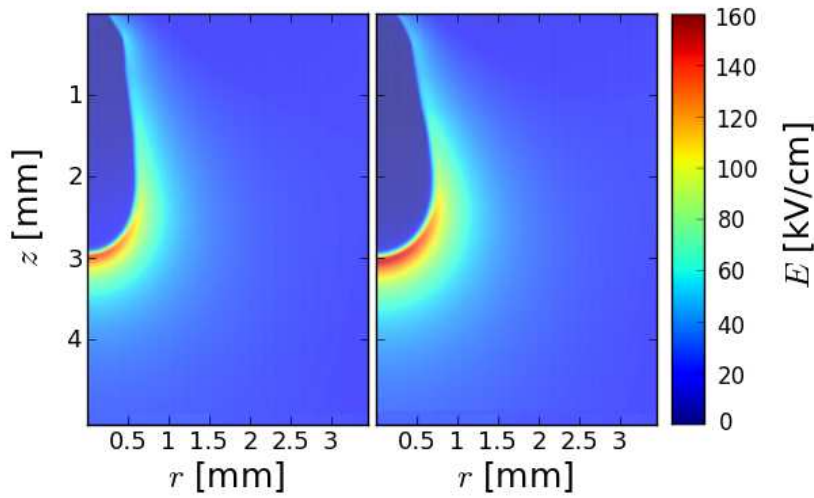


Figure 6.4: Absolute electric field for positive streamers in air at standard temperature and pressure. The streamer on the left uses the new field-dependent transport coefficients while the streamer on the right uses the old constant coefficients. The length of the gap is 8 mm, only the top 5 mm is shown in the figure. Both panels are snapshots taken at times to ensure that both streamers were in a similar stage of propagation and are therefore from different timesteps (left: $t = 4.5$ ns, right: $t = 3.2$ ns).

to be slightly thinner than the one with the constant coefficients. In addition, the field-dependent transport data yield streamers with a maximal electric field that is about 10% lower, as can be seen in figure 6.5. The field-dependent mobility coefficient is higher than the constant value previously used at fields below 63 kV/cm. Consequently, in the area away from the streamer head, the electron mobility will be higher in the simulation with field-dependent data than in the simulation with constant data and electrons flow into the channel more quickly.

In addition, we find that the photo-ionization rate is lower due to the lower maximal electric field in the streamer head, so we conclude that, as seen in figure 6.6, the electron density in front of the streamerhead is lower in the simulations with the field-dependent transport data as less electrons are created by photo-ionization and the electrons drift into the streamer channel more rapidly due to the higher mobility in the background field. The reduced electron density in front of the streamer head can result in slower streamers as seen in chapter 3.

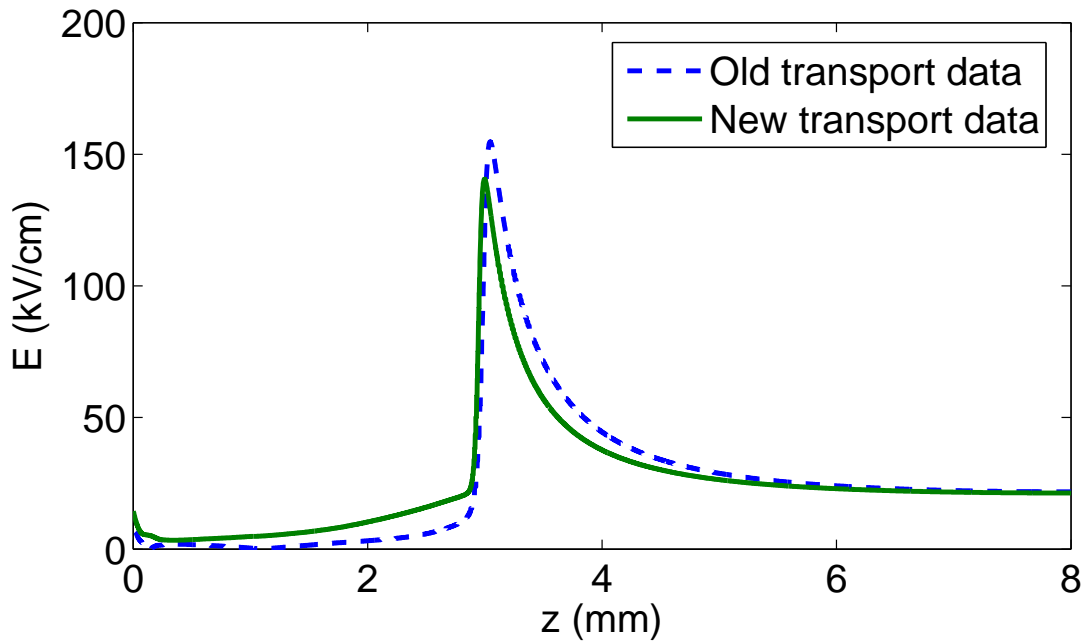


Figure 6.5: Absolute value of the electric field on the streamer axis for positive streamers in air at standard temperature and pressure. The solid green line shows the streamer using the new field-dependent transport coefficients while the dashed blue line shows the streamer using the old constant coefficients. Streamer propagation is from left to right.

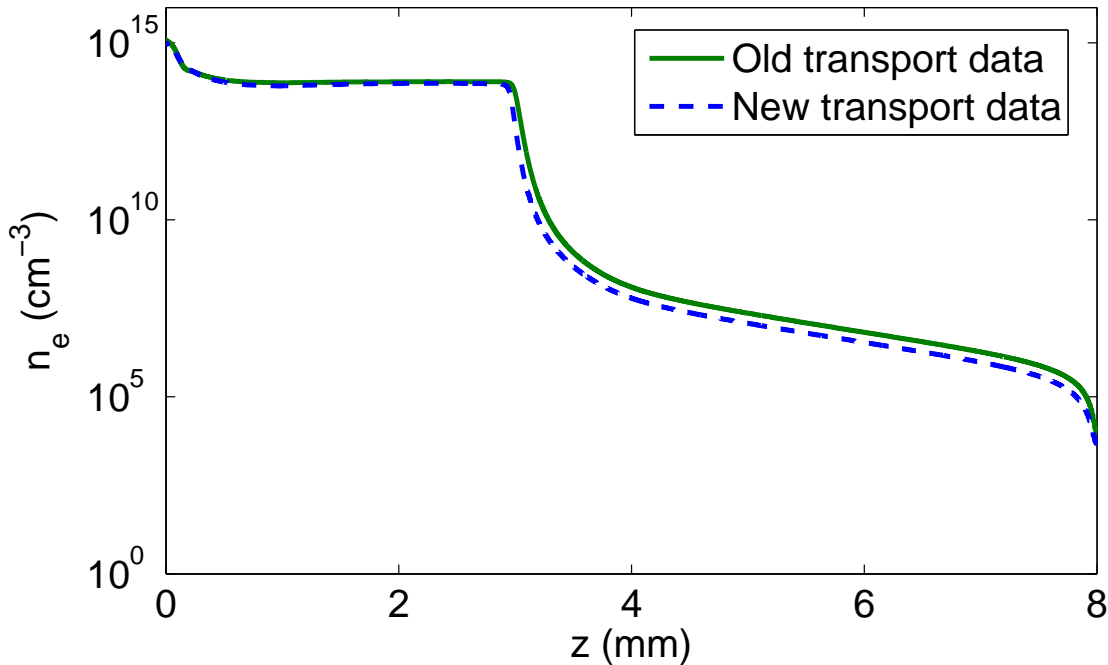


Figure 6.6: Electron density on a logarithmic scale on the streamer axis for positive streamers in air at standard temperature and pressure. The solid green line shows the streamer using the new field-dependent transport coefficients while the dashed blue line shows the streamer using the old constant coefficients. Streamer propagation is from left to right.

6.3 Testing predictions for macroscopic streamer properties

In order to model structures containing many separate streamers, such as sprite discharges, it is required to move away from modelling the dynamics of an individual streamer and its propagation through the medium and consider individual streamers as simple objects that propagate using a small set of simple rules. Therefore it is necessary to be able to characterize a streamer by a small number of parameters, such as radius, velocity, maximal electric field, etc...

6.3.1 Uniformly translating streamers

This characterization involves a uniformly translating streamer, which is a streamer that propagates with a constant velocity and whose properties such as radius and electric field are constant in time. While uniform translation is almost always an approximation, in long systems it can be a good approximation. If we assume uniform translation and apply the following coordinate transformation,

$$\xi = z - vt \quad (6.2)$$

from the (z, t) -frame to the (ξ, t) -frame moving with the streamer velocity, the derivatives with respect to t transforms into

$$\frac{\partial}{\partial t} = \frac{\partial}{\partial t} \Big|_{\xi} - v \frac{\partial}{\partial \xi} \quad (6.3)$$

and due to the uniform translation the time derivative on the right hand side vanishes leaving only a derivative with respect to ξ . Substituting this transformation into the streamer equations 2.20 and 2.21 yields a set of ordinary differential equations that can be studied analytically.

Several authors have used this approach to study the characteristics of a uniformly translating streamer front. Ebert *et al* [93] studied one-dimensional fronts. Naidis [94] has obtained relations between velocity, radius and other streamer properties for positive and negative streamers with photo-ionization. Ratushnaya *et al* [24] derived an expression for the relation between streamer velocity, radius, electron mobility, internal electric field and maximal electric field.

6.3.2 Relation between velocity, interior field, maximal field and radius

While the expression derived by Ratushnaya *et al* explicitly includes a dependence on a field-dependent electron mobility, they compared their result with streamers simulated with constant mobility only. We apply their expression to streamers that have been simulated with field-dependent mobility. The expression derived by Ratushnaya *et al.* is

$$j^- = \frac{2v\epsilon_0 E_{max}}{R} \quad (6.4)$$

where v is the velocity of the streamer, R the radius of curvature of the streamer head, E_{max} the maximal electric field, which is assumed to lie on the symmetry axis just in front of the space charge layer and j^- the electric current density just behind the space charge layer in the streamer head, given by

$$j^- = en_e^- \mu_e(E^-) E^- \quad (6.5)$$

which is the electron density just behind the space charge layer, n_e^- , multiplied by the electron drift velocity, $\mu(E^-)E^-$ (with E^- the electric field just behind the space charge layer), and the electron charge e .

Substituting the expression for j^- from equation 6.5 in equation 6.4 we obtain

$$E^- = \frac{2v\epsilon_0 E_{max}}{en_e^- \mu_e(E^-)} \quad (6.6)$$

which we will refer to as the Ratushnaya-equation. If we rescale this equation to dimensionless units as described in section 2.1.1 we obtain the dimensionless Ratushnaya-equation (the superscript ^d which denotes dimensionless units has been omitted for readability):

$$E^- = \frac{2vE_{max}}{n_e^- \mu_e(E^-)}. \quad (6.7)$$

The Ratushnaya-equation is an expression that relates the electric field in the streamer head to some characteristic streamer properties such as velocity, radius and enhanced electric field. In the case of streamers simulated by Ratushnaya *et al* and in simulations discussed in earlier chapters, where a constant electron mobility was used, equation 6.7 simplifies to an expression from which E^- can be directly calculated:

$$E^- = \frac{2vE_{max}}{n_e^-}. \quad (6.8)$$

The mobility term drops out since in dimensionless units the constant electron mobility is equal to 1. For streamers simulated with field dependent mobility, the mobility data, $\mu_e(E^-)$ is provided as input in tabulated form, the Ratushnaya-equation has to be solved numerically for E^- .

6.3.3 Electron density inside the streamer

We note that as outlined in the appendix of [95] the electron density behind a negative planar streamerfront without photo-ionization can be well approximated by the equation

$$n_e(E_{max}) = \frac{\epsilon_0}{e} \int_0^{|E_{max}|} \alpha(|\mathbf{E}|) dE \quad (6.9)$$

(with $\alpha(\mathbf{E})$ the Townsend coefficient for ionization as discussed in section 2.1) while for positive streamers, with photo-ionization and a curved front, approximation 6.9 for $n_e(E_{max})$ gives only half of the numerical value obtained from simulations [24, 96]. No

explanation for this discrepancy has been given yet. A correct characterization of the electron density as function of the maximal electric field is the second component of the analytical characterization of streamers.

The original derivation of equation 6.9 by Li *et al* [95] uses the Townsend model for impact ionization, equation 2.6, while our simulation uses tabulated reaction coefficients, modeled with equation 1.1. In addition, if an electronegative admixture such as oxygen is present, the effect of attachment should be included as a negative correction to the ionization source. Therefore, we have the following expression for $\alpha(|\mathbf{E}|)$:

$$\alpha(|\mathbf{E}|) = \frac{n(k_i - k_a)}{\mu_e(|\mathbf{E}|)|\mathbf{E}|}, \quad (6.10)$$

with n the neutral density, k_i the combined ionization rate for oxygen and nitrogen impact ionization and k_a the attachment rate.

6.3.4 Comparison between simulation and prediction

In order to verify the validity of the Ratushnaya-equation for streamers with non-constant mobility coefficients, we have simulated a streamer in a longer gap and with a lower voltage, since the derivation of the equation assumes a uniformly translating streamer. With a high voltage, streamers are more likely to accelerate. In addition, in simulations with a short gap between the electrodes, the streamer quickly approaches the cathode which causes the background field in front of the streamer to rise and therefore the streamer to accelerate. We note that the original comparison by Ratushnaya *et al* (figure 5 in [24]) was made with a simulated streamer that was both increasing in velocity and radius, violating the requirement of uniform translation.

We simulated a positive streamer in air (with photo-ionization, without initial background ionization) in a 30 mm needle-plane gap. A voltage of 42.7 kV was applied to the needle electrode. As can be seen in figure 6.7, after the initial formation stage, the streamer enters a stage of constant acceleration until it approaches the cathode and the acceleration rapidly increases. This behavior is similar to that observed by Ratushnaya *et al* in [24]. For further analysis, we have taken simulation data from $t = 12$ ns, which is in the middle of the constant acceleration stage. At this point, the streamer shape is well developed while not yet being strongly affected by proximity to the cathode.

As can be seen in figure 6.8, the radius of the streamer gradually increases with time, as was also seen by Ratushnaya *et al*, who used very similar conditions (electric field, domain size, etc...). We note that at the time-step picked for further analysis ($t = 12$ ns) the streamer channel is already clearly formed, but still only showing minimal signs of expansion.

E_{max} was obtained by finding the maximum of the electric field strength on the streamer axis (plotted in figure 6.9) and was found to be 114 kV/cm. The radius of curvature the streamer was determined by first finding the r -coordinate of the charge maximum while fixing z , for all z in the streamer head area and then fitting a circle to this data. We found $R = 0.25$ mm. n_e was taken as the maximal electron density in the area behind

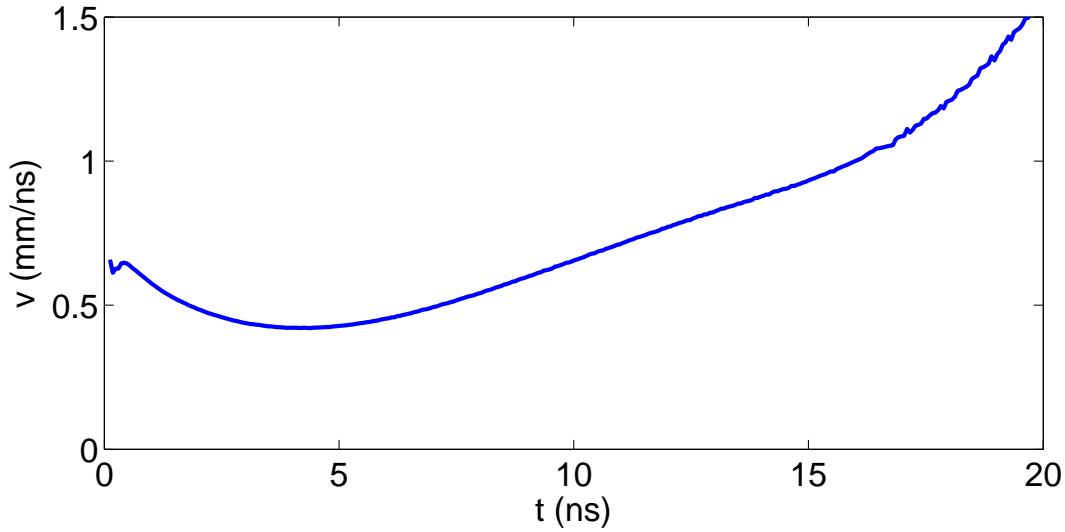


Figure 6.7: Velocity of a positive streamer in air in a 30 mm gap. The voltage applied to the needle electrode is 42.7 kV, the background electric field away from the needle (in the absence of space charges) is 12 kV/cm. The last 5 ns of the simulation, the time interval from 20 to 25 ns, during which the streamer rapidly accelerates as it approaches the cathode, were omitted from the figure.

the streamer front (where we remark that this density is almost constant in the streamer interior), $n_e = 3.43 \times 10^{13} \text{ cm}^{-3}$.

If we solve the Ratushnaya-equation 6.7 for E^- , we obtain $E^- = 3.86 \text{ kV/cm}$. In figure 6.9 this value of E^- was plotted together with the electric field strength on the streamer axis at $t = 12 \text{ ns}$. As can be seen in the figure, while the electric field is not constant in the streamer interior, the computed value of E^- is a very good approximation to the interior field.

If we apply equation 6.9 for the prediction of the electron density behind the front, we obtain a predicted value of $1.68 \times 10^{13} \text{ cm}^{-3}$, a factor of 2.04 lower than the value obtained from the simulation. A discrepancy which is similar to those observed by others, as discussed in section 6.3.3.

We remark that, similarly to results from Ratushnaya *et al*, the requirement of uniform translation of the streamer in the derivation of the Ratushnaya-equation can be fairly lax as in both cases the measured numerical value for E^- matches well with the value predicted by the equation despite the constant acceleration and expansion of the simulated streamers.

6.4 Conclusions

We found that positive streamers are sensitive to the choice of transport data. Replacing the original, constant, diffusion and mobility coefficients by field-dependent coefficients computed with a multiterm Boltzmann solver, caused the streamers to propagate more

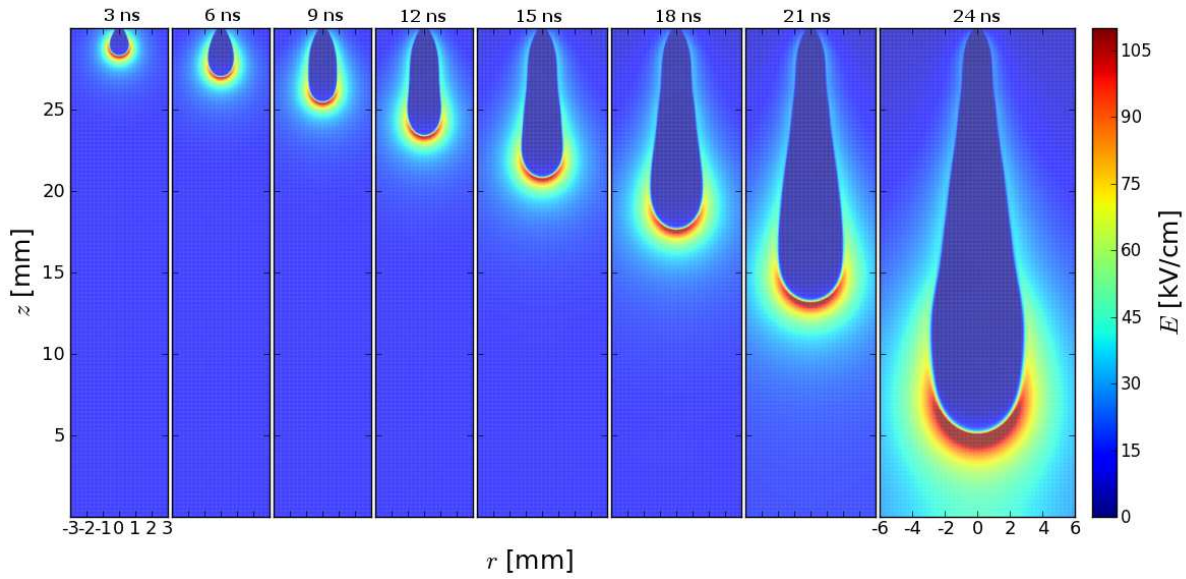


Figure 6.8: Electric field strength of a positive streamer in air in a 30 mm gap ($L_r = 30$ mm, $L_z = 30$ mm). Voltage applied to needle electrode is 42.7 kV, background electric field away from the needle (in the absence of space charges) is 12 kV/cm. Each panel corresponds to a different stage in streamer evolution, with time progressing from left to right. The width of the simulated domain displayed in the first 4 panels is 6 mm, in the next 3 panels 8 mm and 12 mm in the final panel. The total width of the simulated domain is 60 mm. Colour scale is equal for every panel. z and r scales are equal for every panel with aspect ratio 1.

slowly by approximately 30%. Despite the difference in velocity, streamer width and morphology appear unaffected. Nevertheless, when creating streamer simulations, transport data must be selected carefully.

An analytical prediction for the relation between streamer velocity, radius, internal electric field and maximal electric field was by Ratushnaya *et al* for streamer simulations with constant diffusion and mobility coefficients. We adapted this prediction for field-dependent transport data and found it to be in agreement with our simulation results.

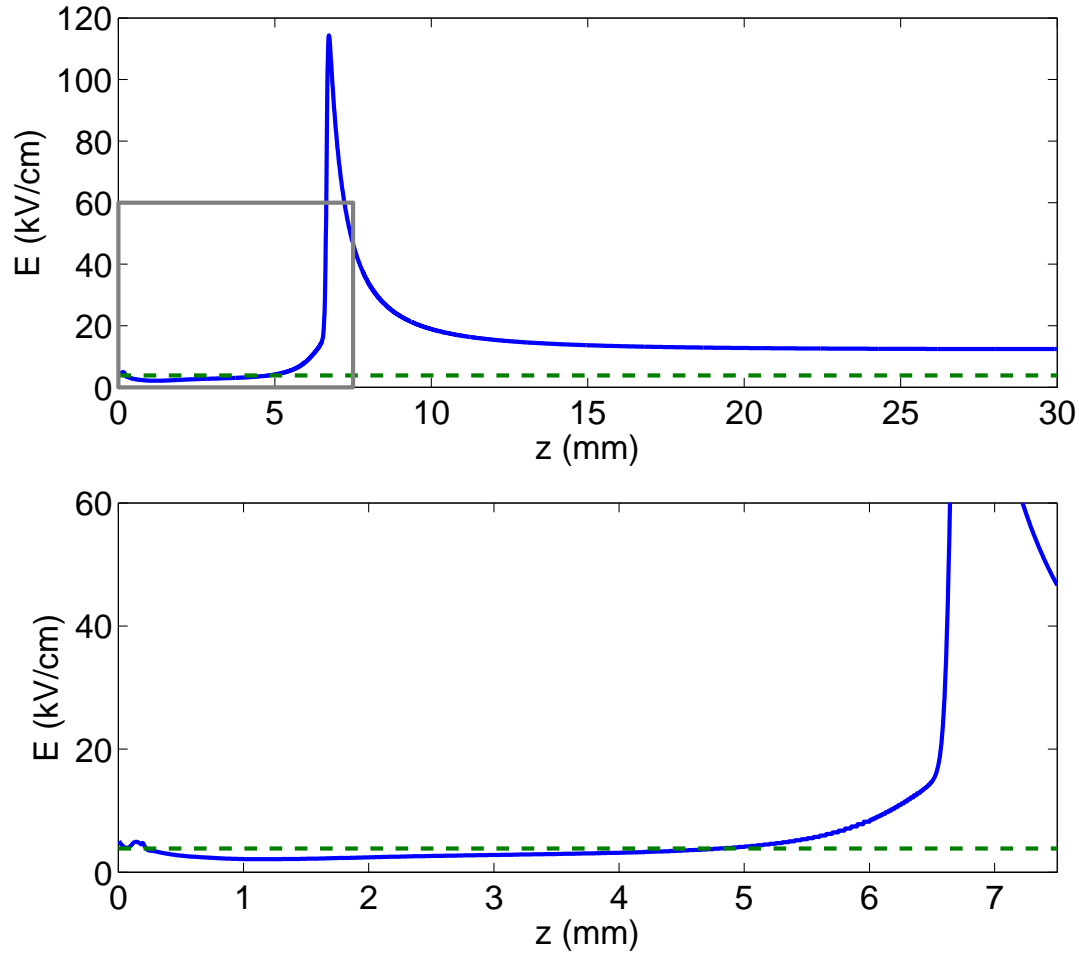


Figure 6.9: Electric field on streamer axis for a positive streamer in air. Dashed green line is the predicted value of the interior electric field E^- from the Ratushnaya-equation 6.7. The top panel depicts the entire z -range of the simulation domain. The rectangle in the bottomleft of the top panel indicates the zoomed in area depicted in the bottom panel.

7.1 Streamers

As discussed in the introduction, streamers are thin, ionized channels that propagate through an otherwise non-ionized background gas under the influence of an electric field. When a sufficiently high electric field is applied to ionizable matter, free electrons can be accelerated and if the electrons can gain sufficient energy, they will ionize the molecules in the background gas, generating an electron avalanche. These avalanches can develop into a streamer that enhances the electric field in front of it, thereby generating additional ionization which extends the streamer. Due to the local field enhancement, the streamer can penetrate regions where the background ionization is too low. A streamer consists of a head, consisting of a thin, curved space charge layer and a channel with high ionization density, but typically low electric field strength.

We distinguish between positive and negative streamers, based on the polarity of the charge in the streamer head. Negative streamers propagate with the electron drift, while positive streamers propagate against the electron drift and need a source of electrons in front of the streamer head. Conceptually, negative streamers are simpler, but experimental and theoretical studies have shown that positive streamers emerge more easily, at lower voltages and propagate with higher velocity than negative streamers.

Streamers occur in nature as the first stage of a spark as well as in lightning discharges, where a large number of streamers forms a corona around the head of the leader that creates the conductive channel for the lightning return stroke to travel through. In the upper atmosphere, sprite discharges occur above thunderclouds after lightning strikes. Sprites consist of large numbers of streamers propagating over tens of kilometers, in the thin air at 40 to 90 km altitude.

7.2 Modeling of streamers

Streamer models can be roughly divided into two categories: particle models and fluid models. Particle models treat electrons as individual particles (possibly using superparticle techniques to have each computational particles represent multiple physical particles) that move through the electric field and collide with neutral molecules and ions. Particle models can be used to study the full physics of the discharge, including stochastic effects and the inception of streamers. However, in longer streamers the number of charged particles becomes too high for current computers and the model runs into memory limits.

Fluid models approximate the individual particles by a density function. Derived from the Boltzmann equation, one can obtain continuity equations for this density function (equation 2.1 and 2.2). This yields a (set of) partial differential equations that can be solved with numerical methods. Fluid models allow for longer streamers to be simulated, but at the expense of approximating the dynamics of individual particles.

Various solutions have been proposed and implemented to combine the advantages of the particle models with the efficiency of the fluid models, such as spatially hybrid models that use a fluid model in the high density low field regions and a particle model in the low density high field regions.

7.3 CStream simulation code

To be able to use more accurate, tabulated, reaction coefficients and field-dependent transport coefficients, we have adapted the existing CStream simulation code and used it for the streamer simulations in this thesis. This code uses a fluid model for particle densities, which is coupled to the Poisson equation for the electric potential. The code uses adaptive grid refinement to resolve small-scale details in areas with high density gradients and high electric fields, while keeping computational cost low by using a relatively coarse grid on the rest of the domain. The simulation code also includes photo-ionization in $\text{N}_2\text{:O}_2$ mixtures and an approximation for needle-plane electrode configurations.

The code includes the **FISHPACK** solver for the Poisson equation. Because of the limitations of the **FISHPACK** solver, the grids for the Poisson equation are not the same as the grids for the density equations. Since **FISHPACK** can't deal with the needle electrode being embedded in the domain, the needle electrode is replaced by a point charge that has a position and charge in such a way that the potential at the location of the needle tip is correct. While the potential in front of the needle is well approximated by this charge-simulation-method, the calculated potential behind the needle tip is not close to the correct potential. Consequently, the density equations can't be solved accurately in the area behind the needle tip. So the computational grid for the density equations does not extend behind the tip of the electrode needle, while the Poisson grid does include the area containing the needle as depicted in figure 2.1.

The user can specify the set of species and reactions to be included in the simulation, as well as system properties such as the gap length between the electrodes, applied voltage, system width and numerical properties such as number of grid points at the coarsest level,

maximum depth of refinement subgrids and refinement criteria.

Chapter 2 describes the CStream code and also serves as a user manual.

7.4 Background ionization as alternative to photo-ionization

Photo-ionization, the mechanism where UV-photons emitted by deexcitation of N_2 -molecules ionize O_2 molecules elsewhere in the domain, is generally assumed to be the main source of free electrons for the propagation of positive streamers. However, the details of the photo-ionization mechanism in $N_2:O_2$ -mixtures are not well known. We have studied an alternative source of free electrons: electron detachment from preexisting background ionization.

We have simulated positive streamers where the photo-ionization mechanism was replaced by a homogeneous background ionization of O_2^- and positive ions. We found that in air at standard temperature and pressure, detachment from background ionization can replace photo-ionization as a source of free electrons. However, in virgin air, background ionization levels (primarily from radioactive materials in buildings) are only at 10^3 cm^{-3} , which in our simulations was insufficient to produce propagating streamers. At higher levels of background ionization, 10^5 cm^{-3} and 10^7 cm^{-3} , positive streamers propagated through the entire electrode gap.

Compared to the simulation with photo-ionization, the streamers with just background ionization were thinner and had a higher maximal electric field. We found that as long as sufficient background ionization is present, decreasing the level of background ionization by 2 orders of magnitude reduces the velocity of the resulting streamer by only 20%.

7.5 Combining background- and photo-ionization

In reality, photo-ionization can't be ignored in air at standard temperature and pressure. We simulated positive streamers to include both photo-ionization and a homogeneous initial background ionization of O_2^- and positive ions. We found that at low levels of background ionization, the effect of photo-ionization completely dominates the effect of background ionization, making the macroscopic properties of streamers with only photo-ionization indistinguishable from those with small amounts of background ionization added.

Above a certain threshold, the effect of adding background ionization becomes noticeable and the velocity of streamers increases. This threshold level depends on the gas mixture. In air, it was found to be approximately 10^{10} cm^{-3} , while in nitrogen with a 1 ppm oxygen admixture, this threshold level drops to 10^6 cm^{-3} . Simple estimates to equate background ionization levels to repetition frequencies of repeated discharges, show a good comparison with experiments on repeated streamer discharges.

7.6 The effect of impurities

We found that, while a source of free electrons in front of the streamer head is required for positive streamers to propagate, the amount of free electrons only has a small effect on how easily streamers emerge and propagate and on the velocities of streamers. Even in very high purity nitrogen, with oxygen admixtures of 1 ppm or less, positive streamers emerge as easily as in air with very similar properties. The main difference between streamers in air and streamers in high purity nitrogen are width and maximal electric field.

The non-local effect of photo-ionization helps to smooth out the steep density gradients in the streamer head. With photo-ionization intensity near the streamer head being 5 orders of magnitude higher in air than in nitrogen with 1 ppm oxygen, this smoothing effect is much more pronounced in air, resulting in smoother gradients and wider streamers. The steeper density gradients in high purity nitrogen enhance the electric field at the tip of the streamer, which increases the rate of impact ionization, which compensates for the reduced number of free electrons in the area near the streamer head produced by photo-ionization.

Since gases with perfect purity are impossible, or at least highly infeasible, to achieve experimentally, the effect of impurities can't be ignored. Our findings obtained from simulations of streamers in high purity nitrogen match experimental findings: Even an admixture of less than 1 ppm of oxygen in nitrogen is enough for positive streamers to propagate, where positive streamer propagation is impossible in 100% pure nitrogen. While we performed simulations of nitrogen with oxygen admixtures as low as 1 ppb, the results of these are not reliable as the extremely low density of oxygen makes the density approximation employed by the fluid model invalid.

7.7 Feather-like structures

In experiments, positive streamers in high purity nitrogen were found to have thin “hairs” connected to the main streamer channel. This was referred to as a “feather-like structure” of the streamer. These feather-like structures were completely absent in streamers in air.

We hypothesized that the hairs in these feather-like structures are avalanches started by single electrons. They are not visible in streamers in air, since the electron density in the region where these avalanches may start (where the electric field strength exceeds the breakdown field) is high enough that there are so many avalanches that they overlap and are not visible individually. In high purity nitrogen, the electron density outside the streamer is much lower due to the lower photo-ionization intensity. Consequently, the number of electron avalanches running towards the streamer head are much lower than in air, which should make them distinct enough from each other to be visible as separate entities.

We used data from simulations in air and in nitrogen with 1 ppm oxygen to estimate the electron density in the area where the electric field exceeds the breakdown field. In air, the electron density in the area where the field is equal to the breakdown field is 10^5 mm^{-3} , while it's only 10^2 mm^{-3} in nitrogen with 1 ppm of oxygen.

We estimated the number of hairs per mm of streamer length. After scaling our simulation results to the parameters of the experiment, we obtained a rough estimate of 3 hairs per mm of streamer length, compared to 1 hair per mm of streamer length observed in the experiment.

However, an accurate investigation of the feather-phenomenon requires the use of a particle model in 3D. The fluid model with cylindrical symmetry that we used is not suitable to study effects of stochastic nature, such as the feather-like structures.

7.8 Estimating background ionization levels

In earlier results, we found that certain levels of background ionization can have an effect on streamer properties. While background ionization is present in buildings at level of about 10^3 cm^{-3} , this is not sufficient to affect streamer propagation in $\text{N}_2:\text{O}_2$ -mixtures. Background ionization left over from a previous discharge can have an effect on the next streamer discharge. After a streamer discharge, a conductive channel with high electron density (approximately 10^{14} cm^{-3} in a gas at standard temperature and pressure) remains. The electrons in this channel will rapidly attach to electronegative species such as oxygen, if they are available in sufficient quantities.

Then, the negative ions (in the case where electrons have attached) or the electrons will recombine with positive ions and the ionization level will decrease. A simple model can provide an estimate to the leftover ionization density as a function of time after a discharge. For any time t relevant to experiments that we compare our results with [15,36] ($t > 10^{-3} \text{ s}$) this estimate is

$$n_i(t) = \frac{1}{k_{rec}t} \quad (7.1)$$

with k_{rec} the recombination rate. The ionization density $n_i(t)$ is independent of the initial ionization density $n_i(0)$ on these timescales for all practical values of k_{rec} and $n_i(0)$. In air at standard temperature and pressure, we found that at $t = 1 \text{ s}$, $n_i = 2 \times 10^5 \text{ cm}^{-3}$, with n_i inversely proportional to t . This makes a repetition frequency of 1 Hz to produce a background ionization that is insufficient to be noticeable in streamers in air.

7.9 Streamer path repetition

The previous estimates of the background ionization levels assume that the leftover ionization after a streamer discharge is constant in the entire domain. In reality, only part of the gas is filled with streamer plasma, while the remainder has ionization densities that are orders of magnitude lower.

We have constructed a model of a decaying streamer channel by assuming that the ionization in the channel diffuses and recombines. The diffusion increases the width of the channel while the recombination lowers its ionization density. Solving this model numerically provides an estimate for the width of the channel and its ionization density as a function of time. Additionally, it provides an estimate for the ionization density in the regions away from the decaying channel.

Using parameters from experiments (streamer channels with width of 0.3 mm and 30 mm apart), we found that 0.1 s after a single pulse in virgin air the ionization density in the center of the channel has decreased from 10^{14} cm^{-3} to $4 \times 10^6 \text{ cm}^{-3}$, while the ionization density between channels increased from 0 to 10^3 cm^{-3} and the channel width increased from 0.3 mm to 5.5 mm. After 1 second, ratio between the ionization density in the center of a channel and between two channels is only 3.4 and the channel has become very faint and spread out.

We have computed an equilibrium background density after many pulses with constant interval. For a repetition frequency of 10 Hz, we found the equilibrium background ionization density to be $2.0 \times 10^6 \text{ cm}^{-3}$. With this background ionization density, 0.1 s after the streamer discharge, the ionization density in the center of the decaying channel is only a factor 3 higher, while the width of the channel has increased to approximately 5 mm. At 1 Hz repetition frequency, the background ionization density in equilibrium is $3.5 \times 10^5 \text{ cm}^{-3}$ and the ratio between the ionization density in the center of the channel and the area between two channels is only 1.23.

In experiments performed in high purity nitrogen at 10 Hz repetition frequency, repeated discharges were seen to not follow the path of previous discharges, which is in agreement with our observation that the streamer channel has already mostly decayed after 0.1 s.

7.10 Effect of choice of transport data on streamer simulations

In other simulations in this thesis, a constant value was used for the mobility and diffusion coefficients, while in reality these coefficients depend on the electric field strength. Using mobility and diffusion coefficients obtained from solving the Boltzmann equation, we have extended the fluid simulation code.

We have found that including these more accurate transport coefficients has had a significant effect on the streamer velocity: Streamers simulated with the field-dependent transport coefficients are slower than those simulated with the previously used constant coefficients, by approximately 30%. On the other hand, other properties such as streamer width and maximal electric field were not affected as much.

The effect of the choice of transport data seems to have a larger effect on the velocity of positive streamers than the precise details of the mechanism that provides the free electrons in front of the streamer head. For example, in earlier simulations we found that artificially decreasing the photo-ionization intensity by a factor of 10 only reduced the velocity of the streamer by 20%.

7.11 Comparison with analytical predictions

In order to model a system with a large number of streamers, the model of an individual streamer needs to be reduced to a small set of macroscopic parameters, such as radius,

velocity and maximal electric field. The relation between these parameters can be derived analytically by assuming a uniformly translating streamer (that is, the streamer has constant velocity and radius) and analyzing the equations of the streamer fluid model in a frame that is comoving with the uniformly translating streamer.

We have taken one such result, the Ratushnaya-equation, which relates streamer radius, velocity, electron density inside the channel and maximal electric field to the electric field in the interior of the streamer and extended it with the field-dependent transport data that we have included in our simulation model. While neither our streamer, nor the one originally studied by Ratushnaya *et al* were precisely uniformly translating, we found that the analytical prediction matched very well with our simulation result.

We also applied a formula to estimate the electron density behind the streamer head as a function of the ionization rate coefficient and the maximal electric field. This formula was originally derived for planar streamer fronts of negative polarity. Application of this formula to curved, positive fronts were found by other authors to show a factor 2 discrepancy between the calculated electron density and the value obtained from the simulation. This discrepancy between prediction and simulation was also present in our result.

7.12 Applications and recommendations for future research

When working with streamers, be it in experiments, simulations or industrial applications, one must take care to anticipate the effects of any impurities in the gas. Indeed, we found that an admixture of 1 ppm of oxygen or less in nitrogen was sufficient for positive streamers to emerge and propagate, where in truly pure nitrogen this is impossible. As an impurity as low as 1 ppm is difficult to achieve for industrial applications, applications using streamers should include a careful study of the contents of the background gas.

We have studied the effect of various parameters on the properties of simulated streamers. For future simulations, these effects can be taken into account when deciding which level of accuracy is required in the model and its parameters.

Many of the results in this thesis are of a descriptive nature, observations of certain phenomena in simulations or calculations. To simulate larger systems with many streamers, it is important to be able to explain and predict the effects that various parameters such as gas composition, photo-ionization properties, applied electric field, pressure, etc... have on macroscopic streamer properties such as velocity, radius and maximal electric field. These predictions can come in the form of analytical relations between the macroscopic properties [94], relations similar to the Ratushnaya equation [24]. With good analytical relations between all relevant properties, it will be possible to use more reduced models to simulate tens to thousands of streamers without having to solve the continuity equations for the entire domain.

The limitations of the fluid model as we have used it have become clear on several occasions. Whether it is extremely low densities of certain species or the lack of stochastic processes, there are physically relevant situations where the predictive power of the current fluid model fails. To increase the range of applicability of the current model, it can be

extended to include stochastic effects [97] or even merged with a particle model to create a spatially hybrid simulation model that can harness the strengths of both fluid and particle models [98].

Replacing the **FISHPACK** solver for the Poisson equation will allow for more complex domains to be studied, including domains that have the electrode embedded as well as setups that include a dielectric, which is relevant for some applications of streamer research. Parallelization of the simulation code will allow for more efficient use of modern multi-core and multi-cpu systems and the ability to simulate larger domains or with higher resolution without increasing the total computation time.

Bibliography

- [1] A. Luque, V. Ratushnaya and U. Ebert, *Positive and negative streamers in ambient air: modeling evolution and velocities*, J. Phys D: Appl. Phys. **41** (2008) 234005.
- [2] A. Luque and U. Ebert, *Density models for streamer discharges: beyond cylindrical symmetry and homogeneous media*, J. Comp. Phys. **231** (2012) 904.
- [3] C. Y. Kao, F. Brau, U. Ebert, L. Schäfer and S. Tanveer, *A moving boundary model motivated by electric breakdown: II. Initial value problem*, Physica D **239** (2010) 1542.
- [4] C. T. R. Wilson, *The electric field of a thundercloud and some of its effects*, Proc. Phys. Soc. London **37** (1925) 32D.
- [5] R. C. Franz, R. J. Nemzek and J. R. Winckler, *Television image of a large upward electrical discharge above a thunderstorm system*, Science **249** (1990) 48.
- [6] D. D. Sentman, E. M. Wescott, D. L. Osborne, D. L. Hampton and M. J. Heavner, *Preliminary results from the Sprites94 aircraft campaign: 1. Red sprites*, Geophys. Res. Lett. **22** (1995) 1205.
- [7] A. Luque and U. Ebert, *Emergence of sprite streamers from screening-ionization waves in the lower ionosphere*, Nature Geoscience **2** (2009) 757.
- [8] S. A. Cummer, N. Jaugey, J. Li, W. A. Lyons, T. E. Nelson and E. A. Gerken, *Submilisecond imaging of sprite development and structure*, Geophys. Res. Lett. **33** (2006) L04104.
- [9] T. Neubert, M. Rycroft, T. Farges, E. Blanc, O. Chanrion, E. Arnone, A. Odzimek, N. Arnold, C.-F. Enell, E. Turunen, T. Bosinger, A. Mika, C. Haldoupis, R. J. Steiner, O. van der Velde, S. Soula, P. Berg, F. Boberg, P. Thejil, B. Christiansens, M. Ignaccolo, M. Fullekrug, P. T. Verronen, J. Montanya and N. Crosby, *Recent results from studies of electric discharges in the mesosphere*, Surv. Geophys. **29** (2008) 71.

- [10] A. Sobota, E. M. van Veldhuizen and W. W. Stoffels, *Discharge ignition near a dielectric*, IEEE Trans. Plasma Sci. **36** (2008) 912.
- [11] G. J. J. Winands, K. P. Yan, A. J. M. Pemen, S. A. Nair, Z. Liu and E. J. M. van Heesch, *An industrial streamer corona plasma system for gas cleaning*, IEEE Trans. Plasma Sci. **34** (2006) 2426.
- [12] A. J. M. Pemen, L. Devi, K. Yan, E. J. M. van Heesch, K. J. Ptasiński, R. Kerst and S. A. Nair, *Plasma-catalytical removal of tars from fuel gas obtained by biomass gasification*, J. Adv. Oxidation Tech. **10** (2007) 116.
- [13] X. Pei, X. Lu, J. Liu, D. Liu, Y. Yang, K. Ostrikov, P. K. Chu and Y. Pan, *Inactivation of a 25.5 μm enterococcus faecalis biofilm by a room-temperature, battery-operated, handheld air plasma jet*, J. Phys. D: Appl. Phys. **45** (2012) 165205.
- [14] N. Yu. Babaeva and M. J. Kushner, *Dynamics of dielectric barrier discharges over wounded skin*, IEEE Trans. Plasma Sci. **39** (2011) 2964.
- [15] S. Nijdam, F.M.J.H. van de Wetering, R. Blanc, E.M. van Veldhuizen and U. Ebert, *Probing photo-ionization: Experiments on positive streamers in pure gases and mixtures*, J. Phys. D: Appl. Phys. **43** (2010) 145204.
- [16] E.J.M. van Heesch, G.J.J. Winands and A.J.M. Pemen, *Evaluation of pulsed streamer corona experiments to determine the O^* radical yield*, J. Phys. D: Appl. Phys. **41** (2008) 2341015.
- [17] T. Verreycken, R. M. van der Horst, A. H. F. M. Baede, E. M. van Veldhuizen and P. J. Bruggeman, *Time and spatially resolved LIF of OH in a plasma filament in atmospheric pressure He-H₂O*, J. Phys. D: Appl. Phys. **45** (2012) 1.
- [18] U. Ebert, S. Nijdam, C. Li, A. Luque, T. M. P. Briels and E. M. van Veldhuizen, *Review of recent results on streamer discharges and their relevance for sprites and lightning*, J. Geophys. Res. **115** (2010) A00E43.
- [19] D. Dubrovin, S. Nijdam, E.M. van Veldhuizen, U. Ebert, Y. Yair and C. Price, *Sprite discharges on Venus and Jupiter-like planets: a laboratory investigation*, J. Geophys. Res. - Space Physics (2010) in press, doi:10.1029/2009JA014851.
- [20] J. R. Winckler, W. A. Lyons, T. E. Nelson and R. J. Nemzek, *New high-resolution ground-based studies of sprites*, J. Geophys. Res. **101** (1996) 6997.
- [21] O. A. van der Velde, A. Mika, S. Soula, C. Haldoupis, T. Neubert and U. S. Inan, *Observations of the relationship between sprite morphology and in-cloud lightning processes*, J. Geophys. Res. **111** (2006) D15203.
- [22] T. Neubert, B. Crosby, T.-Y. Huang and M. J. Rycroft, *ASIM - an instrument suite for the international space station*, in *proceedings of Workshop on Coupling of Thunderstorms and Lightning Discharges to Near-Earth Space* (2009), 8–12.

- [23] Y. Yair, P. Israelevich, A. D. Devir, M. Moalem, C. Price, J. H. Joseph, Z. Levin, B. Ziv, A. Sternlieb and A. Teller, *New observations of sprites from the space shuttle*, J. Geophys. Res. **109** (2004) D15201.
- [24] V. Ratushnaya, A. Luque and U. Ebert, *Electrodynamic characterization of long positive streamers in air*, in preparation .
- [25] The Siglo Database, CPAT and Kinema Software, URL <http://www.siglo-kinema.com>.
- [26] A. Sun, H. J. Teunissen and U. Ebert, *Why single streamers do not exist above the breakdown field in atmospheric air*, revised for Geophys. Res. Lett. (2013).
- [27] A. Sobota, J. H. M. Kanters, F. Manders, M. F. Gendre, J. Hendriks, E. M. van Veldhuizen and M. Haverlag, *Ac breakdown in near-atmospheric pressure noble gases: I. Experiment*, J. Phys. D: Appl. Phys. **44** (2011) 224002.
- [28] T. M. P. Briels, J. Kos, G. J. J. Winands, E. M. van Veldhuizen and U. Ebert, *Positive and negative streamers in ambient air: measuring diameter, velocity and dissipated energy*, J. Phys. D: Appl. Phys. **41** (2008) 234004.
- [29] M. J. Kushner, *Modelling of microdischarge devices: Plasma and gas dynamics*, J. Phys. D: Appl. Phys. **38** (2005) 1633.
- [30] A. Sobota, J. van Dijk and M. Haverlag, *Ac breakdown in near-atmospheric pressure noble gases: II. Simulations*, J. Phys. D: Appl. Phys. **44** (2011) 224003.
- [31] M. Duarte, Z. Bonaventura, M. Massor, A. Bourdon, S. Descombes and T. Dumont, *A new numerical strategy with space-time adaptivity and error control for multi-scale streamer discharge simulations*, J. Comp. Phys. **231** (2012) 1002.
- [32] H. J. Teunissen and U. Ebert, *Controlling the weights of simulation particles: adaptive particle management using k-d trees*, submitted to J. Comput. Phys. (2013).
- [33] C. Montijn, W. Hundsdorfer and U. Ebert, *An adaptive grid refinement strategy for the simulation of negative streamers*, J. Comp. Phys. **219** (2006) 801.
- [34] G. Wormeester, S. Pancheshnyi, A. Luque, S. Nijdam and U. Ebert, *Probing photo-ionization: Simulations of positive streamers in varying $N_2:O_2$ mixtures*, J. Phys. D: Appl. Phys. **43** (2010) 505201.
- [35] G. Wormeester, S. Nijdam and U. Ebert, *Feather-like structures in positive streamers interpreted as electron avalanches*, Jap. J. Appl. Phys. **50** (2011) 08JA01.
- [36] S. Nijdam, G. Wormeester and U. Ebert, *Probing background ionization: Positive streamers with a varying pulse repetition rate and with a radioactive admixture*, J. Phys. D: Appl. Phys. **44** (2011) 455201.

- [37] L. Huxley and R. Compton, *The Diffusion and Drift of Electrons in Gases*, Wiley, New York (1974).
- [38] Y. P. Raizer, *Gas Discharge Physics*, Berlin: Springer (1991).
- [39] A. Davies, C. Davies and C. Evans, *Computer simulation of rapidly developing gaseous discharges*, Proc. IEE **118** (1971) 816.
- [40] W. Hundsdorfer and J. Verwer, *Numerical Solution of Time-Dependent Advection-Diffusion-Reaction Equations*, *Series in Comp. Math.*, volume 33, Springer, Berlin (2003).
- [41] A. Luque, U. Ebert, C. Montijn and W. Hundsdorfer, *Photoionisation in negative streamers: fast computations and two propagation modes*, Appl. Phys. Lett. **90** (2007) 081501.
- [42] J. C. Adams, P. N. Swarztrauber and R. Sweet, *FISHPACK*, URL <http://www2.cisl.ucar.edu/resources/legacy/fishpack>.
- [43] C. Li, U. Ebert and W. Hundsdorfer, *Spatially hybrid computations for streamer discharges: II. Fully 3D simulations*, J. Comput. Phys. **231** (2012) 1020.
- [44] A. Luque, U. Ebert and W. Hundsdorfer, *Interaction of streamers in air and other oxygen-nitrogen mixtures*, Phys. Rev. Lett. **101** (2008) 075005.
- [45] D. van Heesch, *Doxygen*, URL <http://www.stack.nl/~dimitri/doxygen/>.
- [46] E. M. van Veldhuizen, *Electrical Discharges for Environmental Purposes: Fundamentals and Applications*, New York: Nova Science Publishers (2000).
- [47] U. Ebert, C. Montijn, T. M. P. Briels, W. Hundsdorfer, B. Meulenbroek, A. Rocco and E. M. van Veldhuizen, *The multiscale nature of streamers*, Plasma Sources Sci. Tech. **15** (2006) S118.
- [48] U. Ebert and D.D. Sentman, *Streamers, sprites, leaders, lightning: from micro- to macroscales (an editorial review to a cluster issue)*, J. Phys. D: Appl. Phys. **41** (2008) 230301.
- [49] V. P. Pasko, *Red sprite discharges in the atmosphere at high altitude: the molecular physics and the similarity with laboratory discharges*, Plasma Sources Sci. Technol. **16** (2007) S13.
- [50] S.M. Starikovskaia, *Plasma assisted ignition and combustion*, J. Phys. D: Appl. Phys. **39** (2006) R265.
- [51] W. J. Yi and P. F. Williams, *Experimental study of streamers in pure N_2 and N_2 / O_2 mixtures and a 13 cm gap*, J. Phys. D.: Appl. Phys.. **35** (2002) 205.

- [52] T. M. P. Briels, E.M. van Veldhuizen and U. Ebert, *Positive streamers in ambient air and in a nitrogen-oxygen-mixture (99.8:0.2)*, IEEE Trans. Plasma Sci. **36** (2008) 906.
- [53] T. M. P. Briels, E.M. van Veldhuizen and U. Ebert, *Positive streamers in air and nitrogen of varying density: experiments on similarity laws*, J. Phys. D: Appl. Phys. **41** (2008) 234008.
- [54] N. L. Aleksandrov, E. M. Bazelyan and G. A. Novitskii, *The effect of small O₂ addition on the properties of a long positive streamer in Ar*, J. Phys. D: Appl. Phys. **34** (2001) 1374.
- [55] S. Pancheshnyi, *Role of electronegative gas admixtures in streamer start, propagation and branching phenomena*, Plasma Sources Science & Technology **14** (2005) 645.
- [56] H. Raether, *Electron Avalanches and Breakdown in Gases*, Butterworths, London (1964).
- [57] M. Zheleznyak, A. Mnatsakanyan and S. Sizykh, *Photoionization of nitrogen and oxygen mixtures by radiation from a gas discharge*, High Temp. **20** (1982) 357.
- [58] T. H. Teich, *Emission gasionisierender Strahlung aus Elektronenlawinen*, Z. Phys. **199** (1967) 378.
- [59] G. W. Penney and G. T. Hummert, *Photoionization measurements in air, oxygen and nitrogen*, J. Appl. Phys. **41** (1970) 572.
- [60] I. A. Kossyi and V. P. Silakov, *Step photoionization as a mechanism responsible for the Raether paradox*, Plasma Source Science & Technology **14** (2005) 594.
- [61] B. C. O'Neil and J. D. Craggs, *Collisional detachment of electrons and ion molecule reactions in oxygen*, J. Phys. B.: At. Mol. Phys. **6** (1973) 2625.
- [62] D. W. Goodson, R. J. Corbin and Lothar Frommhold, *Electron avalanches in oxygen: Detachment from the diatomic ion O₂⁻*, Phys. Rev. A **9** (1974) 2049.
- [63] A. Doussot, F. Bastien, E Marode and J L Moruzzi, *A new technique for studying ion conversion and detachment reactions in oxygen and in O₂/SO₂ and O₂/N₂ mixtures*, J. Phys. D: Appl. Phys **15** (1982) 2451.
- [64] N. L. Aleksandrov, S. V. Kindysheva, I. N. Kosarev and A. Yu Starikovskii, *Plasma decay in air and N₂ : O₂ : CO₂ mixtures at elevated gas temperatures*, J. Phys. D: Appl. Phys. **41** (2008) 215207.
- [65] N. L. Aleksandrov, *Low-energy electron attachment and detachment in vibrationally excited oxygen*, J. Phys. D: Appl. Phys. **42** (2009) 225210.
- [66] J. Dutton, *A survey of electron swarm data*, J. Phys. Chem. Ref. Data **4** (1975) 664.

- [67] I.A. Kossyi, A. Yu Kostinsky, A. A. Matveyev and V. P. Silakov, *Kinetic scheme of the non-equilibrium discharge in nitrogen-oxygen mixtures*, Plasma Source Science & Technology **1** (1992) 207.
- [68] G.J.M. Hagelaar and L.C. Pitchford, *Solving the Boltzmann equation to obtain electron transport coefficients and rate coefficients for fluid models*, Plasma Sources Science & Technology **14** (2005) 722.
- [69] M. Capitelli, C. M. Ferreira, B. F. Gordiets and A. I. Osipov, *Plasma Kinetics in Atmospheric Gases*, Springer Heidelberg (2000).
- [70] N. A. Popov, *Evolution of the negative ion composition in the afterglow of a streamer discharge in air*, Plasma Phys. Rep. **36** (2010).
- [71] A. Bourdon, V. P. Pasko, N. Y. Liu, S. Celestin, P. Segur and E. Marode, *Efficient models for photoionization produced by non-thermal gas discharges in air based on radiative transfer and the Helmholtz equations*, Plasma Sources Science & Technology **16** (2007) 656.
- [72] G. Steinle, D. Neundorff, W. Hiller and M. J. Pietralla, *Two-dimensional simulation of filaments in barrier discharges*, J. Phys. D: Appl. Phys. **32** (1999) 1350.
- [73] N. Liu and V. P. Pasko, *Effects of photoionization on propagation and branching of positive and negative streamers in sprites*, J. Geophys. Res. **109** (2004) A04301.
- [74] H. Singer, H. Steinbigler and P. Weiss, *A charge simulation method for the calculation of high voltage fields*, IEEE Trans. Power. Appar. Syst. **PAS-93** (1974) 1660.
- [75] M. M. Nudnova and A. Y. Starikovskii, *Streamer head structure: role of ionization and photoionization*, J. Phys. D: Appl. Phys. **41** (2008) 234003.
- [76] S. Nijdam, F.M.J.H. van de Wetering, E.M. van Veldhuizen and U. Ebert, *Diameters of positive streamers in pure N₂/O₂ mixtures*, in *Refereed proceedings of ICPIG 2009* (2009), 10–13.
- [77] C. Li, U. Ebert and W. Hundsdorfer, *3D hybrid computations for streamer discharges and production of run-away electrons*, J. Phys. D: Appl. Phys. **42** (2009) 202003.
- [78] E. Takahashi, S. Kato, A. Sasaki, Y. Kishimoto and H. Furutani, *Single-shot observation of growing streamers using an ultrafast camera*, J. Phys. D: Appl. Phys. **44** (2011) 075204.
- [79] L. Niemeyer, L. Ullrich and N. Wiegart, *The mechanism of leader breakdown in electronegative gases*, IEEE T. Electr. Insul. **24** (1989) 309.
- [80] H. Raether, *Die Entwicklung der Elektronenlawine in den Funkenkanal*, Z. Phys. A **112** (1939) 464.

- [81] U. Ebert, F. Brau, G. Derks, W. Hundsdorfer, C.-Y. Kao, C. Li, A. Luque, B. Meulenbroek, S. Nijdam, V. Ratushnaya, L. SchÃ¶fer and S. Tanveer, *Multiple scales in streamer discharges, with an emphasis on moving boundary approximations*, Nonlinearity **24** (2011) C1.
- [82] N. L. Aleksandrov and E. M. Bazelyan, *Ionization processes in spark discharge plasmas*, Plasma Sources Sci. Tech. **8** (1999) 285.
- [83] D. D. Sentman, H. C. Stenbaek-Nielsen, M. G. McHarg and J. S. Morill, *Plasma chemistry of sprite streamers*, J. Geophys. Res. - Atmospheres **113** (2008) D11112.
- [84] R. M. Snuggs, D. J. Volz, J. H. Schummers, D. W. Martin and E. W. McDaniel, *Mobilities and longitudinal diffusion coefficients of mass-identified potassium ions and positive and negative oxygen ions in oxygen*, Phys. Rev. A **3** (1971) 477.
- [85] A. Bourdon, Z. Bonaventura and S. Celestin, *Influence of the pre-ionization background and simulation of the optical emission of a streamer discharge in preheated air at atmospheric pressure between two point electrodes*, Plasma Sources Sci. Tech. **19** (2010) 034012.
- [86] A. Nikipelov, I. B. Popov, S. Pancheshnyi and A. Yu Starikovskii, *Localized and distributed behavior of nanosecond pulse-periodic discharge in air*, in *Refereed proceedings of ICPIG 2011* (2011), C10–346.
- [87] Z. M. Raspopovic S. Dujko and Z. Lj. Petrovic, *Monte Carlo Studies of Electron Transport in Crossed Electric and Magnetic Fields in CF₄*, J. Phys. D: Appl. Phys. **38** (2005) 2952.
- [88] M. A. Lieberman and A. J. Lichtenberg, *Principles of Plasma Discharges and Materials Processing*, Wiley-Interscience (2005).
- [89] S. Dujko, U. Ebert, R. D. White and Z. Lj. Petrovic, *Electron transport data in N₂-O₂ streamer plasma discharges*, Publ. Astron. Obs. Belgrade **89** (2010) 71.
- [90] Y. Itikawa, A. Ichimura, K. Onda, K. Sakimoto, K. Takayanagi, Y. Hatano and M. Hayashi, *Cross-sections for collisions of electrons and photons with oxygen molecules*, J. Phys. Chem. Ref. Data **18** (1989) 23.
- [91] Y. Itikawa, *Cross sections for electron collisions with oxygen molecules*, J. Phys. Chem. Ref. Data **38** (2009) 1.
- [92] V. D. Stojanovic and Z. Lj. Petrovic, *Comparison of the results of Monte Carlo simulations with experimental data for electron swarms in N₂ from moderate to very high electric field to gas density ratios (E/N)*, J. Phys. D: Appl. Phys. **31** (1998) 834.
- [93] U. Ebert and W. van Saarloos, *Front propagation into unstable states: Universal algebraic convergence towards uniformly translating pulled fronts*, Physica D **146** (2000) 1.

- [94] G. V. Naidis, *Positive and negative streamers in air: Velocity-diameter relation*, Phys. Rev. E **79** (2009) 5.
- [95] C. Li, W. J. M. Brok, U. Ebert and J. J. A. M. van der Mullen, *Deviations from the local field approximation in negative streamer heads*, J. Appl. Phys. **101** (2007) 123305.
- [96] A. Luque and U. Ebert, *Sprites in varying air density: charge conservation, glowing negative trails and changing velocity*, Geophys. Res. Lett. **37** (2010) L06806.
- [97] A. Luque and U. Ebert, *Electron density fluctuations accelerate the branching of streamer discharges in air*, Phys. Rev. E **84** (2011) 046411.
- [98] C. Li, U. Ebert and W. Hundsdorfer, *Spatially hybrid computations for streamer discharges with generic features of pulled fronts: I. Planar fronts*, J. Comp. Phys. **229** (2010) 200.

Streamers

Streamers are thin channels of ionized gas that propagate through an otherwise non-ionized background gas. Streamers occur in nature as part of the precursor to a lightning strike as well as directly in sprites, huge electrical discharges in the atmosphere above thunderstorms. Streamers are a natural phenomenon, but they are also used in various industrial applications ranging from gas cleaning to lighting and biomedical applications such as disinfection.

A streamer is a thin ionized channel created by a propagating head. The interior of the ionized body is electrically neutral and it is surrounded by a space charge layer with a particularly high charge density at the head. This charge enhances the electric field at the streamer head and suppresses it in the ionized interior. In the region of enhanced field, electrons are accelerated to such energies that they can liberate additional electrons from the neutral molecules of the background gas, a process called impact ionization.

One needs to distinguish positive or negative streamers based on the polarity of the charge in the streamer head. The negative streamer has a negatively charged head. Electrons are accelerated outward from the head, in the direction of streamer propagation. For positive streamers, the electrons are accelerated into the streamer channel from the area in front of the streamer head. Even though negative streamers are conceptually simpler, positive streamers occur more easily in nature and experiments.

Since the electrons are accelerated into the positive streamer from the area in front of the streamer head, positive streamers require a source of electrons in front of the streamer head in order to propagate. In air, this source is assumed to be photo-ionization. This process starts when an electron collides with a nitrogen molecule and creates a particular electronically excited state. When the molecule falls back into the ground state, it can emit a photon with sufficient energy to liberate an electron from an oxygen molecule elsewhere in the gas. Another mechanism to provide free electrons is background ionization that is present at the start of the discharge, either from radioactivity or cosmic radiation, or from a previous discharge. Depending on time scales, this background ionization can

either consist of free electrons directly, or of negative oxygen ions from which electrons can detach.

Streamer simulations

One of the primary subjects of this thesis is the study of these sources of free electrons in positive streamers and how their properties affect streamer propagation. For this study, we have used numerical models of streamers to explore a range of scenarios, both mimicking experiments and hypothetical scenarios.

Models for streamers typically fall in one of two categories: Particle models follow the motions of single electrons (or of super-electrons representing many physical electrons) as they move through the electric field and interact with the background gas, while fluid models replace the electrons by an electron density function, that is governed by a partial differential equation, coupled with partial differential equations for other densities and the electric field. While fluid models can't follow the full physics (like realistic streamer branching due to electron density fluctuations or electron run-away phenomena), as they neglect the effects of individual particles, they are more efficient than particle models when it comes to computer resources such as time and memory, which makes fluid models more viable for simulation of longer streamers.

In this thesis we have used and extended a fluid simulation code that was developed by Carolynne Montijn and Alejandro Luque. Chapter 2 of the thesis details the operation of the simulation code, starting with the differential equations that govern the development of the streamer and how these are discretized. We also discuss an important feature of the simulation code, adaptive mesh refinement, which is a technique that allows the code to use finer computational grids in areas where accuracy is needed, while keeping computational cost down by using coarser grids where this is possible. Finally, chapter 2 contains instructions for new users on how to use the code.

Photo-ionization and background ionization

Chapter 3 details the results of an investigation of the different sources of electrons in positive streamers in air and in high purity nitrogen. We compare photo-ionization with detachment from background ionization. Background ionization typically consists of negative oxygen molecules from which electrons can detach if a sufficiently strong electric field is applied. We have investigated whether detachment from background ionization alone is sufficient for positive streamers to propagate. The conclusion is that it is sufficient once the level of background ionization is at least 10^5 cm^{-3} . Ambient air in buildings is estimated to have background ionization levels between 10^3 and 10^4 cm^{-3} , which is not sufficient for positive streamers to propagate without also including photo-ionization. However, at higher levels of background ionization, the speed at which a streamer propagates does not depend strongly on the level of background ionization: An increase in background ionization of 2 orders of magnitude only increased streamer velocity by approximately 20%.

Excluding photo-ionization from the simulation is not realistic, since the existence of the mechanism is well established, even though its precise parameters are not. We have performed simulations combining photo-ionization and background ionization and found that photo-ionization completely dominates streamer properties in air for background ionization levels below 10^{10} cm^{-3} . These background ionization levels are reached in experiments with repeated discharges with a repetition frequency of at least 1 kHz.

Since the photo-ionization mechanism in air requires both nitrogen and oxygen to be present, it was expected that in pure nitrogen, positive streamers would not propagate. However, it is not possible to obtain 100% pure nitrogen and even small admixtures of oxygen in nitrogen turned out to be sufficient for positive streamers to emerge and propagate in experiments. In our simulations, we found similar results: With oxygen concentrations being reduced by over 5 orders of magnitude to 1 ppm, positive streamers still emerge and propagate easily, with velocities comparable to those in air.

Feather-like structures

One aspect of streamers that does change significantly between air and near-pure nitrogen is the morphology of the streamer. Experiments showed that streamers in air are smooth channels, while streamers in near-pure nitrogen have many branches and small hairs, making up a “feather-like structure”. The experimental observations of this feather-like structure are discussed in chapter 4, followed by a theoretical explanation for the phenomenon.

Since the local photo-ionization intensity scales inversely with oxygen density, the density of electrons freed by photo-ionization near the streamer head is expected to be orders of magnitude higher in air than in near-pure nitrogen. We propose that the hairs that make up the feather-like structure are actually individual electron avalanches moving towards the streamer. In air, the electron density in the active area where the local field exceeds the breakdown field (i.e where impact ionization dominates over electron loss processes) is approximately 10^5 mm^{-3} , and therefore we expect these avalanches to be so numerous that they overlap and are not visible as distinct entities.

In near-pure nitrogen (with a 1 ppm oxygen admixture), the electron density in the aforementioned area is much lower, only 10^2 mm^{-3} . Therefore, we can't really speak of a density anymore, but rather of a probability to find an electron in a certain area. This means that electron avalanches will be visible as distinct entities: hairs connecting to a streamer channel.

We remark that in near pure nitrogen the stochastic nature of the free electron distribution becomes relevant and that therefore a fluid model is not suitable to accurately model the formation of feather-like structures. Instead, a particle model or hybrid fluid-particle model should be used.

Background ionization from repetitive discharges

As mentioned above, one of the sources of background ionization in streamer discharges is the ionization left behind by a previous discharge. Without a new ionization source, the ionization level will gradually decrease due to recombination processes. So the level of background ionization at the start of a discharge depends on the time that has passed since the previous discharge. In the context of repetitive discharges, this makes the repetition frequency the factor that determines the background ionization density.

In chapter 5, we estimate the background ionization in air as a function of the time since the previous discharge. First, we assume that all ionization is spread out homogeneously and only consider the loss of ionization due to recombination. We find that the background ionization density at the start of a discharge scales inversely with the time since the previous discharge and is, for the timescales that we're interested in, independent of the level of ionization directly after the previous discharge.

In reality, the ionization will not be spread out homogeneously, but it will be concentrated in the areas where streamer channels have passed. Using data from experiments on the width of streamer channels and the spacing between them, we have formulated a model that combines charged particle recombination with the particle diffusion from the streamer channel. This allows us to examine to what extent a channel is still present after a given amount of time.

First we applied the model to find an equilibrium background density after many discharges; then we found that with a repetition frequency of 10 Hz, the ionization density in the center of where the streamer channel used to be is only 3 times as high as the minimal ionization density in the area between streamer channels. With a 1 Hz repetition frequency, this factor is only 1.23. We predict that under these conditions, streamers will most likely not follow the same path in repetitive discharges, which was confirmed by experiments.

The effect of transport data

The equations that govern the change in particle densities in a fluid model can be separated into three separate terms: Convection, diffusion and reaction. Convection is the movement of charged particles in a direction parallel to the electric field. Diffusion is the movement of particles from areas of high density to areas of lower density. Finally, particles can be created or lost through reactions. In chapter 3, we focused on reactions, primarily detachment, and their effect on streamers.

In the original version of the simulation code, the two parameters that affect convection and diffusion, the mobility and diffusion coefficient respectively, were constant. However, in reality these parameters depend on the local value of the electric field. We have modified the code to include mobility and diffusion coefficients computed with a highly accurate Boltzmann solver. Simulations using these data, as detailed in chapter 6, show that the propagation velocity of streamers depends strongly on the selection of transport data, as we found a 30% difference in velocity between our old, constant parameters and the

field-dependent transport coefficients. On the other hand, streamer width and morphology were not affected.

Finally, we compared the simulations using these field-dependent transport data to analytical predictions for a relation between streamer properties such as radius, velocity and electric field and found that they were in good agreement.

Conclusions

In this thesis, we have studied various aspects of the propagation mechanisms of positive streamers in nitrogen-oxygen mixtures like air. We found that photo-ionization is the dominant mechanism in nearly all scenarios. Only if a large amount of background ionization is present, it can affect the discharge. The precise amount needed depends on ratio of oxygen and nitrogen.

While streamers did propagate in the absence of photo-ionization, the background ionization levels required for this do not occur in virgin air at sea level. In addition, streamers turned out to be remarkably robust against changes in the free electrons density available: Changing the photo-ionization intensity or the background ionization level by one or two orders of magnitude resulted in a change of only a few tens of percent in propagation velocity.

We have proposed a hypothesis for the feather-like structures observed in experiments in near-pure nitrogen, namely electron avalanches that are rare enough to be visible as distinct entities, but a particle model is needed to properly study this phenomenon. Furthermore, a simple diffusion-recombination model was used to compute the remaining ionization after a discharge and to obtain long-term equilibrium levels for the background ionization in repetitive discharges.

Finally, we noticed that while streamers are not very sensitive to the free electrons density available ahead of the streamer, the choice of diffusion and mobility coefficients does affect the streamer velocity significantly. But simulations performed with accurate diffusion and mobility coefficients still agree well with analytical predictions derived for a model with the older, constant coefficients.

Streamers

Streamers zijn dunne kanalen van geïoniseerd gas, die zich voortplanten door een verder niet geïoniseerd achtergrond gas. Streamers komen in de natuur voor als een onderdeel van het proces dat vooraf gaat aan een bliksemflits. Daarnaast komen streamers voor in sprites, gigantische elektrische ontladingen in de atmosfeer boven onweerswolken. Naast een natuurlijk fenomeen, worden streamers ook gebruikt in verscheidene industriële toepassingen, variërend van reiniging van gassen tot verlichting en biomedische toepassingen zoals desinfectie.

Een streamer is een dun, geïoniseerd kanaal dat wordt gecreëerd door een zich voortplantende kop. De binnenkant van dit geïoniseerde geheel is elektrisch neutraal en wordt omringd door een ruimteladingslaag, die vooral in de kop een erg hoge ladingsdichtheid heeft. Deze lading versterkt het elektrische veld bij de kop van de streamer en onderdrukt het in de geïoniseerde binnenkant. In de regio met het versterkte elektrische veld worden elektronen versneld tot ze voldoende energie hebben om meer elektronen los te maken van de moleculen van het achtergrondgas, een proces dat botsingsionisatie wordt genoemd.

Op basis van de polariteit van de lading in de streamerkop wordt er onderscheid gemaakt worden tussen positieve en negatieve streamers. Een negatieve streamer heeft een negatief geladen kop. Elektronen worden vanuit de kop naar buiten toe versneld, in de richting waarin de streamer zich voortplant. Bij een positieve streamer worden elektronen vanuit het gebied voor de streamerkop het kanaal in versneld. Hoewel negatieve streamers conceptueel eenvoudiger zijn, ontstaan positieve streamers gemakkelijker in de natuur en in experimenten.

Gezien de elektronen vanuit het gebied voor de streamerkop de positieve streamer in worden versneld, hebben positieve streamers een bron van elektronen nodig voor de streamerkop om zich voort te kunnen planten. In lucht wordt aangenomen dat fotoïonisatie deze bron is. Dit proces begint wanneer een elektron botst met een stikstof molecuul en een bepaalde elektronisch aangeslagen toestand van het molecuul creëert. Wanneer het molecuul daarna terugkeert naar de grondtoestand, kan het een foton uitzenden dat genoeg

energie heeft om elders in het gas een electron los te maken van een zuurstof molecuul. Een alternatief mechanisme dat vrije electronen kan leveren is achtergrondionisatie die bij het begin van de ontlading al aanwezig is, afkomstig van radioactiviteit of kosmische straling, of van een vorige ontlading. Afhankelijk van de tijdsschalen, kan deze achtergrond ionisatie direct bestaan uit vrije electronen of uit negatieve zuurstofionen, waarvan electronen zich kunnen losmaken via een proces dat “detachment” wordt genoemd.

Streamer simulaties

Een van de hoofdonderwerpen van dit proefschrift is het onderzoek naar deze bronnen van vrije electronen in positieve streamer en hoe de eigenschappen van de bronnen de voortplanting van de streamer beïnvloeden. Voor dit onderzoek hebben we gebruik gemaakt van numerieke modellen van streamers om een scala van scenario's te onderzoeken, zowel scenario's die experimenten nabootsen als hypothetische scenario's.

Modellen van streamers vallen voornamelijk in een van twee categorieën: Deeltjesmodellen volgen de beweging van individuele electronen (of “super-electronen” die elk vele fysische electronen voorstellen) terwijl deze door het elektrische veld bewegen en interacties aangaan met het achtergrondgas. Vloeistofmodellen vervangen de electronen door een electronendichtheidsfunctie, die afhangt van een partiële differentiaalvergelijking en gekoppeld is met partiële differentiaalvergelijkingen voor de dichtheden van andere deeltjes en voor het elektrische veld. Hoewel vloeistofmodellen de volledige fysica (zoals realistische vertakkingen van streamers vanwege fluctuaties in de electronendichtheid of electron run-away verschijnselen) niet kunnen volgen omdat ze de effecten van individuele deeltjes verwaarlozen, zijn ze efficiënter dan deeltjesmodellen als het gaat om computerbronnen, zoals tijd en geheugen, waardoor vloeistofmodellen bruikbaar zijn voor het simuleren van langere streamers.

In dit proefschrift hebben we een simulatieprogramma voor een vloeistofmodel, dat is ontwikkeld door Carolynne Montijn en Alejandro Luque, gebruikt en uitgebreid. Hoofdstuk 2 van dit proefschrift beschrijft het gebruik van het simulatieprogramma, beginnend met de differentiaalvergelijkingen die de ontwikkeling van de streamer beschrijven en hoe deze zijn gediscretiseerd. We bespreken tevens een belangrijk aspect van het simulatieprogramma, adaptieve roosterverfijning, een techniek die het toelaat voor het programma om een fijner computationeel rooster te gebruiken in gebieden waar hoge nauwkeurigheid noodzakelijk is, terwijl de kosten wat betreft rekenkracht beperkt worden door grovere roosters te gebruiken waar dit mogelijk is. Tot slot bevat hoofdstuk 2 instructies omtrent het gebruik van het simulatieprogramma voor nieuwe gebruikers.

Fotoionisatie en achtergrondionisatie

Hoofdstuk 3 beschrijft de resultaten van een onderzoek naar de verschillende bronnen van electronen in positieve streamers in lucht en in zeer zuiver stikstof. We hebben fotoionisatie vergeleken met detachment van achtergrondionisatie. Achtergrondionisatie bestaat meestal uit negatieve zuurstofionen waarvan electronen los kunnen komen (detachment)

als een voldoende sterk elektrisch veld aanwezig is. We hebben onderzocht of detachement van achtergrondionisatie op zichzelf voldoende is voor positieve streamers om zich voort te planten. De conclusie is dat dit zo is wanneer het hoeveelheid achtergrondionisatie minstens least 10^5 cm^{-3} bedraagt. Gewone lucht in gebouwen bevat naar schatting achtergrondionisatie dichtheden tussen 10^3 en 10^4 cm^{-3} , wat niet genoeg is voor positieve streamers om zich voort te planten zonder ook fotoionisatie mee te rekenen. Daarentegen, bij grotere hoeveelheden achtergrondionisatie hangt de snelheid waarmee een streamer zich voortplant niet op sterke wijze af van de hoeveelheid aanwezige achtergrondionisatie: Een toename in de achtergrondionisatie van 2 ordes van grootte resulteerde in een toename van de snelheid van de streamer van slechts ongeveer 20%.

Het weglaten van fotoionisatie in de simulatie is echter niet realistisch, gezien het bestaan van dit mechanisme grondig onderbouwd is, zelfs al zijn de precieze parameters dat niet. We hebben simulaties gemaakt waarbij photoionisatie en achtergrondionisatie zijn gecombineerd en hebben daaruit gevonden dat fotoionisatie de eigenschappen van een streamer in lucht volledig domineert voor dichtheden van achtergrondionisatie lager dan 10^{10} cm^{-3} . Deze dichtheden worden bereikt in experimenten met herhaalde ontladingen met een herhalingsfrequentie van ten minste 1 kHz.

Gezien het fotoionisatie mechanisme in lucht vereist dat zowel stikstof als zuurstof aanwezig zijn, werd er verwacht dat in zuivere stikstof positieve streamers zich niet zouden voortplanten. Het is echter niet mogelijk om 100% zuivere stikstof te verkrijgen en zelfs kleine hoeveelheden zuurstof bleken genoeg te zijn voor het ontstaan en voortplanten van positieve streamers in experimenten. In onze simulaties hebben we vergelijkbare resultaten gevonden: Met zuurstof concentraties die 5 ordes van grootte zijn verlaagd tot 1 ppm, was het nog steeds gemakkelijk voor positieve streamers om te ontstaan en voort te planten, met snelheden die vergelijkbaar zijn met die in lucht.

Veertjes-achtige structuren

Een aspect van streamers dat wel significant verschillend is in lucht en in bijna-zuivere stikstof is de morfologie van de streamer. Experimenten hebben laten zien dat streamers in lucht gladde kanalen zijn, terwijl streamers in bijna-zuiver stikstof bestaan uit vele vertakkingen en kleine haartjes, die samen een “veertjes-achtige structuur” vormen. De experimentele observaties van deze veertjes-achtige structuren worden besproken in hoofdstuk 4, gevolgd door een theoretische verklaring voor dit verschijnsel.

Gezien de intensiteit van de lokale fotoionisatie schaal met het inverse van de zuurstofdichtheid, is het te verwachten dat de dichtheid van elektronen die zijn losgemaakt door fotoionisatie in de buurt van de streamerkop ordes van grootte hoger is in lucht dan in bijna-zuivere stikstof. We stellen voor dat de haartjes waar de veertjes-achtige structuren uit bestaan eigenlijk individuele elektronenlawines zijn die in de richting van de streamer bewegen. In lucht is de electronendichtheid in het actieve gebied waar het lokale elektrische veld sterker is dan het kritische veld (d.w.z. waar botsingsionisatie de processen waar vrije elektronen verloren gaan overheerst) is ongeveer 10^5 mm^{-3} en daarom verwachten we dat deze lawines zo talrijk zijn dat ze overlappen en daarom niet zichtbaar zijn als aparte

entiteiten.

In bijna-zuiver stikstof (met een toevoeging van 1 ppm zuurstof), is de electronendichtheid in het hierboven genoemde gebied veel lager, slechts 10^2 mm^{-3} . Daarom kunnen we niet echt spreken van een dichtheid, maar eerder van een kans om een electron te vinden in een bepaald gebiedje. Dit betekent dat electronenlawines zichtbaar zijn als individuele entiteiten: haartjes die verbonden zijn met een streamerkanaal.

We merken op dat in bijna-zuiver stikstof de stochastische aard van de verdeling van vrije electronen relevant is en dat daarom een vloeistofmodel niet geschikt is om de vorming van veertjes-achtige structuren nauwkeurig te modelleren. In plaats daarvan, zou een deeltjesmodel of een hybride vloeistof-deeltjes-model moeten worden gebruikt.

Achtergrondionisatie door herhaalde ontladingen

Zoals eerder genoemd, is een van de bronnen van achtergrondionisatie in streamer ontladingen, de ionisatie die is achtergebleven na een voorgaande ontlading. Zonder een nieuwe bron van ionisatie zal de ionisatiegraad geleidelijk afnemen door recombinatie processen. Daarom hangt de hoeveelheid achtergrondionisatie aan het begin van een ontlading af van de tijd die is verstreken sinds de vorige ontlading. In de context van herhaalde ontladingen, zorgt dit er voor dat de herhalingsfrequentie de factor is die de hoeveelheid achtergrondionisatie bepaalt.

In hoofdstuk 5 maken we een afschatting van de achtergrondionisatie in lucht als een functie van de verstreken tijd sinds de vorige ontlading. Eerst nemen we aan dat alle ionisatie op homogene wijze verspreid is en beschouwen we enkel het verlies van ionisatie door recombinatie. We vinden dat de hoeveelheid achtergrondionisatie aan het begin van een ontlading omgekeerd evenredig is met de tijd die is verstreken sinds de vorige ontlading en dat deze hoeveelheid, voor alle tijdschalen waarin we geïnteresseerd zijn, onafhankelijk is van de hoeveelheid ionisatie direct na afloop van de vorige ontlading.

In de werkelijkheid is de ionisatie niet op homogene wijze uitgesmeerd, maar is het geconcentreerd in de gebieden waar streamerkanalen zijn gepasseerd. Gebruikmakend van data uit experimenten over de breedte van streamerkanalen en de afstand tussen verschillende kanalen, hebben we een model geformuleerd dat de recombinatie van geladen deeltjes combineert met de diffusie van deeltjes uit het streamerkanaal. Hiermee kunnen we onderzoeken in hoeverre een kanaal is nog steeds aanwezig after een bepaalde tijd.

We hebben het model eerst toegepast om een evenwichtsdichtheid te vinden voor de achtergrondionisatie na vele ontladingen; daarna vonden we dat met een herhalingsfrequentie van 10 Hz de ionisatiedichtheid in het midden van voormalige streamerkanaal slechts 3 keer zo hoog is als de minimale ionisatiedichtheid in het gebied tussen streamerkanalen. Met een herhalingsfrequentie van 1 Hz was deze factor slechts 1,23. We voorspellen dat onder deze omstandigheden het onwaarschijnlijk is dat streamers hetzelfde pad volgen in herhaalde ontladingen, hetgeen is bevestigd door experimenten.

Het effect van transportdata

De vergelijkingen die de verandering van deeltjesdichtheden in een vloeistofmodel beschrijven kunnen worden opgedeeld in drie aparte termen: Convectie, diffusie en reactie. Convectie is de verplaatsing van geladen deeltjes in een richting parallel aan het elektrische veld. Diffusie is de beweging van deeltjes van gebieden met hoge dichtheid naar gebieden met een lagere dichtheid. Ten slotte kunnen deeltjes gecreëerd worden of verloren gaan in reacties. In hoofdstuk 3 hebben we aandacht besteed aan reacties, voornamelijk detachement, en hun effect op streamers.

In de originele versie van het simulatieprogramma, waren de twee parameters die convectie en diffusie beïnvloeden, respectievelijk de mobiliteit en diffusie coefficient, constant. In werkelijkheid hangen deze parameters echter af van de lokale sterkte van het elektrische veld. We hebben het programma aangepast om mobiliteit en diffusie coefficienten te gebruiken die zijn berekend met een zeer nauwkeurige Boltzmann solver. Simulaties die gebruik maken van deze data, zoals in meer detail beschreven in hoofdstuk 6, laten zien dat de voortplantingssnelheid van een streamer sterk afhangt van de keuze van transportdata, gezien we een verschil in snelheid van 30% hebben gevonden tussen onze oude, constante parameters en de veld-afhankelijke coefficienten. Aan de andere kant zijn de dikte van de streamer en de morfologie niet verandert.

Tot slot hebben we de simulaties met deze veld-afhankelijke transportdata vergeleken met analytische voorspellingen van een relatie tussen streamer eigenschappen als straal, snelheid en elektrisch veld en we hebben gevonden dat de simulatie in goede overeenstemming is met de analytische voorspelling.

Conclusies

In dit proefschrift hebben we verscheidene aspecten van de voortplantingsmechanismen van positieve streamers in stikstof-zuurstof mengels zoals lucht bestudeerd. We concluderen dat fotoïonisatie het overheersende mechanisme is in vrijwel alle scenario's. Alleen als er een grote hoeveelheid achtergrondionisatie aanwezig is, kan dit de ontlading beïnvloeden. De precieze hoeveelheid achtergrondionisatie die nodig is hangt af van de verhouding tussen zuurstof en stikstof.

Hoewel streamers zich voort kunnen planten in de afwezigheid van fotoïonisatie, komen de achtergrondionisatiedichtheden niet voor in maagdelijke lucht op zeeniveau. Bovendien blijken streamers opmerkelijk robuust te zijn bij veranderingen in de beschikbare dichtheden van vrije elektronen: Veranderingen van de intensiteit van de fotoïonisatie of de hoeveelheid achtergrondionisatie van een of twee ordes van grootte resulteerden in een verandering van de snelheid van de streamer van slechts enkele tientallen procenten.

We hebben een hypothese voorgesteld voor de veertjes-achtige structuren die in experimenten zijn gezien, namelijk dat deze bestaan uit elektronenlawines die zeldzaam genoeg zijn om zichtbaar te zijn als aparte entiteiten, maar een deeltjesmodel is nodig om dit verschijnsel goed te bestuderen. Vervolgens is een eenvoudig diffusie-recombinatie model gebruikt om de overgebleven ionisatie na afloop van een ontlading te berekenen en

om lange-termijn evenwichtsniveaus te vinden voor de achtergrondionisatie in herhaalde ontladingen.

Tot slot hebben we gemerkt dat hoewel streamers niet erg gevoelig zijn voor de dichtheid van vrije electronen die beschikbaar is voor de streamer, heeft de keuze van diffusie en mobiliteits coefficienten wel een significant effect op de snelheid van de streamer. Maar simulaties die gedaan zijn met nauwkeurige diffusie en mobiliteits coefficienten zijn nog steeds in goede overeenkomst met analytische voorspellingen die afgeleid zijn voor een model met de oudere, constante coefficienten.

As my thesis draws to an end and with it the more than 4 years that have gone into it, the time has come to reflect back on this period and give thanks to those that have, directly or indirectly, supported me in my work or in other parts of my life.

First I would like to thank Ute, my promotor and supervisor. I don't think I know anyone more dedicated to the pursuit of science and that served as an inspiration. Even though you almost constantly had a stack of papers, proposals, reviews and such to finish, there was always time to pop in for a question, something that I should've made more use of, when looking back.

My copromotors, Alejandro and Sander, each helped me in a different way. Alejandro got me started with his simulation code and, while moving to Spain not long after I joined, was always ready to assist when I couldn't tell my `doubles` from my `ints` anymore. And thanks to Sander I have experimental results that served as a comparison for my simulations and as a starting point for new questions to be answered.

The streamer-group at CWI has an interesting setup, being led by a physicist (Ute), but with Willem and Margreet as staff members representing mathematics and computer science respectively. This interplay between the different perspectives on the subject was very interesting and also reflects my personal interests. I am grateful to have been able to access these diverse views and approaches to the questions that arose.

I'd also like to thank other colleagues from my group for making my time at CWI very enjoyable. In reverse alphabetical order starting from the third letter of the name: Sasa, Christoph (I think I ended with a positive pingpong-record), Igor, Jannis, Anna M, Anna D, Delyan, Valeria, Anbang, Chao, Aram (sorry for crashing your MacBook so often, but you should just get a normal computer!). Thanks to the support staff, in particular the secretaries Nada and Martine for helping with all the non-scientific matters.

Ook buiten werktijd zijn er mensen geweest die mij op allerhande manieren hebben bijgestaan. Allereerst mijn familie, Jan, Karin & Veron. Hoewel ik dat wellicht niet altijd duidelijk laat zien, is het feit dat ik weet dat wat er ook gebeurt, jullie altijd voor mij klaar staan als het nodig is, een grote geruststelling voor mij. Ik ben erg gelukkig dat ik nu ben waar ik ben en dat is grotendeels dankzij jullie. Tevens wil ik mijn schoonfamilie,

Marie-Andrée, Karin & Chiel, Yvonne & Jurian bedanken voor de gezelligheid en hulp met allerlei dingen de afgelopen jaren.

Ik bedank mijn vrienden van de universiteit (& partners) voor vele jaren gezelligheid tijdens films, spelletjes, vakanties, roleplaysessies, BBQs en veel meer. Bedankt, Mark, Maaïke & Johannes, Ernst & Vincent, Nora & Menno en Ilaan. Vincent in het bijzonder bedankt voor het ontwerpen van de omslag van dit proefschrift.

Een tweede groep mensen waar ik al jaren met veel plezier mee om ga, zijn de begeleiders van de Vierkant voor Wiskunde zomerkampen. Het was op een Vierkant kamp dat ik mij voor het eerst echt op mijn plek voelde, in 2000. Sindsdien hebben de zomerkampen er jaar in jaar uit voor gezorgd dat die groepsaccommodatie in Lunteren voor mij een soort “home away from home” is geworden. Hoewel de volgende lijst met namen lang niet compleet is, wil ik toch een aantal mensen noemen: Martin, Demian, Simeon, Gerwin, Hildo, Martine, Nick, Lesley, Bertram, Oscar, Susanne, Wolf, Mignon & alle anderen, bedankt!

Nicole, we zijn inmiddels bijna 10 jaar bij elkaar en ik kan me niet voorstellen hoe mijn leven er zonder jou uit zou zien. You bring just the right amount of order to my chaos and just the right amount of chaos to my order. Waar we ook terecht zullen komen in de volgende 1, 5 of 50 jaar, de gedachte dat we het samen zullen doen geeft mij het vertrouwen dat het geweldig zal zijn. Thanks for keeping me (somewhat) sane.

Tot slot is er Gwen. Kleine, lieve Gwen, het zal nog wel even duren voor je dit kunt lezen, maar goed. Ik vraag me af of dit proefschrift eerder of later af is dankzij jou. Later, omdat het na jouw geboorte moeilijk was om weer terug aan het werk te gaan. Eerder, omdat het feit dat jij thuis was mij de motivatie gaf om het proefschrift eindelijk maar eens snel af te maken. Hoe dan ook, sinds jij er bent lijkt al het andere zo veel minder belangrijk. Ik hoop dat wanneer je dit leest, je nog net zo’n vrolijke, vriendelijke en enthousiaste meid bent zoals nu.

Curriculum Vitae

Gideon Wormeester was born on 01-06-1985 in Apeldoorn, Netherlands.

After finishing VWO in 2002 at Gymnasium Apeldoorn in Apeldoorn, Netherlands, he completed a Bachelors in Mathematics and in Physics, followed by a Masters in Mathematics at the University of Utrecht, Netherlands. In 2008 he graduated within the mathematical logic group on non-standard models of arithmetic. From november 2008 he started a PhD project at Centrum Wiskunde & Informatica (CWI) in Amsterdam, Netherlands, of which the results are presented in this dissertation.